Schweizerische Eidgenossenschaft
Confédération suisse
Confederazione Svizzera
Confederaziun svizra

Federal Department of the Environment, Transport, Energy and Communications DETEC

Swiss Federal Office of Energy SFOE
Energy Research and Cleantech Division

Final report dated March 24, 2026

Demonstration of high-performance CO_2-selective graphene membranes for energy-efficient carbon capture

EfficientCapture

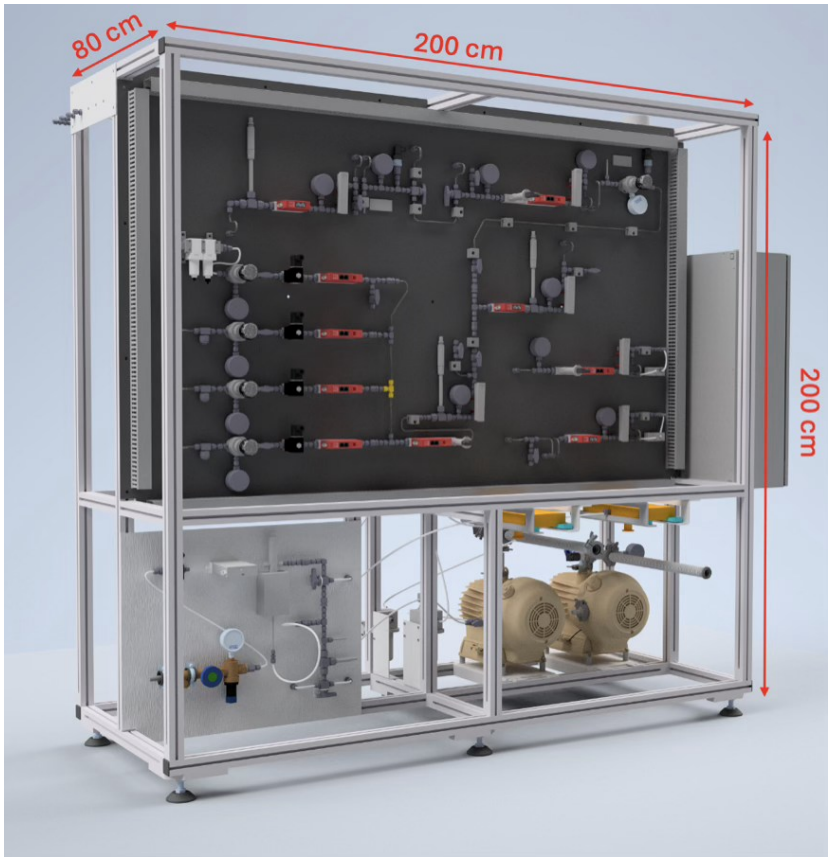

Source: ©Laboratory of Advanced Separations, EPFL; 2025

Location: Bern

Publisher:
Swiss Federal Office of Energy SFOE
Energy Research and Cleantech
CH-3003 Bern
www.bfe.admin.ch

Co-financing:
École Polytechnique Fédérale de Lausanne (EPFL)
Canton of Valais
GAZNAT

Subsidy recipients:
École Polytechnique Fédérale de Lausanne (EPFL)
Rue de l'Industrie 17, Case Postale 440, CH-1950 Sion

GAZNAT
Av. Général-Guisan 28, 1800 Vevey

Authors:
Dr. Jian Hao, Dr. Marina Micari, Prof. Kumar Varoon Agrawal
Laboratory of Advanced Separations (LAS), EPFL
kumar.agrawal@epfl.ch

SFOE project coordinators:
Men Wirz, Men.Wirz@bfe.admin.ch
Elena-Lavinia Niederhäuser, lavinia.niederhaeuser@bfe.admin.ch

SFOE contract number: SI/502268-01

Zusammenfassung

Die erfolgreiche Umsetzung des vom Schweizer Bundesrat festgelegten Netto-Null-Ziels erfordert eine rasche Entwicklung energieeffizienter Technologien zur CO_2-Abscheidung. Dieses Projekt basiert auf einer neuartigen zweidimensionalen (2D) Membrantechnologie der EPFL, die atomar dünne, poröse Graphenfilme (PG) als CO_2-selektive Schicht nutzt. Ziel des Projekts ist die Skalierung dieser Technologie auf Metermaßstab sowie der Nachweis einer CO_2-Abscheidung von 1 kg pro Tag.

Im Verlauf des Projekts wurden mehrere wesentliche Innovationen eingeführt, die zu einer deutlichen Reduktion der Herstellungskosten von PG-Membranen führten, eine homogene Porenbildung über große Flächen ermöglichten und die Herstellung großflächiger Membranen mit attraktiver Leistungsfähigkeit erlaubten. Es wurde erfolgreich ein skalierter Reaktor in Betrieb genommen, der die Synthese von Graphen im Metermaßstab in einem einzigen Prozessschritt ermöglicht. Darüber hinaus wurde ein weiterer skalierter Reaktor zur kontrollierten Oxidation von Graphen entwickelt, mit dem sich hochdichte Poren im Ångström-Bereich für die CO_2-Trennung erzeugen lassen. Dieser Reaktor erlaubt insbesondere die Herstellung von Proben mit Flächen bis zu 500 cm^2.

Wir zeigen, dass der Stofftransport des Oxidationsmittels entscheidend für eine gleichmäßige Oxidation großflächiger Graphenfilme ist. Zudem wurden Cross-Flow-Module für die Verarbeitung von Membranen unterschiedlicher Größen (1, 10, 100 und 500 cm^2) entwickelt und erfolgreich validiert. Die Rissbildung während des Graphentransfers, die bislang die Reproduzierbarkeit einschränkte, konnte durch ein neuartiges Verfahren eliminiert werden, das auf empfindliche Floating- und Handhabungsschritte verzichtet. Dadurch ist die Herstellung hochleistungsfähiger Graphenmembranen mit nahezu 100% Erfolgsrate möglich. Insgesamt konnte die Reproduzierbarkeit und Zuverlässigkeit der Membranherstellung deutlich verbessert werden.

Abschließend wurde ein zweistufiger Membranprozess entwickelt und optimiert, mit dem eine CO_2-Reinheit von 95% sowie eine Rückgewinnungsrate von 90% erreicht werden. Eine zweistufige Pilotanlage wurde an der EPFL in Betrieb genommen und zeigte eine langfristig stabile Leistung der Graphenmembranen unter simulierten Rauchgasbedingungen. In Zusammenarbeit mit GAZNAT konnte zudem die Stabilität der Graphenmembranen bei der Trennung von CO_2 aus realem Rauchgas erfolgreich nachgewiesen werden.

Résumé

La réalisation réussie de l'objectif de zéro émission fixé par le Conseil fédéral suisse nécessite le développement rapide de technologies de captage du carbone à haute efficacité énergétique. Ce projet s'appuie sur une technologie innovante de membranes bidimensionnelles (2D) développée à EPFL, utilisant des films de graphène poreux (PG) d'épaisseur atomique comme couche sélective au CO_2. Le projet vise à passer à l'échelle (membranes de taille métrique) et à démontrer une capacité de captage de 1 kg de CO_2 par jour.

Au cours du projet, plusieurs avancées majeures ont été introduites, permettant de réduire significativement les coûts de production des membranes PG, d'assurer une formation uniforme des nanopores sur de grandes surfaces, et de produire des membranes de grande taille présentant des performances attractives. Nous avons notamment mis en service un réacteur à l'échelle pilote capable de synthétiser du graphène de taille métrique en un seul lot. Par ailleurs, un réacteur de mise à l'échelle pour l'oxydation contrôlée du graphène a été développé, permettant la formation de pores de taille angströmique à haute densité pour la séparation du CO_2. Ce réacteur permet en particulier la préparation d'échantillons allant jusqu'à 500 cm^2.

Nous démontrons que le transfert de masse de l'agent oxydant joue un rôle déterminant pour garantir une oxydation homogène sur de grandes surfaces de graphène. Nous avons également développé et

validé des modules à écoulement tangentiel (cross-flow) pour le traitement de membranes de tailles croissantes (1, 10, 100 et 500 cm^2). La formation de fissures lors du transfert du graphène, qui limitait auparavant la reproductibilité, a été éliminée grâce à un protocole innovant évitant les étapes délicates de manipulation et de flottation du graphène. Cette approche permet la fabrication de membranes de haute performance avec un taux de réussite proche de 100%. Notre méthode de fabrication améliore ainsi significativement la reproductibilité et la fiabilité du procédé.

Enfin, nous avons développé et optimisé un procédé membranaire en deux étages permettant d'atteindre une pureté en CO_2 de 95 % et un taux de récupération de 90%. Une unité pilote à deux étages a été mise en service à l'EPFL, démontrant la stabilité à long terme des membranes en graphène dans des conditions simulées de gaz de combustion. En collaboration avec GAZNAT, nous avons également démontré la stabilité de ces membranes pour la séparation du CO_2 à partir de gaz de combustion réels.

Summary

A successful realization of the zero-emission target set by the Swiss Federal Council requires a rapid development of energy-efficient carbon capture technology. This project builds on the EPFL's novel two-dimensional (2D) membrane technology using atom-thick, porous graphene (PG) film as a CO_2-selective layer. The project aims to scale up the technology (meter-scale membrane) and demonstrate the capture of 1 kg CO_2/day.

During the project, we introduced several interventions that significantly reduced PG membrane production costs, enabled uniform pore formation over a large area, and enabled the preparation of large-area PG membranes with attractive performance. We successfully commissioned a scaled-up reactor capable of synthesizing meter-scale graphene film in a single batch. We also developed a scaled-up reactor capable of controlled oxidation of graphene to form high-density Å-scale pores for CO_2 separation. In particular, this reactor can prepare samples that are up to 500 cm^2 in size. We show that oxidant mass transfer is crucial for achieving uniform oxidation of large-area graphene. We have developed and validated cross-flow modules for handling graphene membranes of increasing size (1, 10, 100, and 500 cm^2). Crack formation during graphene transfer, which also limits reproducibility, is eliminated using a novel protocol that avoids delicate floating and handling of graphene, enabling the fabrication of a high-performance graphene membrane with a near 100% success rate. Our fabrication method has improved the reproducibility and success rate of graphene membrane preparation. Finally, we developed and optimized a two-staged membrane process to achieve 95% CO_2 purity and a 90% recovery rate. We also commissioned a two-stage membrane pilot plant at EPFL. The pilot plant demonstrated long-term stability of the graphene membrane in simulated flue gas. In collaboration with GAZNAT, we demonstrated the stability of graphene membranes in separating CO_2 from real flue gas.

Contents

Abbreviations

2D: Two-dimensional

AC-HRTEM: Aberration-corrected high-resolution transmission electron microscopy

CHP: Combined heat and power

CFD: Computational fluid dynamics

CVD: Chemical vapor deposition

GPU: Gas permeation unit (1 GPU = 3.35×10^{-10} mol m^{-2} s^{-1} Pa^{-1})

IPCC: Intergovernmental panel on climate change

LAS: Laboratory of Advanced Separations

MRF: Mechanically-reinforcing support film

NSLG: Nanoporous single-layer graphene

PES: Polyethersulfone

PG: Porous graphene

PTMSP: Poly(1-trimethylsilyl-1-propyne)

PDMS: Polydimethylsiloxane

SLG: Single-layer graphene

SS: Stainless-steel

1 Introduction

1.1 Background information and current situation

The sixth assessment report by IPCC highlights the necessity to restrict the global temperature rise to within 1.5 ºC from the pre-industrial levels, which requires the reduction of CO_2 emissions from industrial point sources as well as the atmosphere (negative emission).[1–3]

Among point sources, power plants are the largest emitters, with CO_2 concentrations in flue gas ranging from 4% to 13%.[4,5] The captured CO_2 can then be converted into CH_4 using renewable electricity.[6] This can be added to the gas grid, reducing overall carbon emissions. Naturally, for the successful implementation of capture while meeting Switzerland's energy needs, the development and deployment of energy- and cost-efficient capture technology are of paramount importance.

The need for energy-efficient technology stems from the high energy cost of CO_2 capture using currently commercially available technology, which relies on absorption in an amine-based solvent (Figure 1a). Here, the high cost (>CHF 50-110/tonCO_2) mainly arises from the requirement to regenerate liquid amines by thermal treatment.[7,8] High-performance membrane-based capture processes can reduce the capture penalty because they do not rely on expensive thermal energy but instead use electrical energy (compression/vacuum) to create a concentration gradient across the membrane (Figure 1b). The commercial membrane-based capture technology uses dense polymeric films as the selective layer. The state-of-the-art polymeric films have shown promising CO_2/N_2 performance.[5] However, there is an opportunity (i) to significantly improve separation performance, especially the CO_2 permeance, which affects the needed membrane area and, therefore, the capital cost, and (ii) to improve the operational lifespan of the membranes, especially considering the acidic contaminations in the flue gas (SOx and NOx). A thermally and chemically stable nanoporous inorganic material-based selective layer has an intrinsic advantage of high CO_2 permeance and improved thermal and chemical stability.

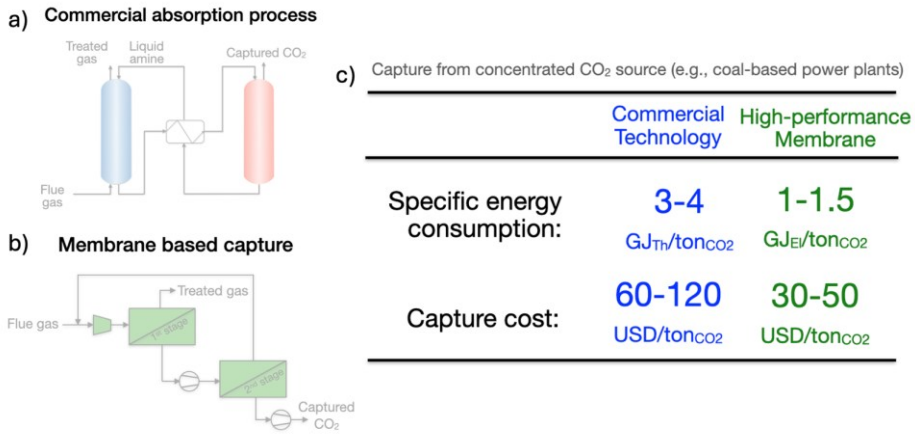

Figure 1. Carbon capture process illustration: (a) commercial absorption process, and (b) membrane-based capture. (c) The comparison of the capture cost from a techno-economic analysis.

LAS at EPFL has developed an atom-thin porous graphene film for high-performance carbon capture. We have demonstrated high carbon capture performance with CO_2 permeance approaching 10000 GPU and CO_2/N_2 selectivity close to 20, which can then be further increased based on pore edge functionalization.[9–12] The CO_2 permeance, which determines the needed membrane area, is 3-4 fold

better than that of commercial membranes. Technoeconomic analysis of these membranes indicates significant energy and cost savings for carbon capture (Figure 1c).[8,13]

1.2 Novel porous graphene membrane

The graphene membrane described here refers to a porous graphene film with a selective layer thickness of just one atom.[14] Graphene is an allotrope of carbon formed of a single layer of graphite where carbon atoms are arranged in sp^2-hybridization. As a result, pores in graphene constitute the thinnest possible permselective layer. The single-atom thickness of the pore results in an extremely short molecular diffusion path length and a high gas permeance.[15] If small pores, similar to the size of gas molecules, are incorporated in graphene, the separation of gas molecules takes place based on the relative rate of diffusion of gas molecules from the pore (Figure 2). This rate of diffusion depends on the energy barrier of the molecule to cross the pore, which, in turn, depends on the relative size difference of gas molecules with respect to the graphene pore, a concept known as molecular sieving.[16–19] In the separation of flue gas, two major components are CO_2 and N_2. Luckily, CO_2 is smaller than N_2 (kinetic diameters of 0.33 and 0.364 nm, respectively), allowing one to target its separation from graphene pores. Another pathway that affords selectivity to CO_2 is the competitive adsorption of CO_2 vs N_2 on graphene pores. This is especially manifested when the graphene pores are functionalized (e.g., with an O or N functional group).[12,19] In our case, since pores are created by oxidation, the pores are decorated with O functional groups (epoxy, ether, semiquinone).

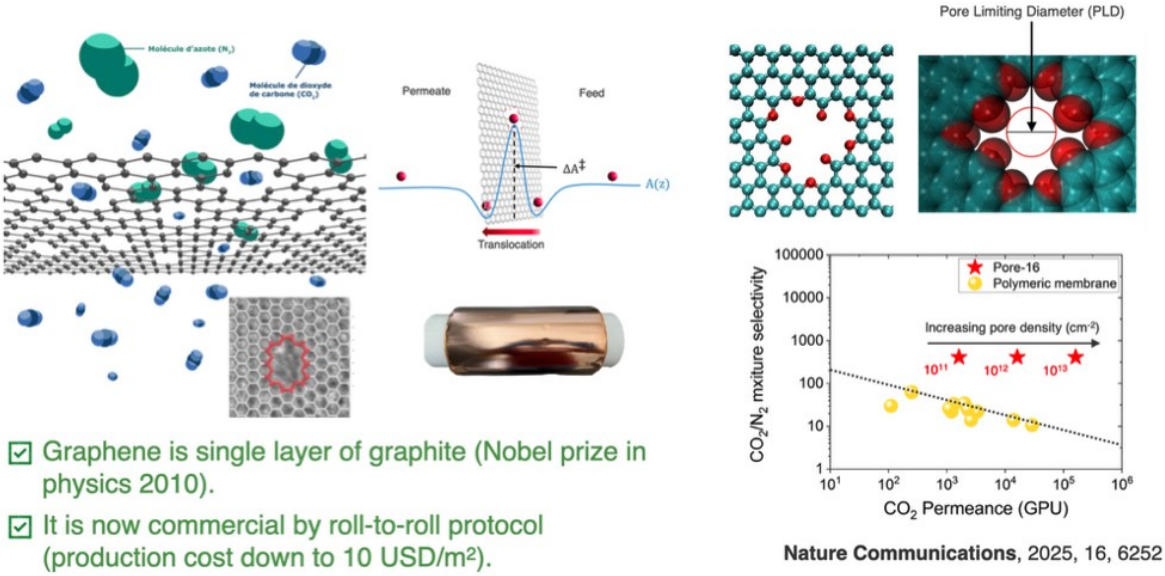

Figure 2. Concept of CO_2 separation using graphene membranes hosting Å-scale pores. A single-atom-thick graphene layer containing Å-scale pores enables selective CO_2 transport via size sieving and adsorption-assisted translocation, while larger molecules, such as N_2, are hindered. The pore-limiting diameter and pore chemistry govern the energy barrier for transport. Increasing pore density dramatically enhances permeance while maintaining high CO_2/N_2 selectivity, enabling performance beyond conventional polymeric membranes. Graphene can be produced by roll-to-roll manufacturing at projected costs down to USD 10/m2 supporting scalable deployment for carbon capture applications.

The advantage of graphene membranes over commercial membranes, such as those made of polymer, comes from the fact that graphene pores allow rapid transport of gas molecules. As a result, graphene membranes exhibit higher CO_2 permeance than polymeric membranes, which is advantageous for reducing the required membrane area and, therefore, the capture cost. This also becomes extremely

useful for membrane compaction, especially when space for installation is at a premium (offshore facilities, transportation sector, etc.).

Porous graphene has another advantage. It has high chemical, thermal, and mechanical robustness. Therefore, one can expect graphene membranes to have a much longer lifetime, especially in the presence of acidic impurities such as NOx and SOx. Based on this, we expect the membrane to last at least 5 years.

Graphene can be synthesized by different methods.[20,21] While it was famously first isolated by peeling layers of graphite using the mechanical exfoliation method with scotch tape, modern industrial applications rely on a more scalable chemical vapor deposition (CVD) process.[22,23] In this method, the carbon-rich gas, like methane, is decomposed at approximately 1000 ºC and forms a single layer of ordered carbon on the surface of a catalytic substrate (copper foil), resulting in a single-atom-layer with low density of intrinsic defects. Although this established process produces a nearly perfect lattice, such pristine graphene is impermeable to any gas molecules. To use it as a gas-separation membrane, a precise pore-forming process must be applied to create molecular pathways, followed by careful transfer of the graphene layer onto a mechanically robust porous support.[24] As briefly illustrated in Figure 3, this multi-step membrane fabrication process has the potential of being produced in a continuous, roll-to-roll manner.

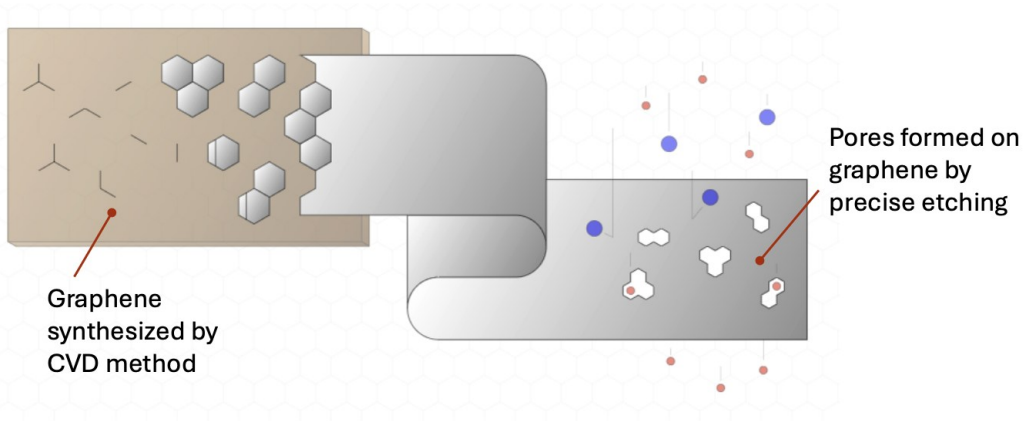

Figure 3. Schematic illustration of the porous graphene fabrication process.

Scaling the production of graphene membrane faces two primary hurdles: achieving precise pore formation and ensuring the defect-free transfer of graphene onto a porous support. Our group has systematically addressed the former by investigating the underlying mechanism of pore formation (Figure 4).[17–19,25] We select ozone as an advantageous etchant: its gaseous phase ensures high uniformity and scalability across large areas, while its high reactivity allows for fine pore size control. The ozone etching process begins with the chemisorption of ozone onto the graphene lattice to form epoxy clusters, which evolve from monomers into dimers, cyclic trimers, and eventually linear trimer chains. These clusters introduce significant local strain, leading to C-C bond cleavage and the formation of ether groups at the core. When sufficient energy is provided, such as heating or exposure to UV light, these cluster gasify, leaving behind pores terminated by ether or semiquinone groups.[11,25,26] Ultimately, the size of the pore can be finely tuned by controlling the size of the epoxy cluster and the amount of energy applied during the gasification stage.

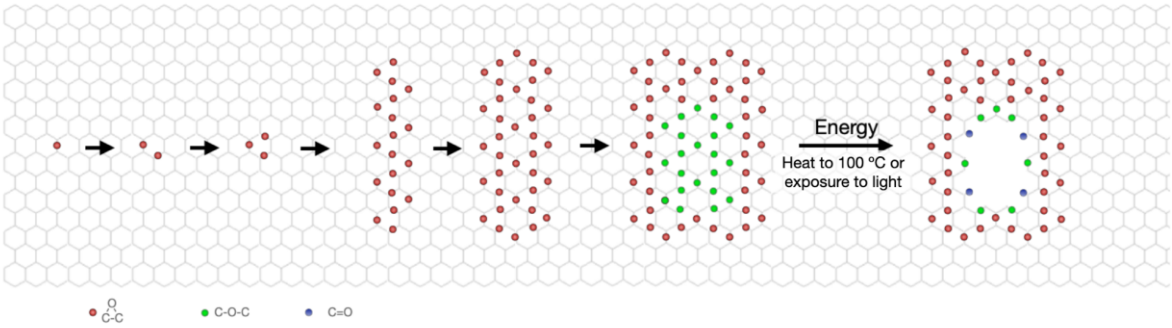

Figure 4. Mechanism illustration of pore formation on graphene lattice by ozone.

The second major hurdle, the transfer of graphene, has historically seen limited progress due to the physical risks inherent in the conventional process.[27] As illustrated by the SEM image in Figure 5, this typically involves chemically etching away the Cu growth substrate and manually scooping the ultra-thin graphene onto a porous support, a delicate procedure prone to tears and cracks that are detrimental for gas separation membranes. Consequently, developing a fabrication method that bypasses this fragile transfer step is essential for achieving the reliability required for the scale-up of graphene membranes.[28]

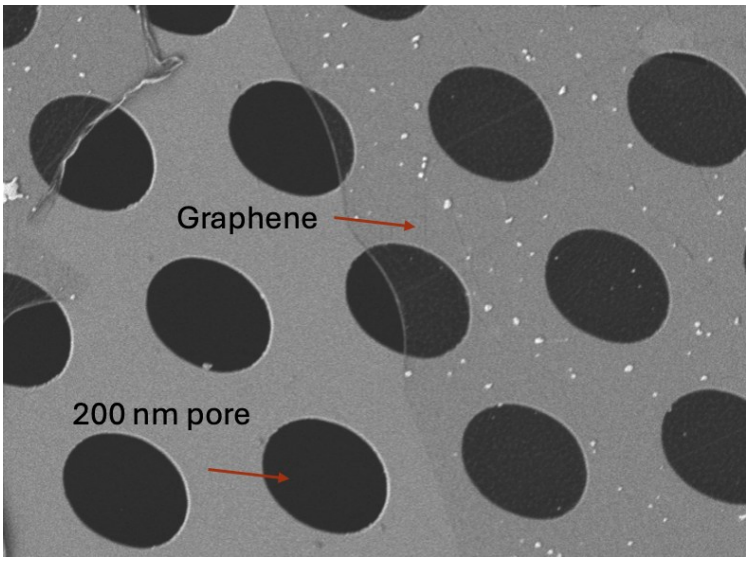

Figure 5. SEM image of graphene transferred on a support with 200 nm pores.

1.3 Purpose of the project

Our techno-economic analysis indicates that a double-stage membrane module fitted with high-performance graphene membranes with only a small membrane area of 0.04 m^2 is sufficient for capturing 1 $kgCO_2$/day (our target rate) in an energy-efficient manner.[13] Given the high potential of this technology in addressing the important issue of global warming, its further scale-up and demonstration are attractive. Therefore, the project will seek to scale up the production of nanoporous graphene films, membrane elements, and membrane modules. Subsequently, the project will build a two-stage membrane process to capture CO_2 from flue gas with the help of our industrial collaborators.

1.4 Objectives

This project aims to scale up porous graphene films hosting Å-scale pores for gas separation to a large area (50 cm^2 scale for a single coupon). The project then intends to develop a membrane element and module using graphene film as the selective layer. The membrane will be implemented in a two-stage membrane process to capture CO_2 at the rate of 1 kg/day from a simulated CO_2/N_2 gas mixture.

Overall, by testing high-performance membranes, we aim to validate the techno-economic analysis (Table 1).

Table 1. Techno-economic analysis of carbon capture from different feed conditions.

Feed Condition	**Recovery**	**Purity**	**Specific Energy Demand (GJ/tonCO_2)**	**Capture Cost ($/ton$CO_2$)**	**Membrane Lifespan (year)**
Flue gas (12% CO_2)	90% CO_2	95% CO_2	1.5	41	5
Biogas (45% CO_2)	96% CO_2, 91% CH_4	90% CO_2, 96% CH_4	0.7	38	5

Our specific objectives are:

1. Scale-up production of high-performance graphene membranes (target area 0.1 m^2) using intrinsically scalable fabrication methods that are capable of yielding m^2 graphene membranes in a single synthesis batch.
2. Develop compact plate-and-frame membrane modules with a low-volume footprint and high packing density (100-300 m^2/m^3), low pressure drop, and low concentration polarization.
3. Build a membrane skid consisting of a double-stage membrane process with recycle, and demonstrate its efficacy for capturing 1 kg CO_2 from a gas mixture representing flue gas from a waste incinerator with a recovery of 90% and a purity of 95%.
4. Demonstrate membrane stability by continuously online monitoring the performance data.

2 Description of facility

2.1 Membrane production

As a part of the project, we have built a dedicated scale-up laboratory to produce high-quality graphene membranes in a clean environment. The equipment includes an ISO 5 cleanroom (Figure 6), a homemade reactor to produce porous graphene at meter-scale (Figure 7 and Figure 8), a scaled-up oxidation reactor to synthesize porous graphene (Figure 9), and a large-area spin-coater (Figure 10) to deposit a thin protective and mechanically-reinforcing polymeric film on graphene.

The cleanroom (ABN Cleanroom Technology, ABNCR-22 580, ISO 5) has an air exchange rate of 70 times per hour and less than 1000 1-µm-sized particles per cubic meter. It covers an area of 4 m × 3.5 m. The cleanroom is designed so that all gas connections enter the cleanroom without disrupting the cleanroom module. There is also air conditioning in the side clean room to ensure the enclosure's temperature does not rise when ovens heat to high temperatures.

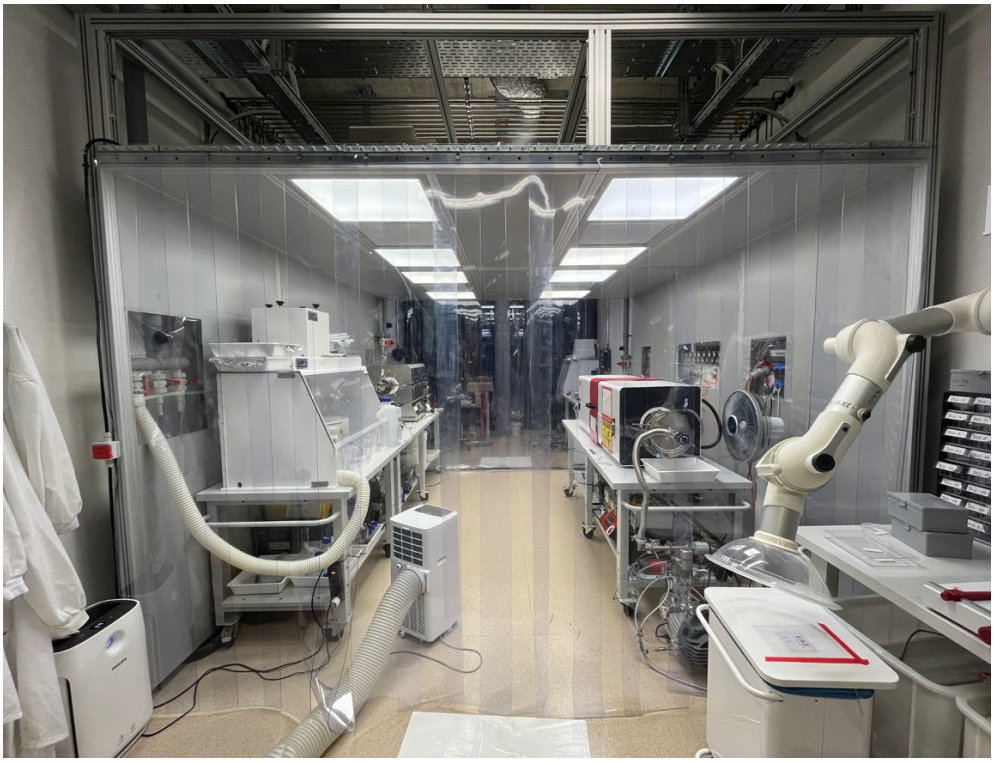

Figure 6. The membrane scale-up laboratory at EPFL.

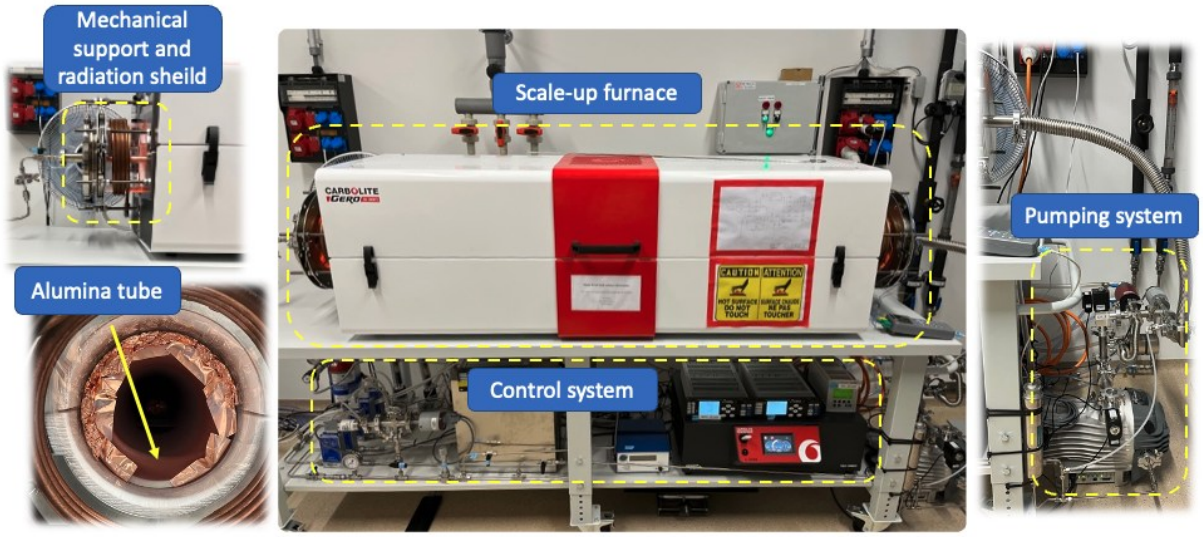

Figure 7. Large-scale CVD furnace for graphene synthesis.

The large-scale CVD furnace is custom-made in the laboratory. It is composed of a heating furnace (Carbolite, 1200 ºC Split Tube Furnace, TS3 12/200/1200, with a controller; see Figure 7) with a 1.2 m uniform heating zone up to 1200 ºC and a quartz tube with an outer diameter of 20 cm. Inside the quartz tube, an alumina tube (Zibo Highlion New Material Co., Ltd, 1.5 m long, outer diameter of 18 cm, inner diameter of 16 cm) is placed to reduce the contamination from the quartz tube. This is because, during the heating of Cu foil above 600 ºC, the reaction between Cu vapor and quartz produces SiO_x particles and contaminates the Cu surface.

It can be used to produce graphene coupons with a width of 12 cm and a length of 1 m. The furnace is equipped with various systems for the controlled and safe production of graphene. We customized a stainless-steel mechanical support to withstand the compression force from the metal flanges during pumping. We realized that it is extremely crucial to balance the mechanical force on the quartz tube when the vacuum is applied. This is where the mechanical support is crucial (shown on the left side of Figure 7). We also added a customized copper radiation shield near the edge of the heating zone inside the quartz tube to reduce the flange temperature during synthesis. The system is pumped through a scroll vacuum pump (Plasmadiam, nXDS 10i), and the pressure is monitored by several pressure transducers (MKS, Vacuum Pressure Transducer, 1000 Torr, and 1 Torr). A gas regulating valve (Pfeiffer, RVC 300) is integrated to regulate the system pressure during synthesis. The synthesis can be fully automated by creating LabView programs to interact between these devices and a laboratory PC, and the software interface is shown in Figure 8.

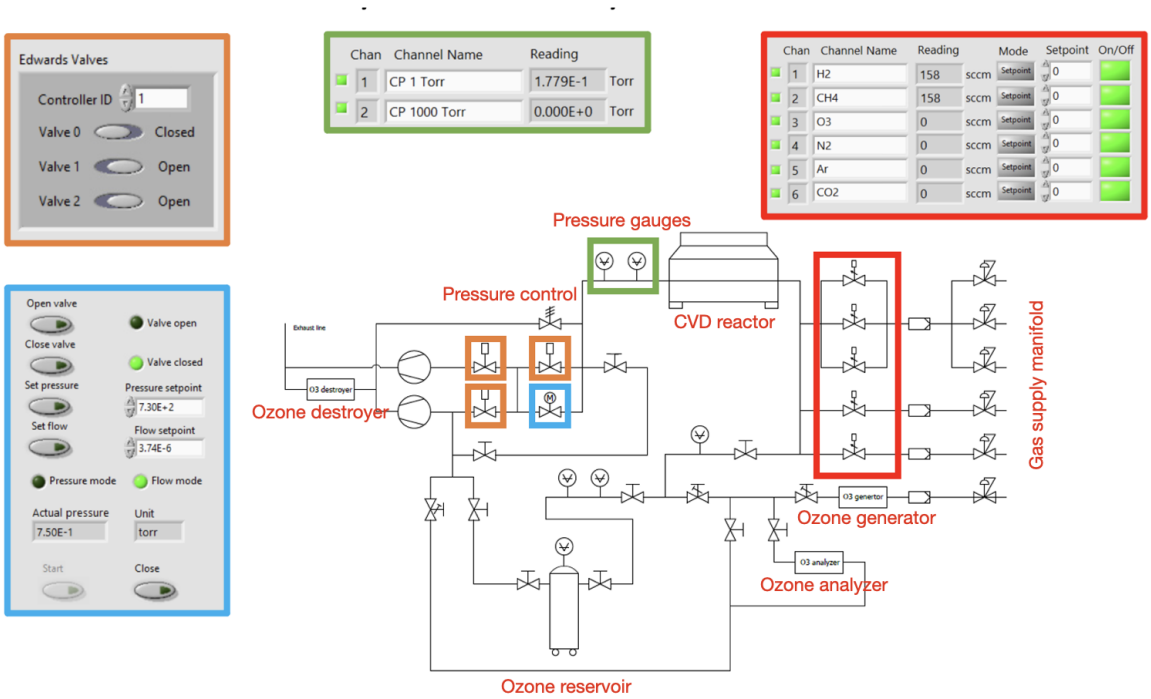

Figure 8. Process flow diagram for the large-scale CVD reactor for producing nanoporous graphene.

The graphene oxidation reactor, which creates pores in graphene, is equipped with a furnace (Nabertherm, Split Tube Furnace, RSH, Figure 9) that houses a 12 cm-diameter quartz tube. The reactor can be heated to a temperature of 1100 ºC, and its pressure can be controlled by a vacuum pump. The pressure is monitored by a Baratron absolute manometer (MKS). The reactor can house graphene coupons with a width of 11 cm and a length of 50 cm. The reactor is fed with an ozone supply via an

ozone generator (Absolute Ozone, Atlas 60) with a concentration of 8-10% ozone in oxygen and a flow rate of up to 2 l/min at atmospheric pressure. It is also fed with argon and hydrogen, which is used to clean the graphene surface from contamination. The laboratory is equipped with ozone sensors and an automated ozone flow cutoff system in case of a leak of ozone.

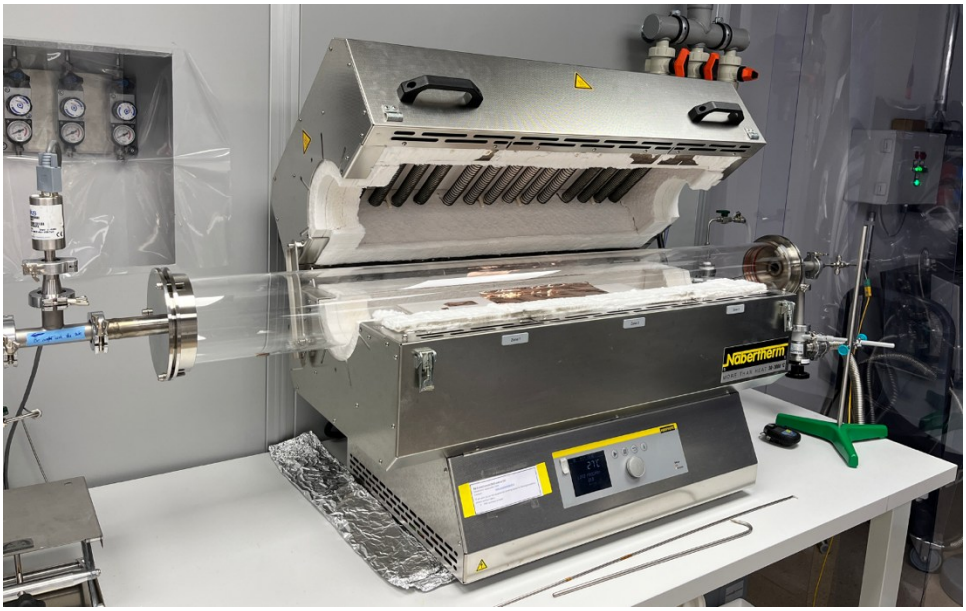

Figure 9. Large-scale tube furnace for ozone functionalization on graphene.

The laboratory is also equipped with a large area spin coater (Laurell Technologies Corporation, WS-650Hz-15NPPB) capable of coating thin polymeric film for large substrates (up to 30 cm diameter coupons, Figure 10). For meter-scale graphene membranes, this is a sufficient and convenient route to reliably coat a thin polymeric film. The spin coater is housed in a ventilated hood, which allows one to use organic solvent-based coating suspension.

Figure 10. Large-area spin coater hosted inside a ventilated hood.

A dedicated space outside the Engerypolis campus is built for testing and demonstrating carbon capture from a gas mixture using porous graphene membranes (Figure 11). Pure CO_2, N_2, and O_2 gases can be supplied from gas cylinders to mimic the composition of the flue gas. An automated testing system has

been built with remote monitoring functionality to generate continuous data for evaluating the long-term stability of the graphene membrane (Figure 69). Moreover, gas tanks containing a simulated flue gas mixture containing SO_x/NO_x contaminants are housed in the facility to test the membrane's stability under flue gas conditions.

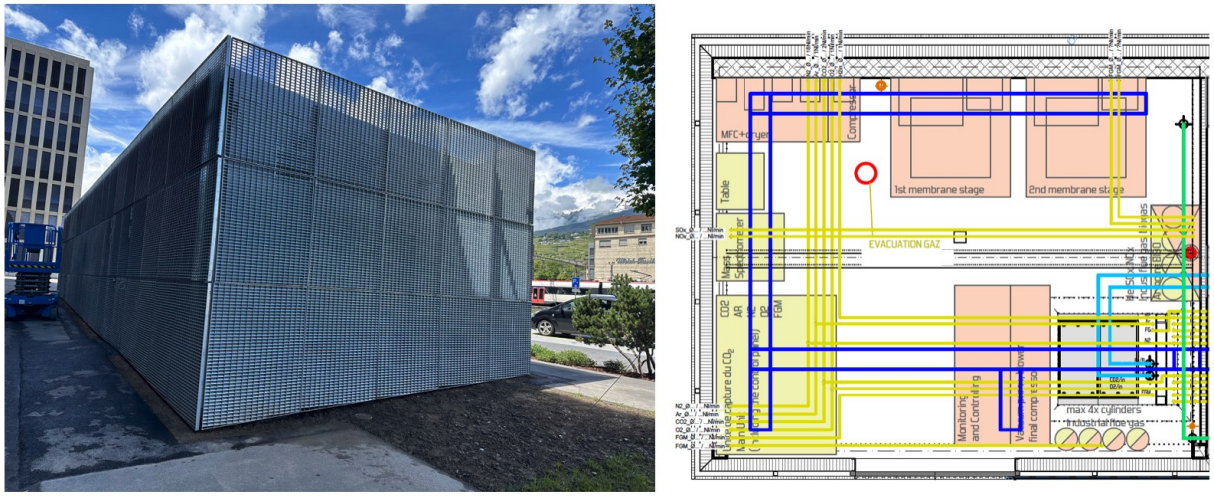

Figure 11. Dedicated space in Energypolis campus (Sion) for the demonstration of graphene membrane-based carbon capture

2.2 Membrane setup

The prepared membrane is first assembled in a membrane module (see the next section for the preparation technique), and the module is then inserted into a permeation measurement setup to validate the gas separation property. Figure 12a shows a schematic illustration of the permeation setup at a laboratory scale, and Figure 12b shows examples of different segments. Essentially, feed gas is introduced to the membrane, with part of it passing through the membrane and the rest going into the retentate. The membrane enables selective permeation for CO_2. As illustrated in Figure 12c, the membrane has a higher CO_2 transport rate than N_2, resulting in CO_2 enrichment on the permeate side.

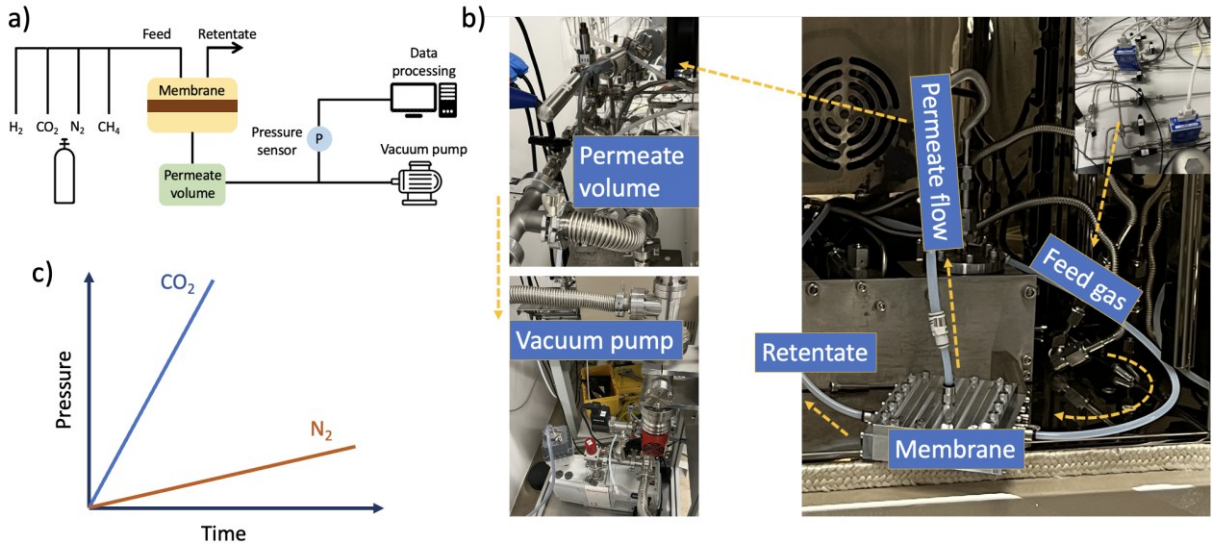

Figure 12. (a). Schematic illustration of the membrane separation process on a laboratory scale. (b). Examples of different segments of the membrane permeation setup. (c). Schematic illustration of membrane permeation results showing that CO_2 gas is passing through the membrane faster than N_2.

We have also developed and commissioned a membrane pilot plant to demonstrate stable operation with high CO_2 recovery and purity (Figure 13 and Figure 14). Briefly, a simulated flue gas containing ~12% CO_2 is fed to the pilot plant, where a two-stage membrane process (50 cm^2 each, as shown in Figure Figure 14) purifies the CO2 with a high purity rate (target > 95%) and a high recovery rate (target >90%). A detailed process flow diagram for a two-stage membrane module for carbon capture is shown in Figure 13.

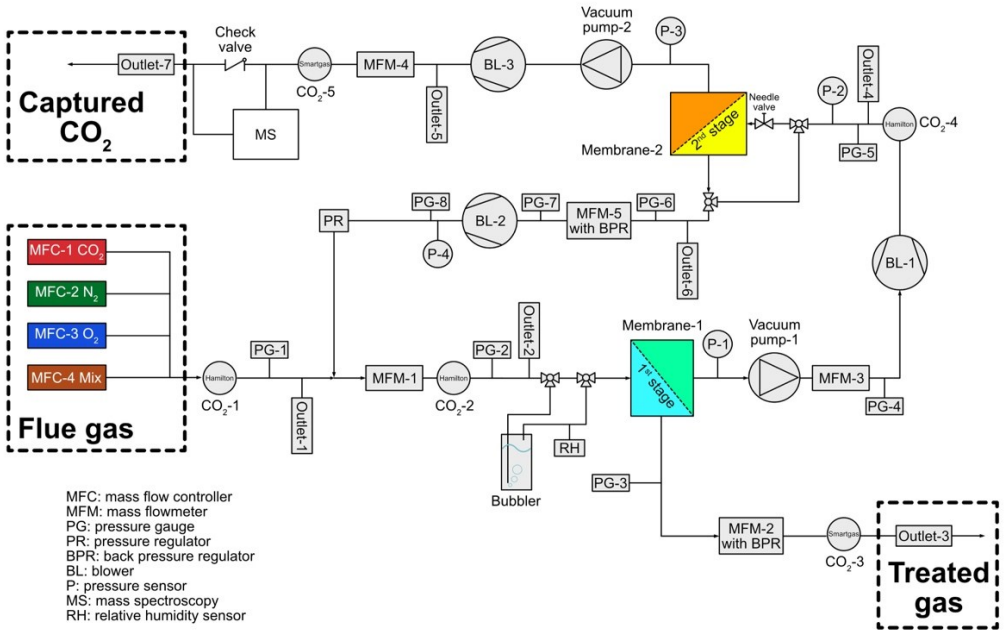

Figure 13: Process flow diagram of the two-staged membrane skid (see pictures of the skid in Figure 10).

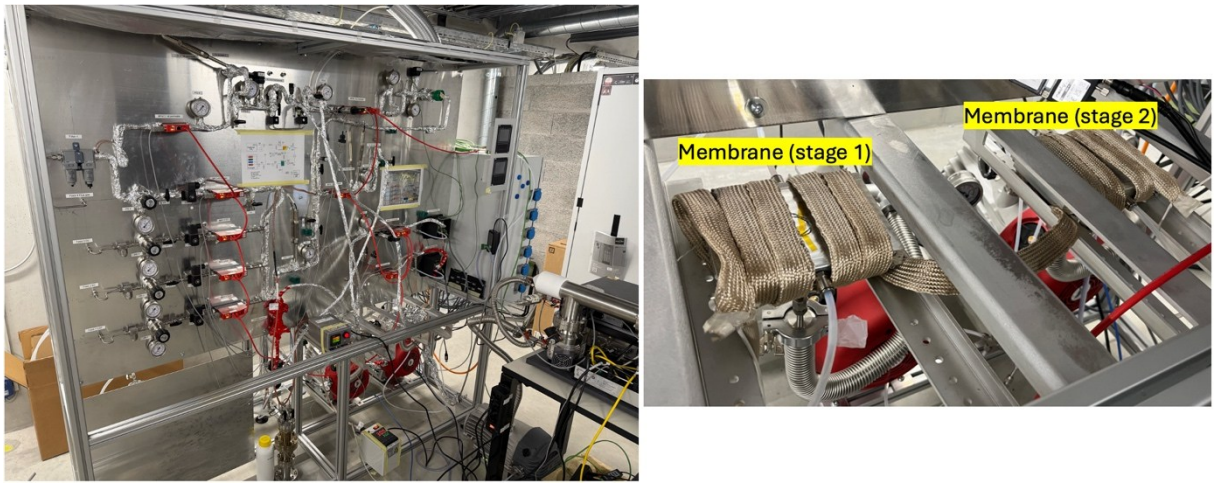

Figure 14. The two-staged membrane skid (left). Right: The two membrane modules are highlighted on the right.

3 Procedures and methodology

3.1 Project procedure

The fulfillment of this project can be described in the following procedures:

1. Building a cleanroom facility-based laboratory (ISO 5) that reduces particulate contamination for the production and processing of clean graphene membranes.
2. Designing and assembling the experiment setup for CVD synthesis of graphene.
3. Designing and assembling experiment setups for pore incorporation in graphene by oxidation ozone.
4. Optimizing the experimental parameters to synthesize graphene with high quality (I_D/I_G band ratio less than 0.1, characterized by Raman spectroscopy) and high porosity (pore density of 3×10^{11} cm^{-2}, characterized by AC-HRTEM analysis).
5. Optimizing and scaling up the membrane module for reproducible membrane fabrication and reliable mixture gas separation.
6. Constructing membrane separation units in the lab to understand performance.
7. Simulating the membrane process model and conducting a technoeconomic analysis to determine the optimal configuration for the membrane process (pressure ratio, area, recycle in the two-stage membrane, etc.).
8. Building a two-stage membrane separation setup to validate the performance of our membrane process.

To realize high-performance graphene membranes, our strategy was the following:

1. Studying the key factors that affect the quality of graphene synthesized by the CVD approach. This includes surface quality of Cu (roughness, contamination), Cu annealing conditions, CVD synthesis temperature, synthesis pressure, and precursor concentration.

2. Studying the influence of different ozone gas reaction parameters on the porosity and the pore size distribution of graphene by directly analyzing the membrane performance. Here, CO_2 permeance is an indicator of porosity in graphene, whereas CO_2/N_2 selectivity is an indicator of efficacy in creating a narrow pore size distribution. Key parameters studied for this were reactor geometry (diameter), temperature uniformity, ozone flow rate and velocity, reaction temperature, time, and Cu surface roughness during the reaction. The latter was optimized by annealing the porous graphene in a hydrogen atmosphere at various temperatures to get a smooth Cu surface.
3. Designing the membrane mechanical reinforcement strategy for defect-free membrane fabrication, as well as the membrane module geometry for efficient single component or mixture gas separation.

3.2 Synthesis of high-quality, large-area single-layer graphene

The procedure for the synthesis of high-quality single-layer graphene in the scale-up CVD furnace consists of several steps. This starts with cleaning the surface of the as-received Cu foil (Roth, 100 µm thick) using an acid treatment. Briefly, Cu foil is cut into desired sizes and undergoes an acid treatment to remove the surface coatings or impurities, which can be preserved after graphene synthesis. The acid treatment is performed by first immersing the Cu foil in 4 wt% nitric acid for 10 min, followed by 4 washes in deionized water. The resulting Cu coupon is then inserted into the CVD reactor for synthesis.

In the CVD reactor, organic contaminants are removed by exposing Cu to CO_2. This is followed by H_2 annealing to remove native oxide groups on Cu, CVD graphene synthesis, and finally cooling (Figure 15). CO_2 cleaning is performed below 1020 ºC under ambient pressure, after which the atmosphere is changed to H_2/Ar for Cu annealing. The annealing procedure is optimized near the melting point of Cu, followed by stepwise cooling to the CVD growth temperature (1020 ºC). The synthesis is done at 190 mTorr maintained by flowing 3 and 9 sccm of H_2 and CH_4, respectively. After 30 min of synthesis, the furnace is cooled naturally.

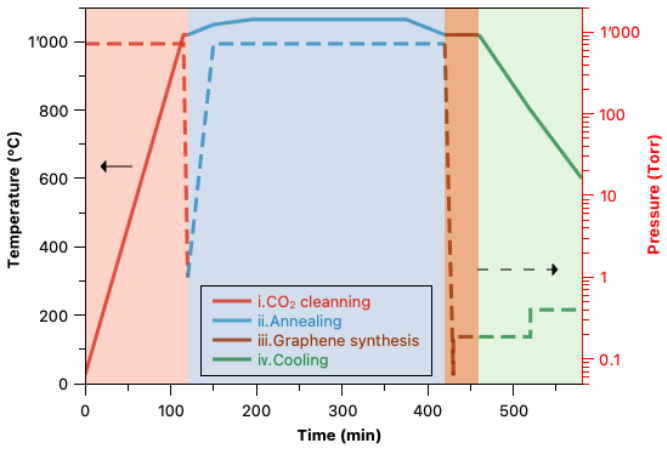

Figure 15. Large-scale CVD protocol for graphene synthesis.

3.3 Pore opening in graphene by ozone treatment

The oxidation of graphene was systematically optimized based on an improved fundamental understanding of graphene oxidation in O_3, based on recent studies from our group.[17–19,25] The

experiment setup illustration of ozone oxidation is shown in Figure 16a, and the process of oxidation consists of four consecutive steps (Figure 16b):

1. Graphene is first cleaned in a reductive atmosphere at 600 ºC to remove the surface contamination on graphene as well as reduce any oxidation on the substrate (Cu).
2. Graphene is then exposed to ozone flow (1 bar, 8% in O_2) after cooling the sample to the oxidation temperature (50-80 ºC). The sample is typically exposed for 1-6 h, during which the temperature is maintained or cooled to room temperature (see results sections). During this process, oxygen clusters form on the graphene lattice. There are a few parameters to tune to maximize the cluster density, including the ozone reaction temperature and time, and the gas velocity across the sample. It should be noted that ozone is generated by the ozone generator, which requires 30 min to reach a steady state. Therefore, ozone flow is initiated at least 30 minutes before ozone is injected into the reactor. During this time gap, the generated ozone is similarly purged into the evacuation system after being destroyed by an ozone destroyer.
3. The above step generates oxygen clusters on graphene, which are typically 2-3 nm in size. Pores are opened within these clusters by gasification of these clusters by heating to 150-200 ºC in an argon atmosphere.
4. Cu surface is usually oxidized and becomes rough during the oxidation step (Figure 16c, d). Our efforts to prepare membranes using as-oxidized graphene failed, likely because it is challenging to transfer graphene from a very rough oxidized Cu foil. To improve the membrane quality, the oxidized Cu surface is reduced. For this, the sample is reduced under H_2/Ar at 500-600 ºC.

The extent of oxidation on the graphene lattice can be characterized through gas permeation studies. The more the sample is oxidized, the higher the membrane permeance will be. But at the same time, there is also a trade-off between membrane permeance and selectivity. The loss of selectivity at higher pore density is because neighboring pores may coalesce to form larger pores that are not selective. The process is then optimized to obtain overall high performance.

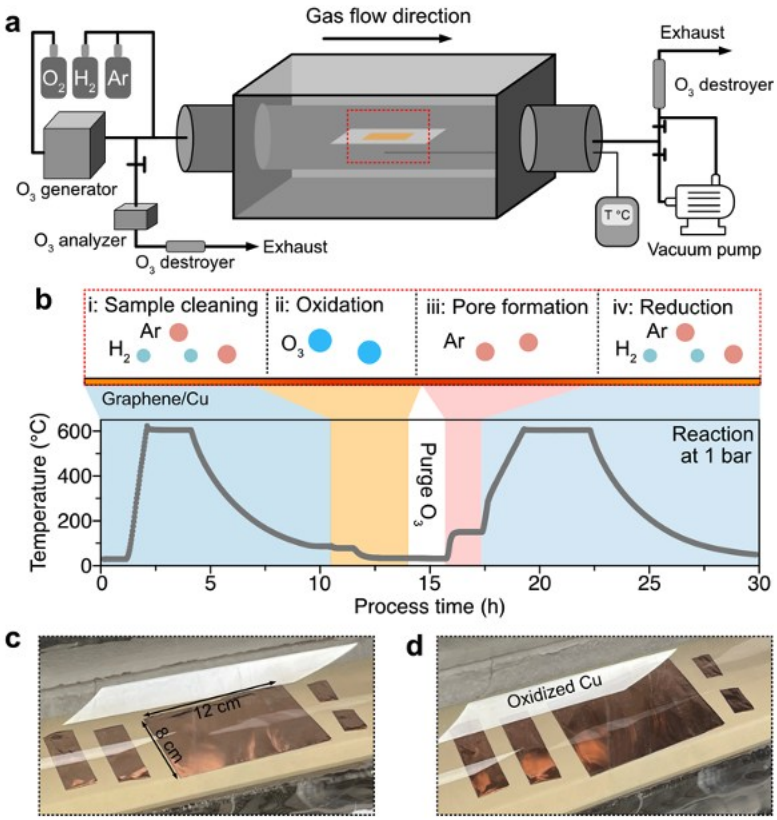

Figure 16. Scaled-up reactor for pore incorporation in graphene. (a). Schematic illustration of the ozone functionalization setup. (b). Oxidation schemes with corresponding temperature profiles used in the process. Photos of graphene resting on Cu before (c) and after oxidation (d) where color change of oxidized Cu can be visualized.

3.4 Membrane fabrication

The MRF approach has been reported to address the crack formation in graphene during its transfer. While centimeter-scale membranes have been reported, the success rate has been low due to stress generated in the film during wet-chemical etching of the film, where the film is floated. To address this issue, we developed a facile transfer strategy involving a novel membrane module architecture (Figure 17a, b). This involved coating an MRF (PTMSP or PDMS) on PG to a target thickness of approximately 1 µm (Figure 17c). The resulting Cu/PG/MRF was placed on a porous membrane support (PES), ~0.2 µm pores (Figure 17d), resting on a macroporous stainless steel (SS, Figure 17e) mesh. The step-by-step assembly of the module, with a stacking order of Cu/PG/MRF/PES/SS mesh, is illustrated in Figure 17f. The module was sealed by two rubber gaskets (Figure 17b) and was compressed by two cover plates (Figure 17f, panels i and ii).

The stacking order, Cu/PG/MRF/PES/SS mesh, exposes Cu foil on one side of the module, allowing one to etch and remove Cu directly from the assembled module. This effectively eliminated the need to float graphene. After sealing the module, the exposed Cu was placed in contact with a cell hosting a Cu etchant (1 M $FeCl_3$, Figure 17f, panel iii). During etching, PG reinforced by MRF was secured in the module.

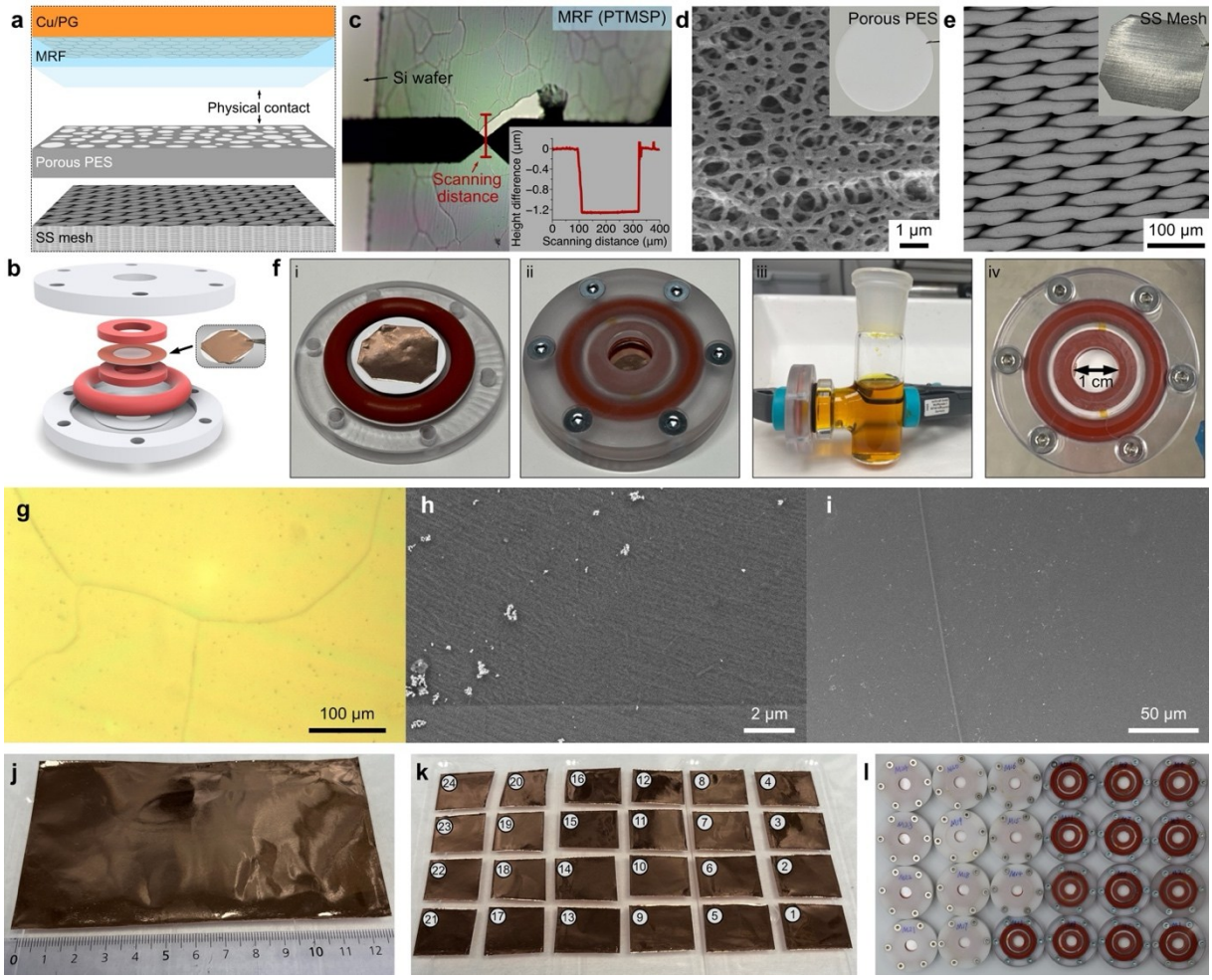

Figure 17. Crack-free direct transfer of graphene inside the membrane module. Schematic illustration of graphene transfer strategy (a), and the architecture of the membrane module (b). (c). Optical microscope image of the MRF transferred on a Si/SiO_2 wafer. The inset shows the film thickness characterization. SEM images of commercial PES support (d) and SS mesh (e). The insets are pictures of the two supports. (f). Pictures of stacked membrane assembly hosting Cu/PG/MRF/PES/SS mesh (panels i and ii), etching setup for Cu (panel iii), and as-prepared graphene membrane module after etching Cu foil (panel iv). Optical (g), and SEM (h, i) images of graphene surface after removal of Cu. A ~8 × 12 cm^2 graphene coupon (j) is cut into 24, 2 × 2 cm^2 small coupons (k). (i). All 24 coupons in panel (j) lead to successful 1-cm-scale membranes. Half of the membrane modules were assembled with transparent cover plates to reveal the sealing.

Optical microscope (Figure 17g) and SEM images (Figure 17h, i) of the graphene surface after Cu removal reveal no visible cracks. The white particles observed in Figure 17h are residues from the etching of Cu foil. The reproducibility of this transfer strategy was assessed by cutting a ~8 × 12 cm^2 graphene coupon (Figure 17j) into 24 2 × 2 cm^2 coupons (Figure 17k) and fabricating membranes from each (Figure 17l).

The simple design of this module enabled upscaling the membrane element. However, the circular disk design of the module limits the ability to achieve the practical cross-flow configuration. Therefore, larger decimeter-scale cross-flow modules were designed by including cross-flow permeation channels (Figure 18). The membrane stacking order and Cu etching strategy were identical (Figure 18a). The module consisted of a symmetrical body frame and two identical cover plates, each accommodating two 5-cm^2 membrane elements, thereby increasing packing density. A cross-flow channel was created by cutting slits along the sides of the module (Figure 18b). Cu foil in the assembled module could be removed by

flowing the etchant through the cross-flow slits (Figure 18c). This exposed the graphene and created a feed channel for gas-permeation experiments. The cover plate on both sides had a central opening serving as a permeate window. This module could be further scaled into a larger one capable of hosting two 5 × 10 cm^2 membrane elements (Figure 18d).

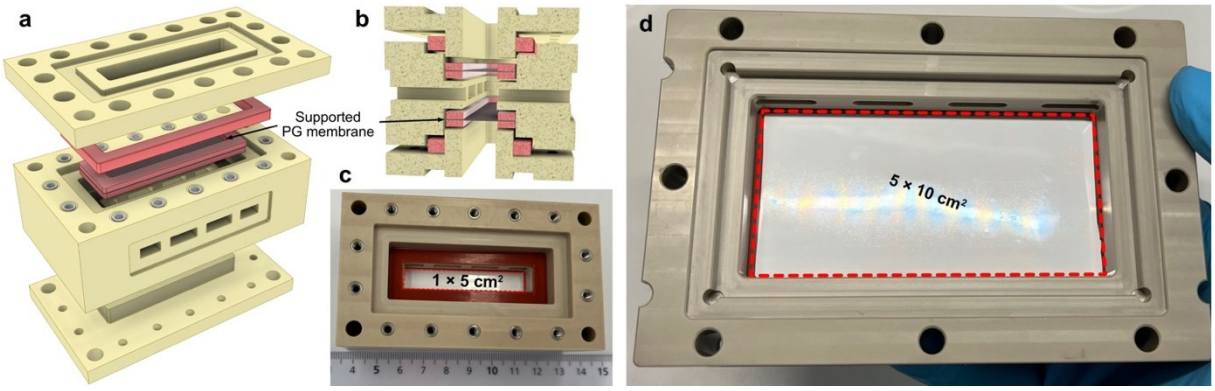

Figure 18. Graphene membranes prepared in large-area cross-flow modules. Three-dimensional model of the upgraded membrane module architecture (a), and the corresponding cross-section view showing the cross-flow slits (b). Photos of successfully prepared 1 × 5 cm^2 (c) and 5 × 10 cm^2 graphene membranes (d).

For multicomponent gas separation, the current membrane module suffers from concentration polarization, mainly due to the large feed channel gap. One major consequence is that the separation efficiency of more permeable gas, CO_2, will be compromised, especially at lower feed compositions. To solve this, the membrane module was further optimized with a reduced feed channel gap of 200 µm (Figure 19).

Figure 19. 3D design of the optimized membrane module with negligible concentration polarization effect.

3.5 Permeation test

The robustness of the graphene membrane is validated by permeation measurements using a constant-volume variable-pressure setup (Figure 12a). Very briefly, the membrane is exposed to the feed gas (single component). Permeate collects in a fixed volume, leading to an increase in permeate pressure. This is then used to calculate the membrane permeance as a function of feed gas type and membrane temperature. To evaluate the mixture gas, the permeate gas is sent to a gas chromatograph for gas composition analysis.

3.6 Membrane process validation

The membrane performance under realistic conditions is validated on a home-made two-stage membrane separation unit. The process flow diagram and the photo of the setup are shown in Figure 13 and Figure 14. The simulated flue gas can be supplied either from a gas tank containing a gas mixture or by mixing pure gases to the target composition. Water vapor can be introduced by passing the feed gas through a bubbler. In the two-stage membrane separation process, we can continuously evaluate membrane performance (recovery and purity) through online monitoring and control.

4 Activities and results

4.1 Summary of activities

The activities detailed in this report cover the full aspects of graphene membrane production, from synthesis and pore optimization to a functional two-stage membrane process demonstration. To ensure high-quality graphene while using low-cost copper foil, we developed an acid pretreatment that yields a smooth, contamination-free substrate surface. Utilizing a custom-built, large-scale CVD reactor designed to minimize impurities, we successfully synthesized high-quality single-layer graphene. To bridge the gap to scalability, we engineered a transfer technique that achieves a near 100% success rate for 1 cm^2 membranes, which we then scaled to 50 cm^2 modules designed to mitigate concentration polarization. Our ozone-based pore-formation process was also optimized across multiple experimental setups to ensure reproducibility and scalability. Finally, we modeled and validated a two-stage membrane separation process, testing it under simulated flue gas conditions over a long time period. This rigorous testing has provided a deep understanding of critical operational parameters and confirmed the long-term stability of our membranes in realistic testing conditions.

4.2 Preparation of low-cost Cu foil

Our proof-of-principle results on high-performance graphene membranes were obtained on expensive Cu foil with a cost of over 8000 CHF/m^2. To decrease this cost, we chose low-cost Cu foil alternatives (Table 2).

Table 2. Comparison of the Cu substrate used in this work and the market.

Supplier	Catalog No.	Purity	Thickness (μm)	Price (USD/m^2)*	Demonstration of high-quality graphene	Demonstration of gas-sieving graphene membranes
Nilaco	CU-113221	99.99+%	25	16735	Yes	No
	CU-113263	99.9%	50	35	Yes	No
Strem	STR93-2994	99.9%	50	9100	Yes	Yes
Sigma-Aldrich	349208	99.98%	25	2473	Yes	No
Goodfellow	1000070388	99.9%	50	1598	Yes	No
Alfa Aesar	13380.cv	99.9%	127	740	Yes	Yes
	46986.RH	99.8%	25	214	Yes	Yes
Basic Copper	cu-3mil-6in-4ft cu-3mil-bulk-roll	99.9%	76	156 39	Yes	No
Roth	8540.2	99.9%	100	100	Yes	Yes, this work
MTI KJ group	BCCF-25u-B	99.8%	25	29	Yes	No
Kunshan Luzhifa Electronic Technology Co., Ltd.		99.97%	50	10	Yes	No
Alibaba	C1100	99.9%	100	10	Yes	Yes, this work

*Note: the price is based on those available in the year 2024.

A 100 μm-thick Cu foil from Carl Roth®, at a cost (laboratory price) of 87 CHF/m^2, was chosen because it aligns with the cost projection in the technoeconomic analysis. We note that the cost at scale can be significantly lower. The cost of the Cu foil could be further reduced to 10 USD/m^2 (see Table 2), where high-quality graphene could also be synthesized from cheap Cu foil sourced from Alibaba. The Cu foil is processed to reduce surface roughness and contamination by a simple acid treatment described in section 3.2 (Figure 20).

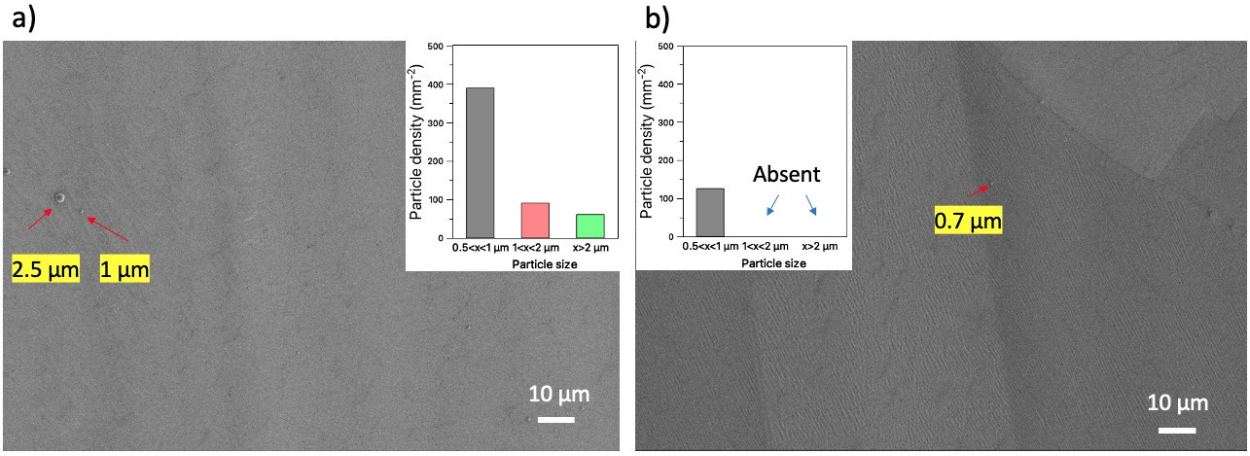

Figure 20. SEM image of graphene surface synthesized on (a) as-received Cu and (b) treated Cu. The inset is the contamination particle density after graphene synthesis.

4.3 High-quality, large area graphene synthesis:

Using the above-mentioned CVD synthesis method, large-area graphene coupons (11 x 26 cm) were successfully synthesized (Figure 21). The high quality of graphene is confirmed by Raman spectroscopy. The Raman spectrum reveals a negligible defect peak (*D* peak), while a map of peak intensity ratio (I_D/I_G) shows that the quality of graphene is uniform (Figure 22). Figure 23 shows that the graphene has similar quality throughout the entire reactor.

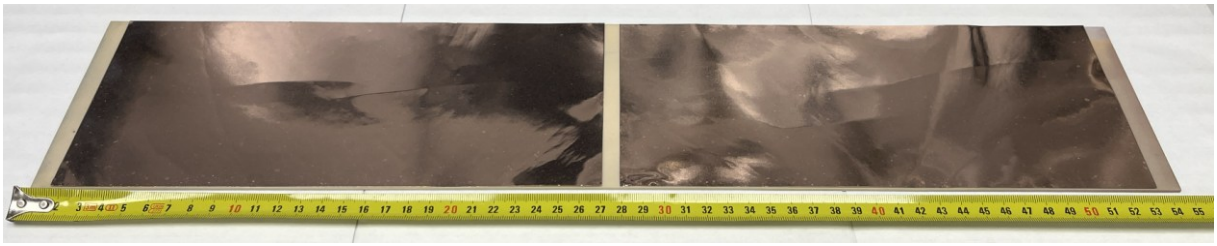

Figure 21. Large coupons of graphene synthesized in the large-scale CVD furnace.

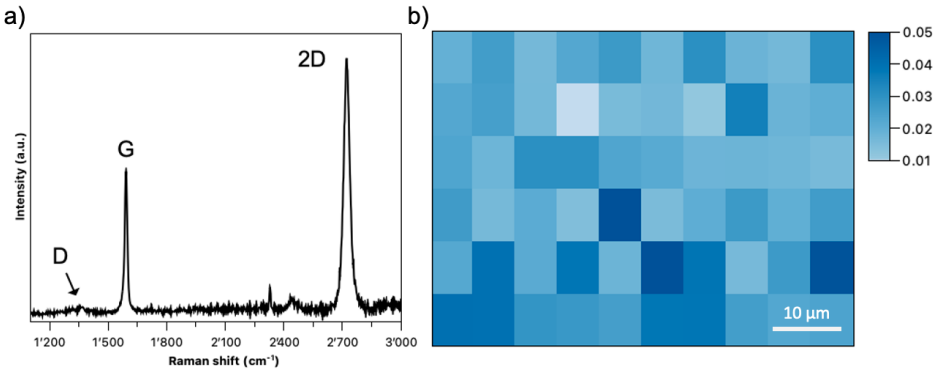

Figure 22. (a) Raman spectrum of SLG, and (b) the color map of I_D/I_G ratio on a 60 x 40 µm^2 area.

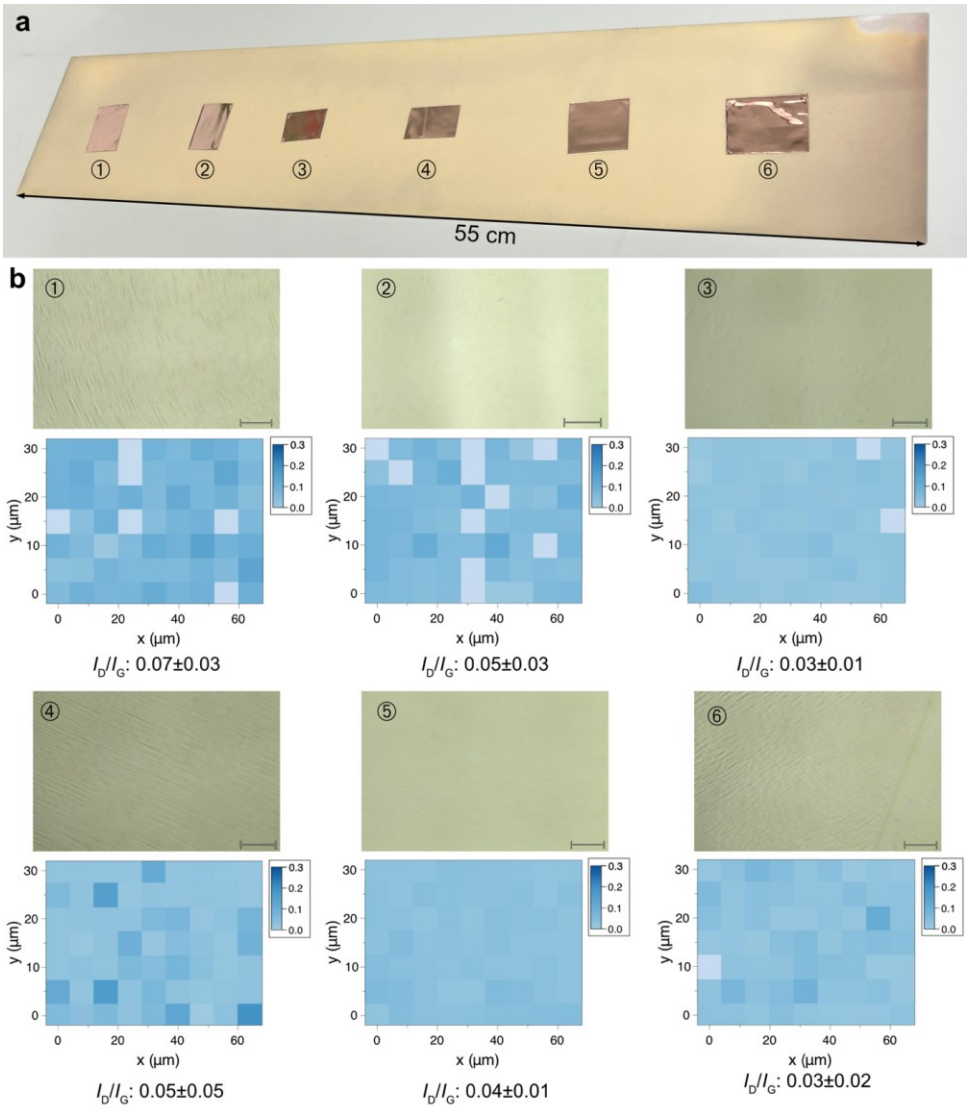

Figure 23. (a) Photo of six graphene coupons grown at different positions on the 55 cm-long sample plate. (b) Optical microscope image (top) and the Raman mapping of D and G peak intensity ratio (bottom) of the graphene sample located at the positions 1, 2, 3, 4, 5, and 6, respectively. The scale bar is 10 μm.

4.4 Uniform oxidation of large-area graphene

Our research systematically explores the parameters of graphene pore formation to ensure high performance during scale-up. We have identified that flow uniformity, temperature consistency, gas velocity, and the dimensions of the reaction zone are the critical factors controlling both membrane porosity and gas permeance (measured in GPUs). Through the iterative development of multiple reactor designs, testing various tube diameters and heating sources, we have determined that a large-diameter furnace provides the optimal environment for uniform, scalable oxidation. This setup allows the treatment of large graphene coupons (27 cm x 12 cm) with a success rate approaching 100% under the given process conditions. Current optimization efforts focus on maximizing ozone reactivity through optimal O_3 flow control and transitioning the reaction to room temperature. This shift away from the

current 80 ℃ setpoint aims to prevent the oxidation of the underlying copper foil, as surface roughness from oxidized copper can compromise the integrity of the atom-thick graphene film.

Another interesting learning was the management of ozone. At the start of the project, we stored ozone in a 250 L reservoir tank (Figure 24) to allow direct injection into the CVD reactor after graphene synthesis. This allowed the reaction to continue for a certain time with a continuous ozone flow in a large-volume CVD reactor (60 liters), which was otherwise not possible. We have now moved to a smaller reactor volume (thanks to our discovery that a smaller volume with higher ozone velocity is a critical parameter for porosity incorporation), where we find that a 2 L/min flow of ozone directly from the ozone generator is sufficient to induce reaction for porosity incorporation. In this view, we have stopped storing ozone in the tank. This also helps us manage safety in the lab (in case of an ozone leak from the tank). We also realized that the concentration of stored ozone in the tank is lower (~4-5%) compared to that generated by the generator (~8%). This could be due to ozone degradation in the storage tank. By avoiding ozone storage, we ensured a continuous 8% ozone supply to the reactor.

Figure 24. Ozone reservoir for rapid injection into the CVD furnace.

Below are the details of our optimization.

Optimization of pore formation in the 5-cm-diameter chamber

As shown in Figure 25, we built a 5 cm-diameter reaction chamber for ozone optimization to obtain preliminary data. The sample was first cleaned externally in a tube furnace and then immediately transferred into the reaction chamber. A thermocouple is placed near the sample position to monitor the reaction temperature. Figure 26 shows the color change of the sample during the process. After ozone treatment, the oxidation of the substrate is reflected in a darker color change, and it returns to its original color after reduction. The aspect of color is important and helpful because the oxidized Cu is quite rough. Our attempts to make membranes by skipping the reduction step failed, underlying the importance and need of making the Cu surface smooth by reduction.

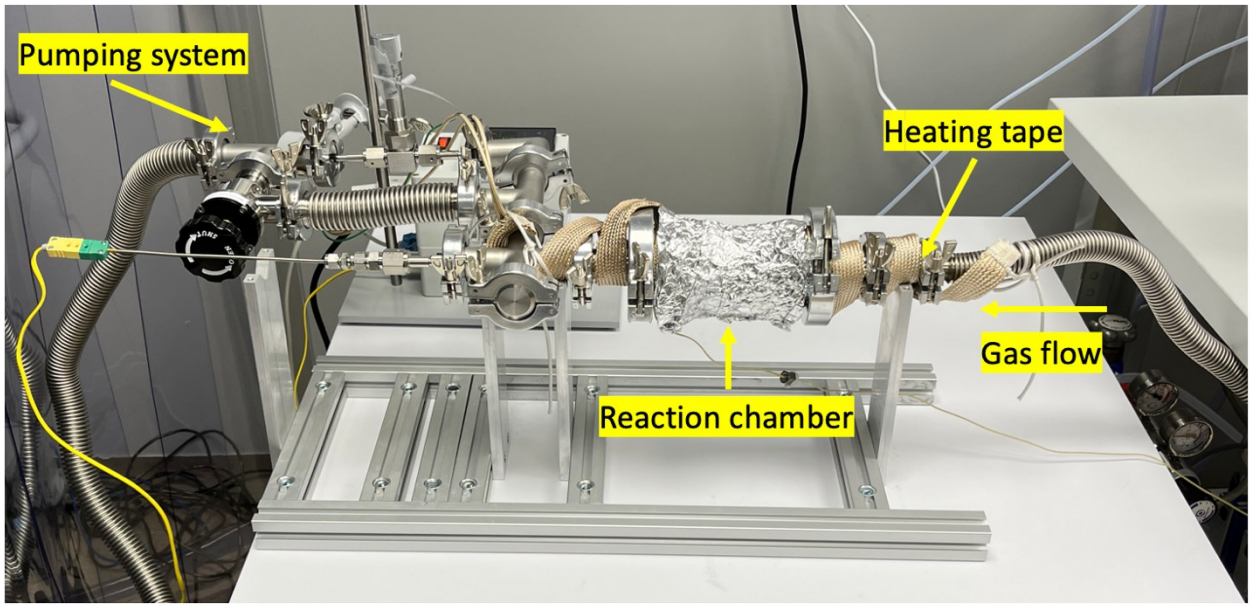

Figure 25. The 5-cm-diameter reaction chamber for ozone-based pore formation in graphene. The sample is placed inside the reaction chamber.

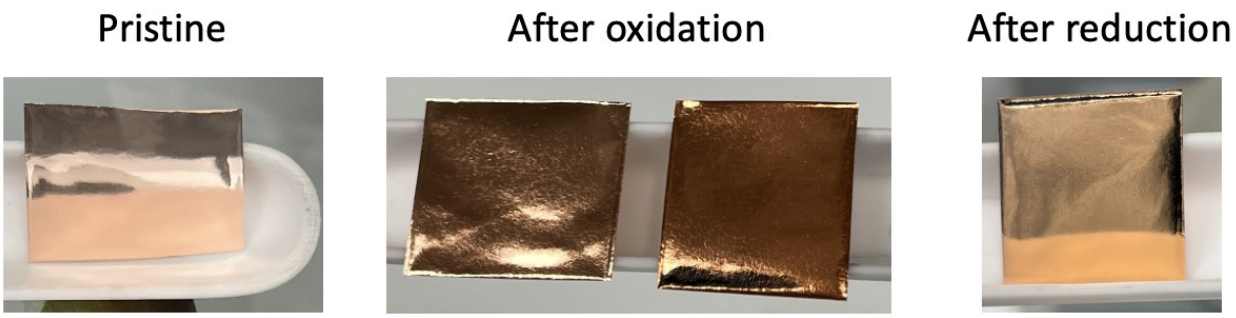

Figure 26. The color change of the sample at different steps of the reaction.

The ozone oxidation was initially conducted at 80 ºC for 1 h with an ozone flow rate of 500 ml/min. Since the reaction temperature is relatively high, we also applied a stabilization step, which cools the sample with the same ozone flow to room temperature. After oxidation, we transferred and assembled the graphene in our 1-cm membrane module. The extent of ozone oxidation was characterized by the gas permeation study. Figure 27 shows the CO_2 gas permeance and CO_2/N_2 gas pair ideal selectivity of pristine graphene and the graphene oxidized under different conditions. All membranes show a higher gas selectivity than the supporting layer, reflecting a highly reproducible membrane fabrication strategy we developed in the past years. We observe a noticeable improvement in CO_2 permeance for oxidized graphene, indicating a successful pore formation by ozone reaction. However, the gas selectivity is only marginally improved, and there is a big variation in gas permeance. This shows that the pore etching is not uniform, and the size distribution is broad.

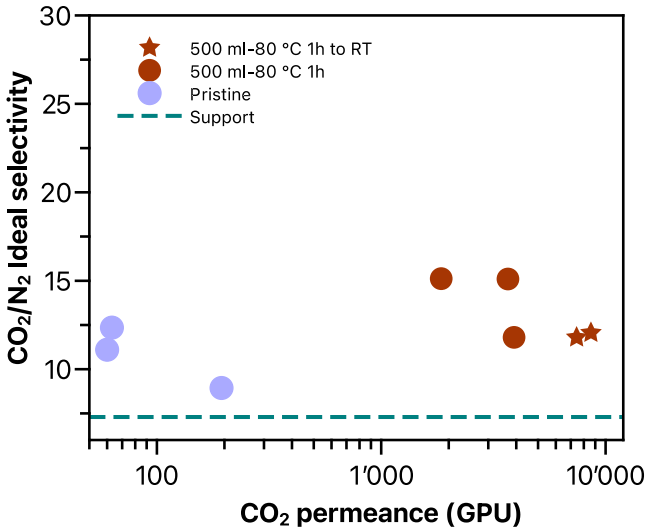

Figure 27. Gas permeation results of the ozone-oxidized graphene from 5-cm-diameter chamber.

Optimization of pore formation in the 16-cm-diameter chamber

We upgraded the reaction chamber to a 16-cm-diameter tube to improve uniformity and scalability simultaneously (Figure 28), while the experimental procedure remained the same.

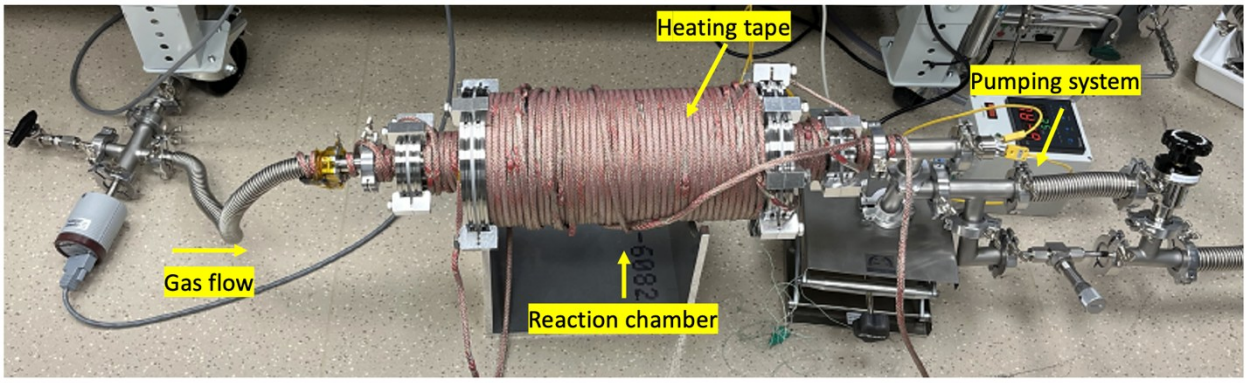

Figure 28. ⌀16 cm chamber for ozone functionalization.

Before optimization, we initially conducted CFD simulations using basic fluid modeling software (Autodesk CFD) to understand the gas flow profile within the reaction chamber, which had never been done during our previous optimization processes. These early simulations revealed that our initial chamber was too small to facilitate a uniform gas flow across large samples. Based on the CFD result, we further developed a larger reactor where the gas flow profile is much more uniform.

Figure 29 shows the gas velocity comparison between ⌀5 cm and ⌀16 cm chambers at the same flow rate.

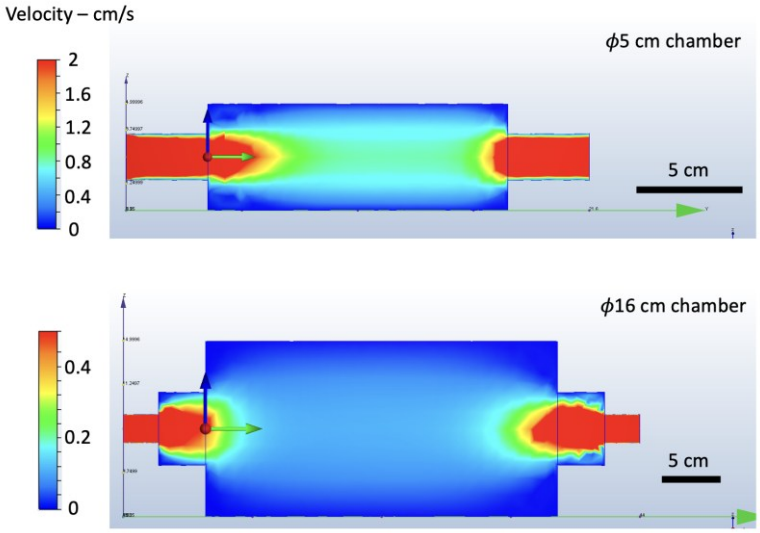

Figure 29. Computational fluid dynamics (CFD) simulation of the gas velocity in different reaction chambers. The simulation was performed on a basic fluid modeling setup using Autodesk CFD.

It is clear that the gas velocity across the sample is dependent on the geometry of the reaction chamber. Under the same gas inlet flow rate, the 16-cm-diameter chamber gives a slow but uniform gas velocity (average gas velocity from the entire reaction chamber: ~0.12 cm/s), while that in the 5-cm-diameter chamber is fast but not uniform (average ~1.2 cm/s).

As with the 5-cm-diameter chamber, we examined the gas permeance of the membrane prepared under the same conditions. We observe that the increase in CO_2 permeance becomes less as the reaction chamber diameter increases. Given that the gas velocity in the 16-cm-diameter chamber is about 10 times slower than in the 5-cm-diameter chamber, the gas velocity could play an important role in increasing the pore density of the oxidized graphene. We also used a higher gas inlet flow rate for the ozone reaction. The result (Figure 30) shows that the membrane gas permeance varied widely from 5000 GPU to 10000 GPU, close to the permeance of the polymer support (10000 GPU), at the expense of gas selectivity. The CFD simulation (Figure 31) indicates that as the gas inlet flow rate in the 16-cm-diameter chamber increases, the uniformity of the gas velocity decreases drastically, which makes ozone oxidation difficult to control. We note that the region of interest for the analysis of gas velocity and uniformity is at the center of the reactor, which is where the sample is placed. These simulation results provided us, for the first time, with a clear insight into the gas flow profile, transforming our approach from empirical testing to a systematic optimization of reactor geometry.

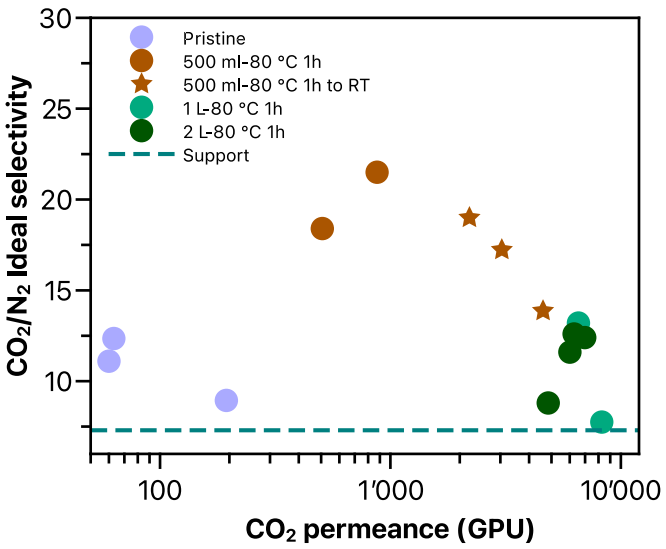

Figure 30. Gas permeation results of the ozone-oxidized graphene from the 16-cm-diameter chamber.

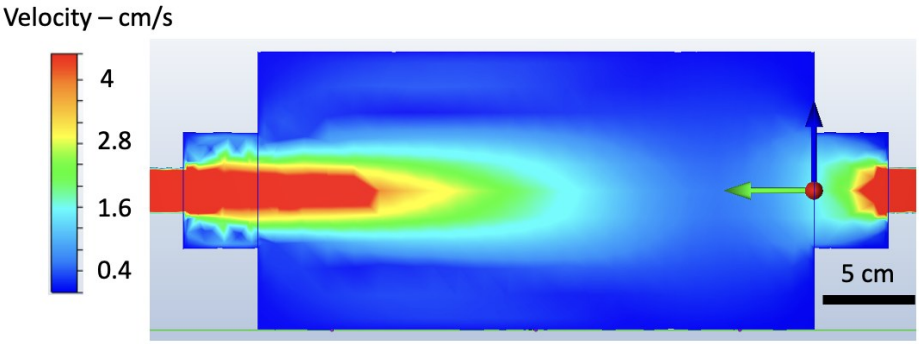

Figure 31. CFD simulation of the gas velocity in the 16-cm-diameter chamber with a flow rate of 2 l/min.

Optimization of pore formation in the 2.5-cm-diameter quartz reactor

From a fluid dynamics perspective, the uniformity of gas velocity is inherently linked to the length and aspect ratio of the reaction chamber. Figure 32 shows the CFD simulation of the gas velocity in a 2.5-cm-diameter quartz tube under 0.5 and 2 l/min. A smaller tube diameter naturally results in a much faster gas velocity. At the same time, uniformity is improved due to the developed flow profile, as indicated by a thin, slow boundary layer near the tube wall and a consistent gas velocity in the middle of the tube. The modified setup is shown in Figure 33, and the gas permeance of the membrane oxidized in this setup under the same conditions is shown in Figure 34.

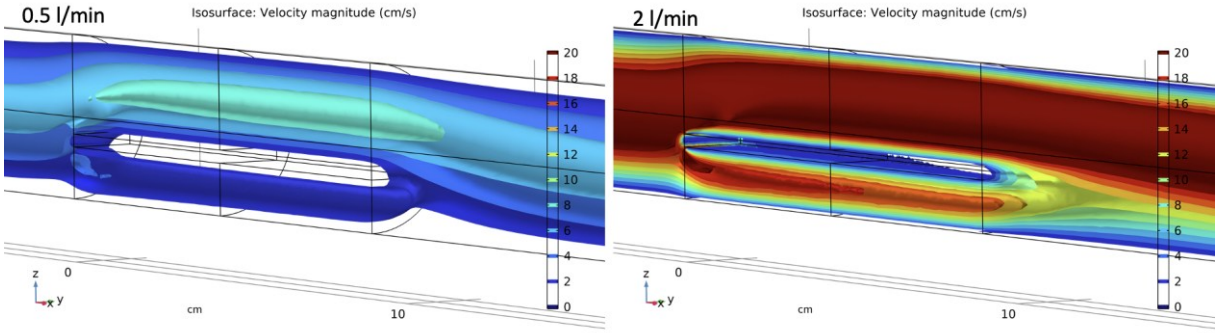

Figure 32. CFD simulation of the gas velocity in the 2.5-cm-diameter tube with a flow rate of 500 ml/min and 2 l/min. A sample plate was placed in the reaction chamber.

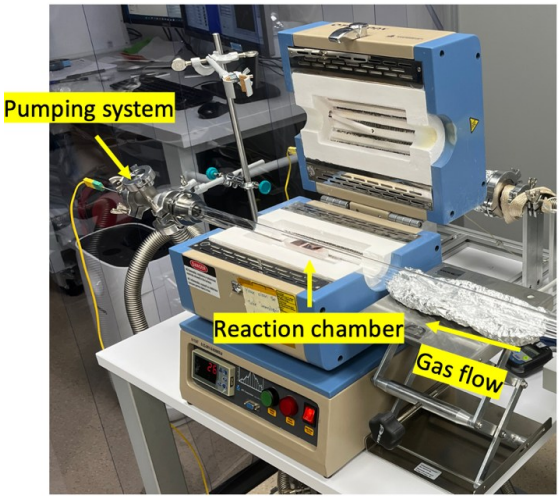

Figure 33. The 2.5-cm-diameter quartz tube furnace for ozone functionalization.

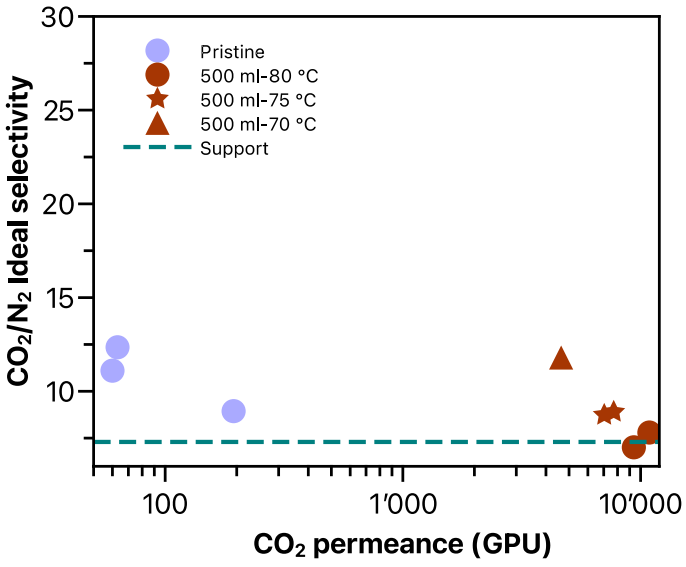

Figure 34. Gas permeation results of the ozone-oxidized graphene from the 2.5-cm-diameter quartz tube furnace.

The graphene treated under the same conditions (flow rate: 500 ml/min, temperature: 80 ℃) was highly defective, with both the permeance and the gas selectivity close to the support. The increased oxidation extent on the graphene lattice is attributed to the high gas velocity in the 2.5-cm-diameter tube. As we decrease the oxidation temperature, the gas permeance of the membrane goes down, while the selectivity doesn't obviously improve.

The contrast in experimental results between the small chamber and the tube furnace strongly suggests that a tubular geometry is significantly more advantageous for achieving a well-developed and stable gas flow profile. While this conclusion is a fundamental principle of fluid dynamics, the CFD simulation results were instrumental in providing the empirical insight needed to apply this knowledge to our specific system. By visualizing the flow behavior, we were able to confirm that the tubular design naturally facilitates the transition to a more predictable and uniform environment, which is essential for consistent large-scale graphene oxidation.

Optimization of pore formation in the 12-cm-diameter quartz tube furnace

Based on these iterations, we finally upgraded the oxidation setup in a 12-cm-diameter quartz tube furnace. Based on the CFD simulation (Figure 35), we believe the oxidation reaction in this tube furnace is moderate, uniform, and scalable. This is confirmed by the preliminary gas permeation results of the membrane prepared under a flow rate of 2 l/min at 85 ℃. As shown in Figure 36, the CO_2 permeance is averaged around 1000 GPU, and the CO_2/N_2 selectivity is about 20.

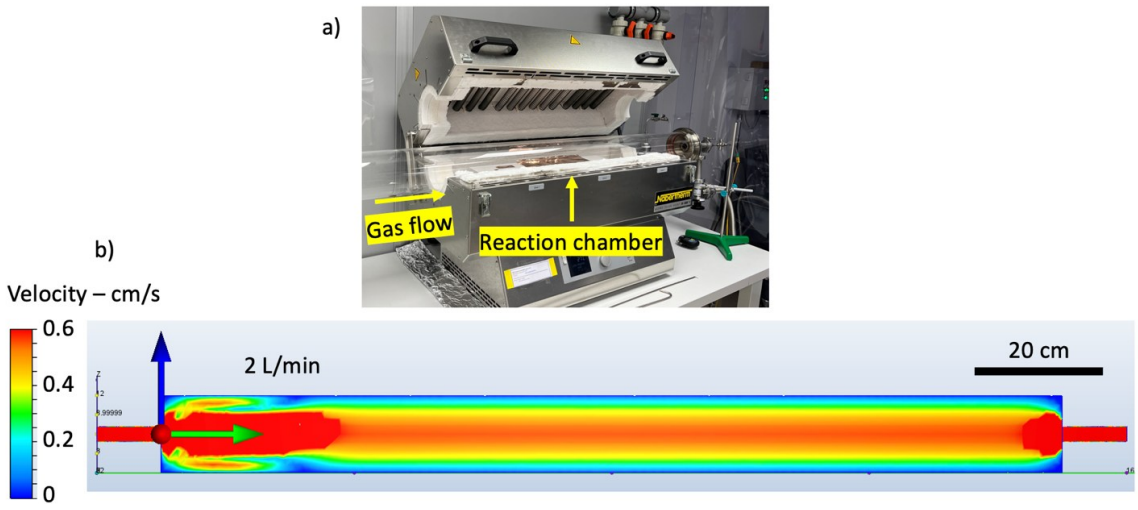

Figure 35. a) Picture of the 12-cm-diameter quartz tube furnace for ozone functionalization. b) CFD simulation of the gas velocity in the ⌀12 cm tube with a flow rate of 2 l/min. The gas velocity scale is exaggeratedly zoomed in to show that the gas flow becomes uniform after 30 cm from the inlet.

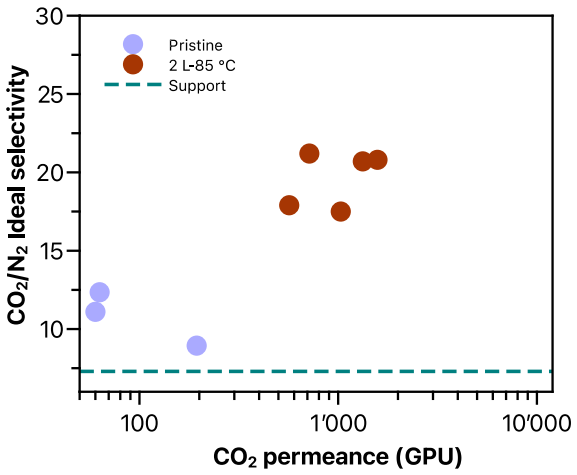

Figure 36. Gas permeation results of the ozone-oxidized graphene from the 12-cm-diameter quartz tube furnace.

To further refine this, we transitioned to more detailed Multiphysics simulations using COMSOL to specifically model mass transfer limitations. These models utilize a laminar flow regime, as the calculated Reynolds number (Re) remains well below the turbulent threshold (Re < 2000) for these flow rates and diameters. The simulations were validated by comparing the predicted CO_2 permeance trends with experimental data. Figure 37 shows the simulated iso-surface plot of the gas velocity within the above-mentioned 12-cm-diameter quartz reactor (with an inlet flow rate of 2 l/min in the tubular reactor where a substrate holding Cu/graphene was placed).

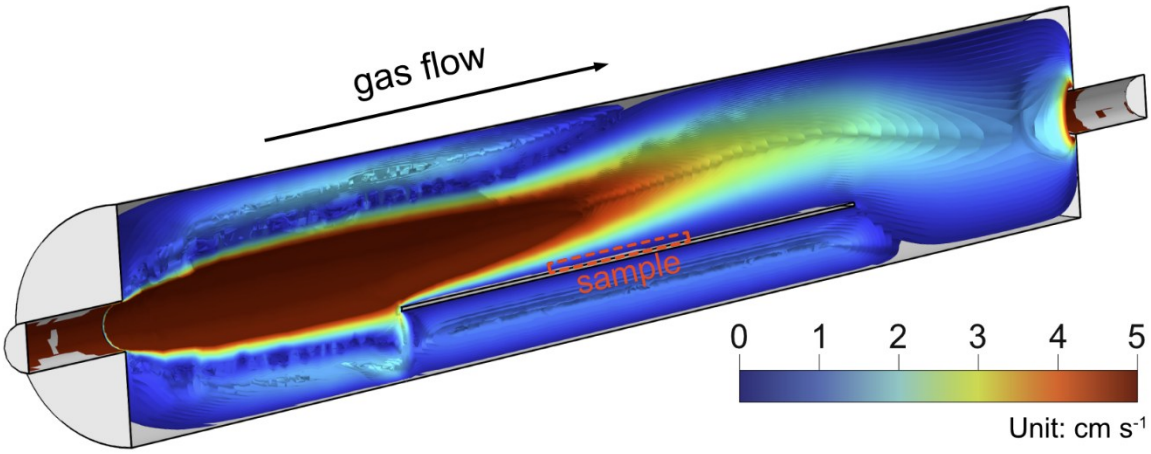

Figure 37. COMSOL simulated gas flow profile: iso-surface plot of gas flow velocity in the 12-cm-diameter quartz reactor with the sample substrate.

The highest velocity was near the center of the reactor. This is because of the small cross-sectional area of the gas delivery system relative to the reactor. The former was essentially a tube with an inner diameter of 2.2 cm. A boundary layer could be observed near the substrate where the gas velocity was significantly reduced. A 2D plot of the gas velocity, 1 mm above the substrate, on a 6 × 16 cm area at the center of the substrate is shown in Figure 38. The influence of the reactor geometry is apparent with varying gas velocity in different parts of the reactor. The gas flow was highest in the center and decreased at the edges of the reactor. While this is a standard phenomenon for pipe flow, its impact on

atomic-layer chemistry is significant. The average gas velocity near graphene was 0.06 ± 0.04 cm/s, indicating an uneven flow. To ensure the accuracy of these values, we utilized a “fine” mesh from COMSOL to avoid the influence of the mesh size. A mesh sensitivity analysis was not performed because the reactor geometry in the immediate vicinity of the sample position remained unchanged across our primary comparisons. Since all other boundary conditions and parameters were held consistent, our analysis focused exclusively on the macroscopic difference between distinct reactor geometries. By maintaining a stable mesh configuration in the region of interest, we ensured that the observed variations in the gas flow profile were a direct result of the geometric changes. Consequently, this high standard deviation in velocity is a direct reflection of significant velocity variations across the substrate. Such non-uniformity is undesirable for scaling up production, as a consistent flow profile is essential for achieving uniform pore incorporation across the entire graphene surface.

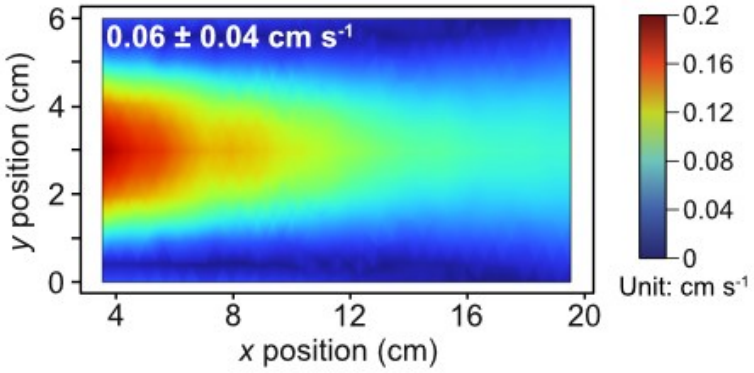

Figure 38. COMSOL CFD simulation results from the unmodified reactor: extracted gas velocity 1 mm above the substrate in the middle of the reactor (see Figure 37) with a sample size of 6 × 16 cm^2.

To address the issues of non-uniformity and high standard deviation, we developed a novel method that alleviated the mass transfer limitation in the O_3-led oxidation reaction. By placing a quartz semi-cylindrical block (12 cm in diameter) in the reactor, we effectively occupied the bottom half of the unnecessary space for the ozone reaction. Figure 39 shows the tubular reactor hosting the semi-cylindrical block and a 55 cm-long graphene substrate plate. Attributing to the reduction in the cross-sectional area of the flow by the block, the gas develops a laminar flow at a short distance after the inlet (Figure 40). A 2D plot of the gas velocity near graphene reveals a significantly uniform flow profile (Figure 41). The velocity increased threefold to 0.17 ± 0.02 cm/s, with the standard deviation dropping to a negligible level. This led to a significant improvement in the porosity of graphene, reflected by a drastically improved CO_2 permeance. After ozone oxidation, Raman spectroscopy is used to characterize graphene. An example in Figure 42a clearly shows that defects are introduced on the graphene lattice because the *D* peak is introduced. Figure 42b shows a uniform oxidation achieved by our approach.

An average CO_2 permeance from the 1-cm-scale membranes of 13105 GPU and CO_2/N_2 selectivity of 15.1 could be achieved. Furthermore, 50-cm^2-sized PG membranes in the 5 × 10 cm^2 cross-flow module yielded attractive separation performance with CO_2 permeance of up to 11799, and CO_2/N_2 selectivity of up to 17.6, respectively (Figure 43, Figure 44). This performance is highly competitive to those from the state-of-the-art and commercial membranes (Figure 45).

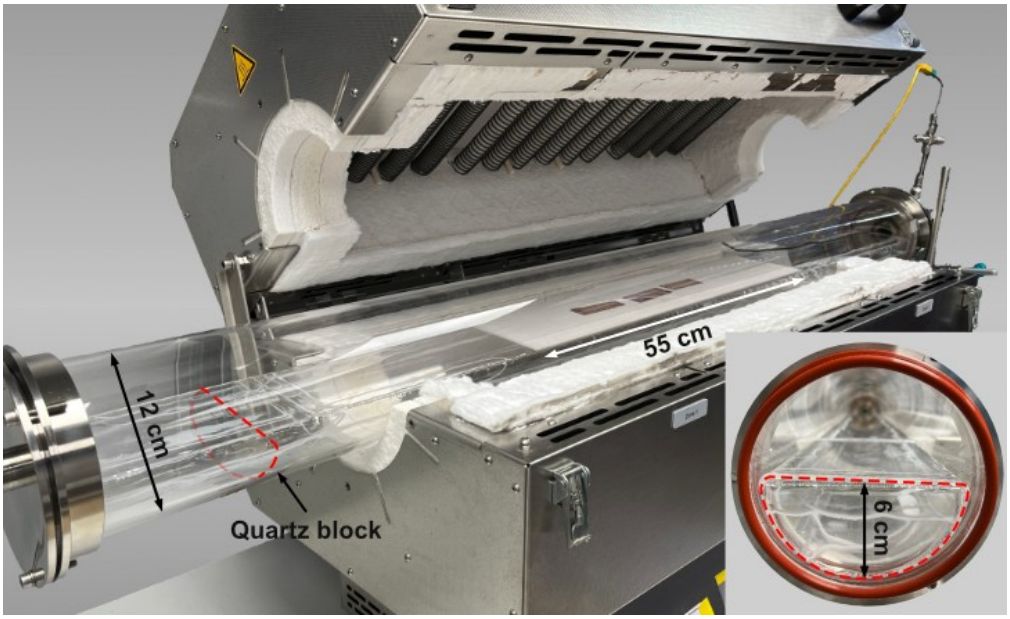

Figure 39. Picture of the modified ozone oxidation reactor hosting a quartz semi-cylindrical block (12 cm in diameter). The inset is the side view of the reactor with the quartz block

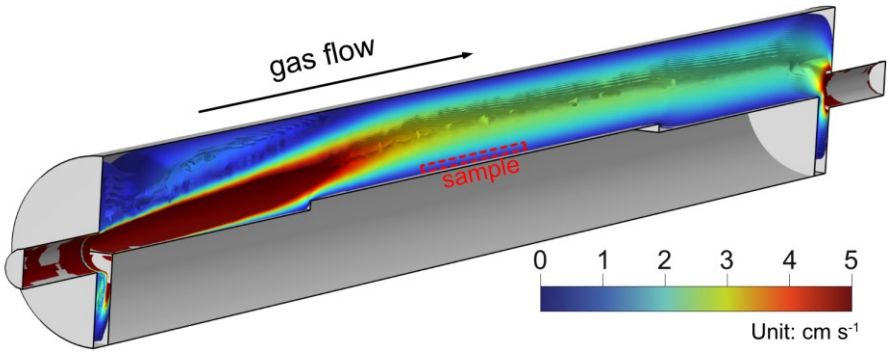

Figure 40. COMSOL simulated gas flow profile: iso-surface plot of gas flow velocity in the reactor with the sample substrate on the quartz block.

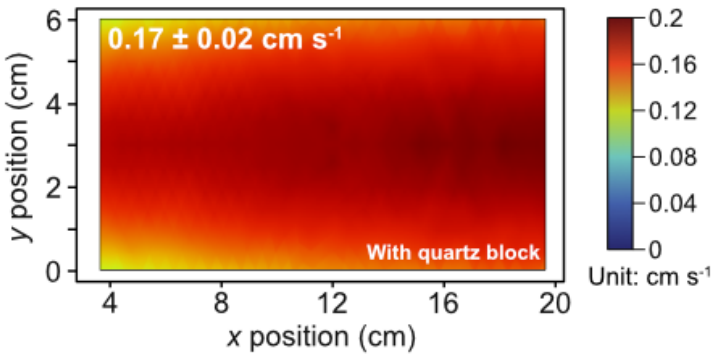

Figure 41. COMSOL CFD simulation results from the modified reactor: extracted gas velocity 1 mm above the substrate in the middle of the reactor (see Figure 40) with a sample size of 6 × 16 cm^2.

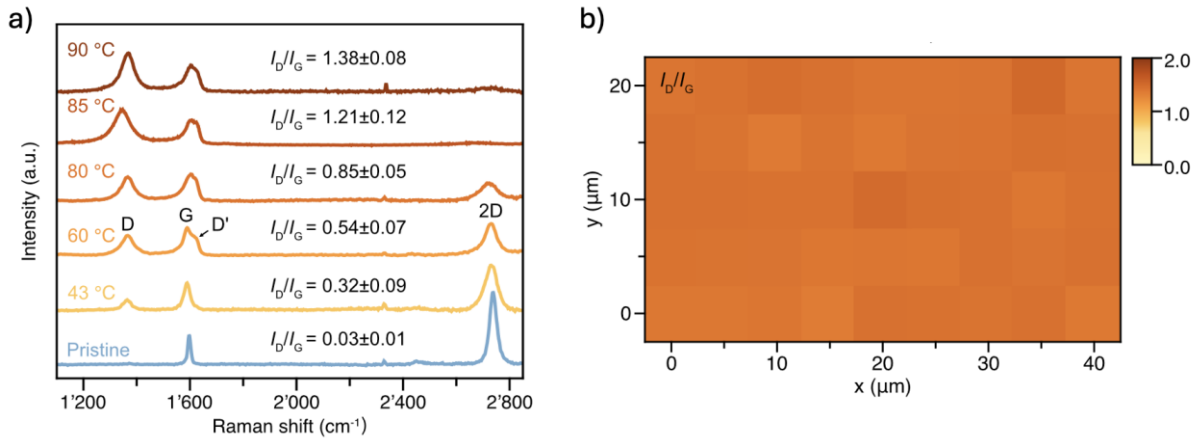

Figure 42. (a). Raman spectra of graphene under various temperatures for oxidation. The spectra have been normalized to the G band intensity. (b). Raman mapping of D/G peak intensity ratio of graphene oxidized at 90 °C across an area of 20 × 40 µm^2.

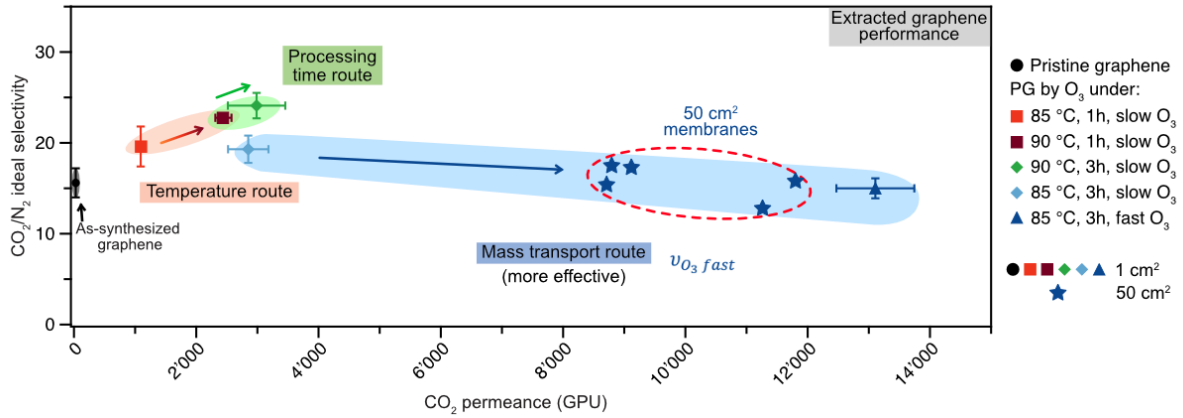

Figure 43. Gas permeation results of as-synthesized graphene (black) and PG (colored) membranes at 1 cm^2 and 50 cm^2-scale. The ozone oxidation was optimized by different reaction routes: temperature, processing time, and mass transport routes. The permeance of PG is extracted from the membrane using the resistance model.

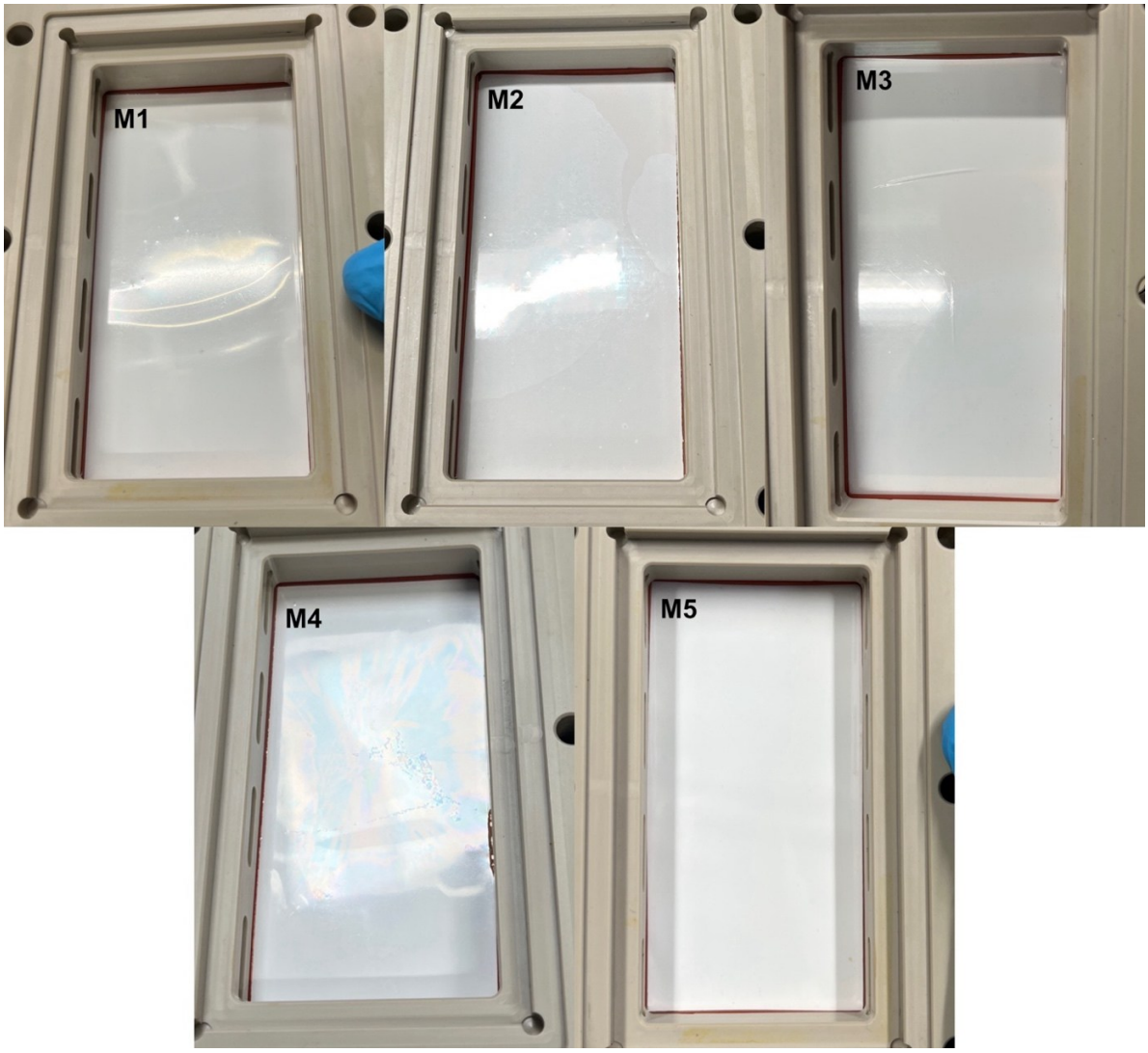

Figure 44. Pictures of five 50 cm^2 porous graphene membranes.

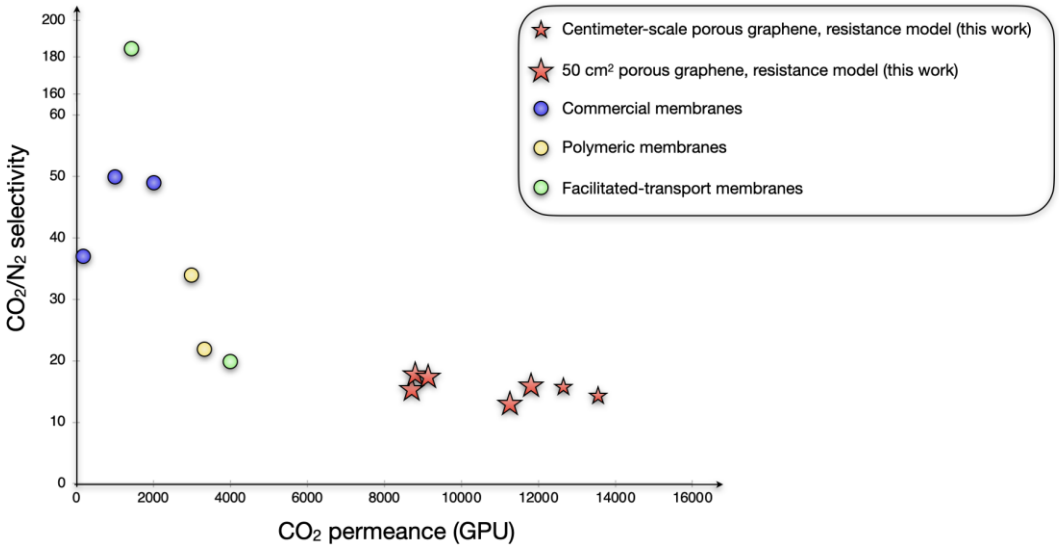

Figure 45. Comparison of carbon capture performance of porous graphene membrane.

AC-HRTEM images of graphene under an oxidation condition using fast and slow ozone gas velocity were collected. Several CO_2-selective pores were observed on porous graphene (Figure 46). Pores formed by missing N carbon atoms are denoted as pore-N, where N is an integer. Pores smaller than pore-10 are considered to be CO_2-impermeable. The density of CO_2-permeable pores under the fast ozone was two times higher than the slow ozone condition (Figure 47). The pore size distribution (Figure 48) shows that the fast ozone velocity is optimal. Above all, a carefully designed scaled-up reactor and transfer strategy allows one to achieve attractive performance from large-area graphene membranes.

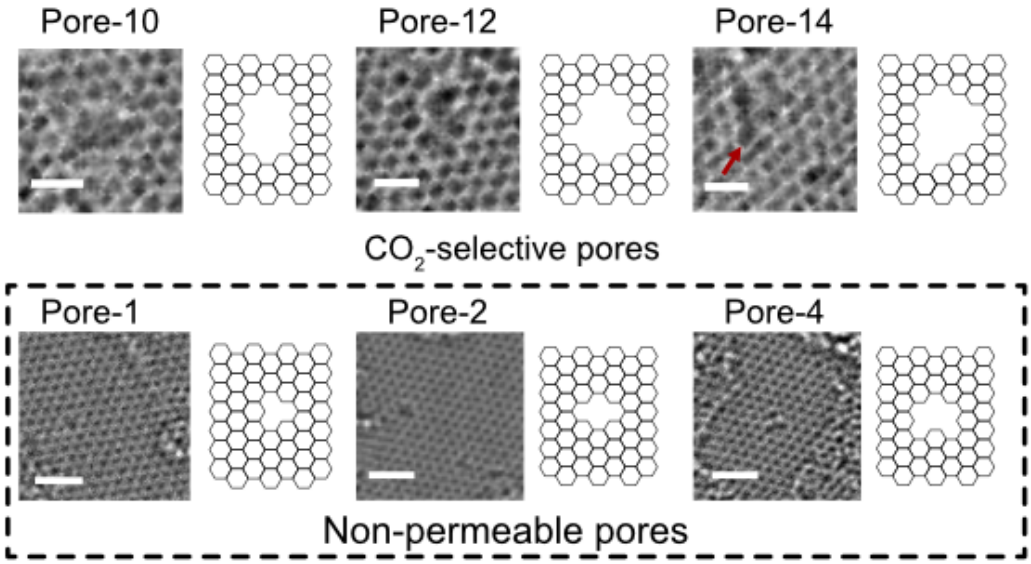

Figure 46. AC-HRTEM images of pores generated under an oxidation condition using fast ozone velocity. Scale bar: 0.5 nm for Pore-10, 12, and 14, 1 nm for Pore-1, 2, and 4.

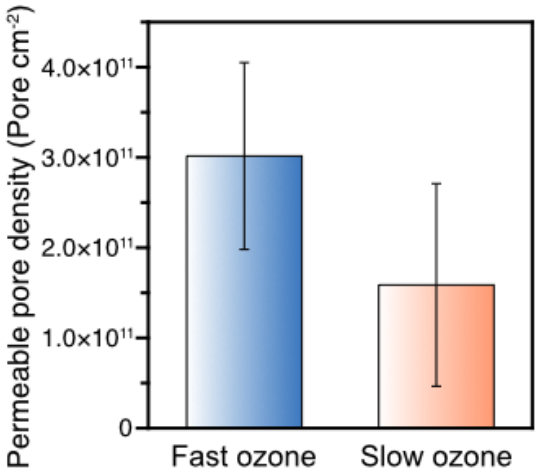

Figure 47. Density of CO_2-permeable pores as a function of the ozone velocity. The error bars represent the standard deviation from 5 AC-HRTEM images.

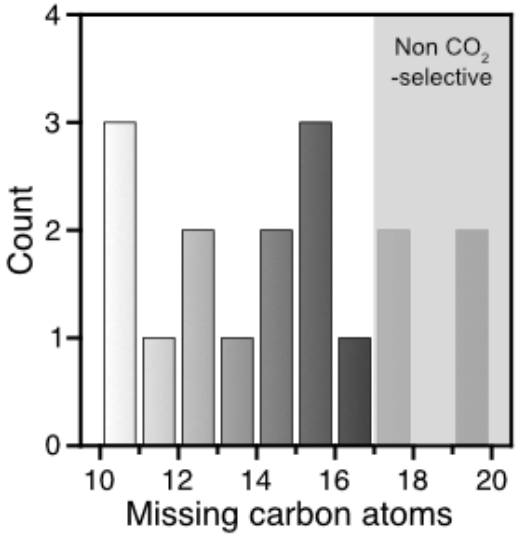

Figure 48. Size distribution of CO_2-permeable pores under fast ozone velocity obtained from the AC-HRTEM images.

4.5 Development of membrane modules

Module design – selection of channel thickness to reduce non-ideal effects

The practical module would not mimic the centimeter-scale module's design but rather the plate-and-frame module shown in Figure 18. It contains two membrane sheets that are separated by a small distance. The selection of the distance between the sheets within the module is important because this distance corresponds to the thickness of the feed channel and therefore affects the stream velocity. The channel thickness is designed to reduce two non-ideal effects of the membrane process related to velocity: concentration polarization and feed-side pressure drop.

With concentration polarization, the concentration of the permeable component at the membrane interface is lower than in the bulk, thereby reducing the driving force across the membrane. The

concentration profile along the thickness direction depends on the component's transport in the channel and through the membrane. To reduce concentration polarization, we would need a channel as thin as possible, since ideally the concentration profile in each section should be flat to maximize the driving force. On the other hand, a thinner channel results in higher velocity and higher pressure drop.

When the transport coefficient through the membrane (permeance) is higher, the concentration at the membrane interface is depleted, leading to stronger concentration polarization. Therefore, with high permeance, we need to use thinner channels to reduce concentration polarization, whereas with lower permeance, larger channels can be used.

From a practical point of view, a larger channel thickness is easier to achieve, which reduces the pressure drop. Thus, the selected channel thickness is the largest thickness at which concentration polarization remains limited. We investigated a range of thicknesses from 200 to 1500 µm for global CO_2 recovery between 50 and 90% (fixed purity of 98%). The process comprises two membrane stages: the second is fed by the permeate from the first, and the retentate from the second is recycled and mixed with the feed to the first.

We evaluated the impact of channel thickness on the membrane area of the first stage, since it typically accounts for most of the total membrane area (Figure 49). The membrane area increases significantly with increasing channel thickness, particularly at large recovery values. However, the impact of channel thickness is almost negligible at the lowest investigated recovery (50%).

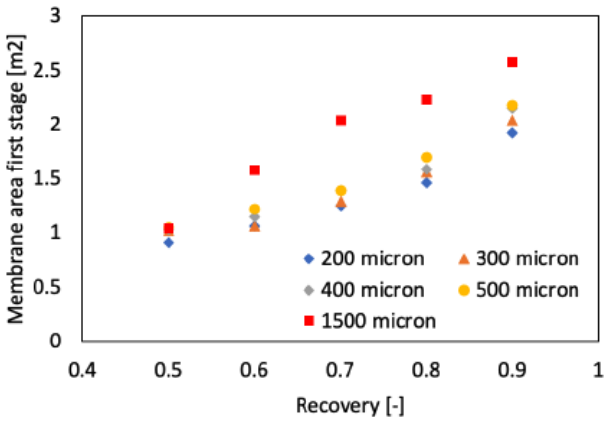

Figure 49. Membrane area in the first stage at variable global recovery and variable channel thickness. Final CO_2 purity target of 98%. Feed pressure in the first stage equal to 3 bar and permeate pressure equal to 0.01 bar. The membranes used for this plot have CO_2 permeance of 1000 GPU and CO_2/N_2 selectivity of 15.

Module design – initial experimental validation with prototype

We applied the same membrane reinforcement strategy and designed a new membrane module to increase the actual membrane area from ~ 1 cm^2 to 10 cm^2, and to 50 cm^2. Figure 50 shows the 3D model of the membrane module, and Figure 51 and Figure 52 show the step-by-step assembly of the 10 cm^2 and 50 cm^2 membranes, respectively.

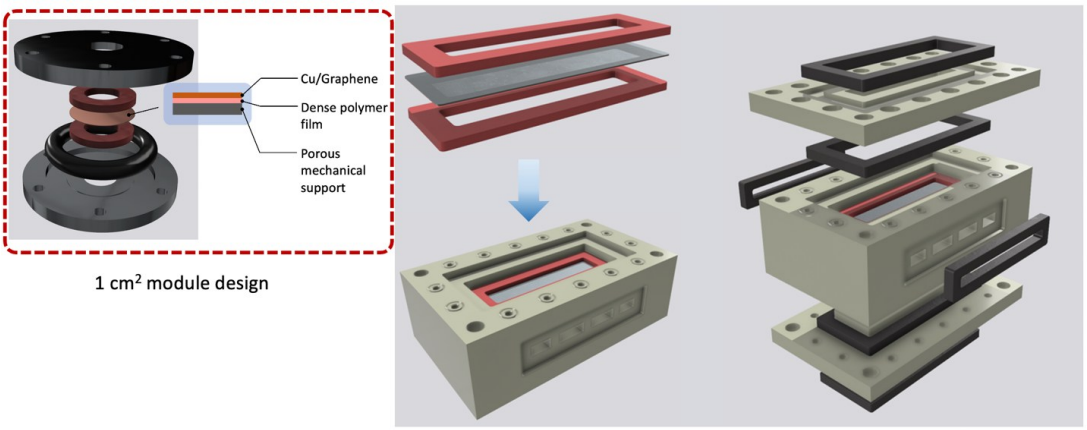

Figure 50. 3D model of the membrane module.

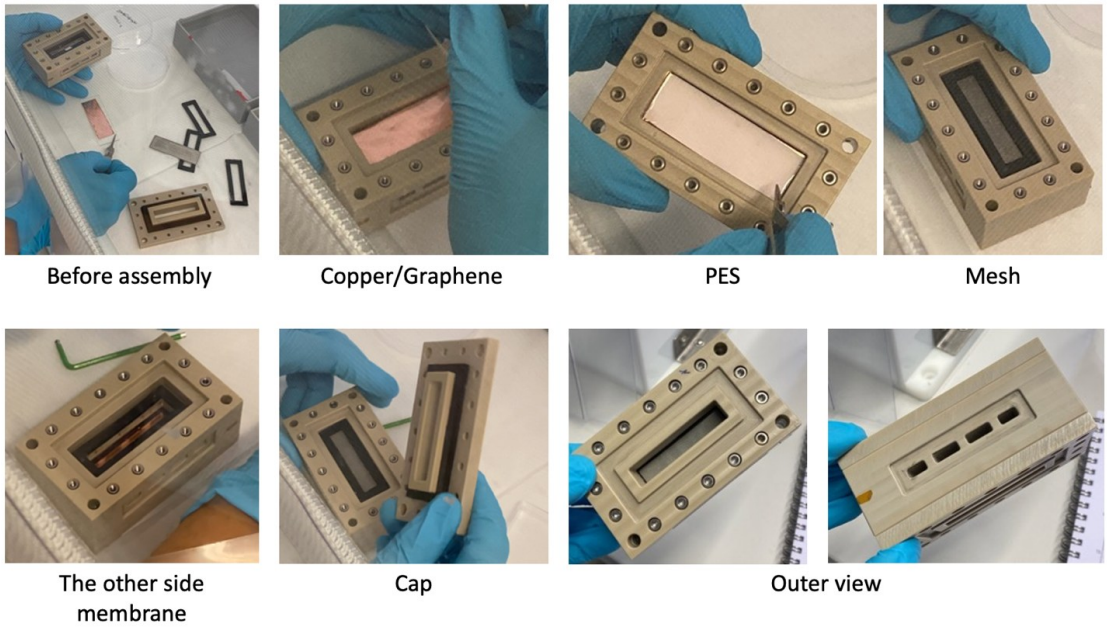

Figure 51. Step-by-step assembly of 10 cm^2 membrane module.

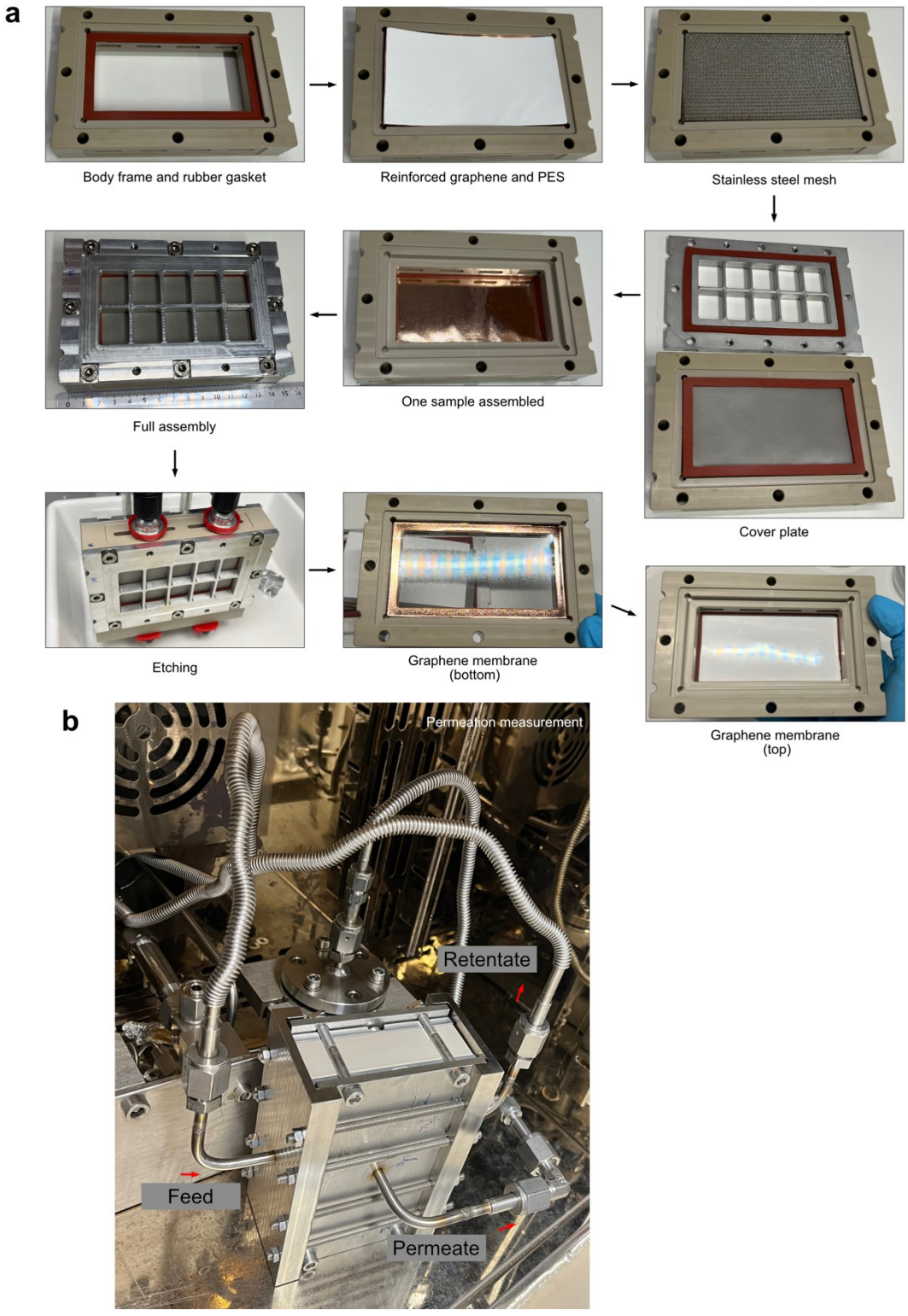

Figure 52. a) A step-by-step fabrication of 5 × 10 cm^2 graphene membrane using the modified membrane module, and b) pictures of the module for gas permeation measurement.

In our first prototype (Figure 50), there is a large (~9.6 mm) gap between the two membrane elements assembled in the module on the feed side of the membrane. As expected from the modeling section, this led to an issue with concentration polarization when the feed gas is a mixture of CO_2 and N_2 at a CO_2 permeance of 1000 GPU. To solve this, we reduced the gap in the feed channel gap to 1.6 mm by placing a rectangular block inside the membrane module (Figure 53). Figure 54 shows the resulting normalized CO_2 permeance as a function of CO_2 feed concentration from a commercial polydimethylsiloxane (PDMS) membrane with different feed channel thicknesses. It is clear that the concentration polarization effect is reduced when the sample gap becomes thinner. In the next step, we will design a membrane module with an even thinner gap (e.g., 0.2 mm) to avoid concentration polarization.

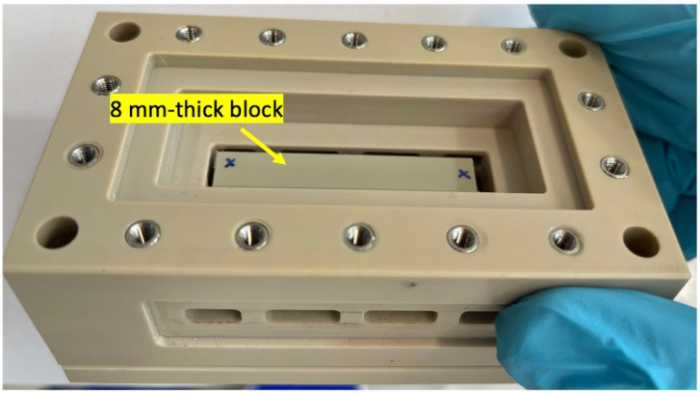

Figure 53. The block stuck in the membrane module to reduce the concentration polarization effect.

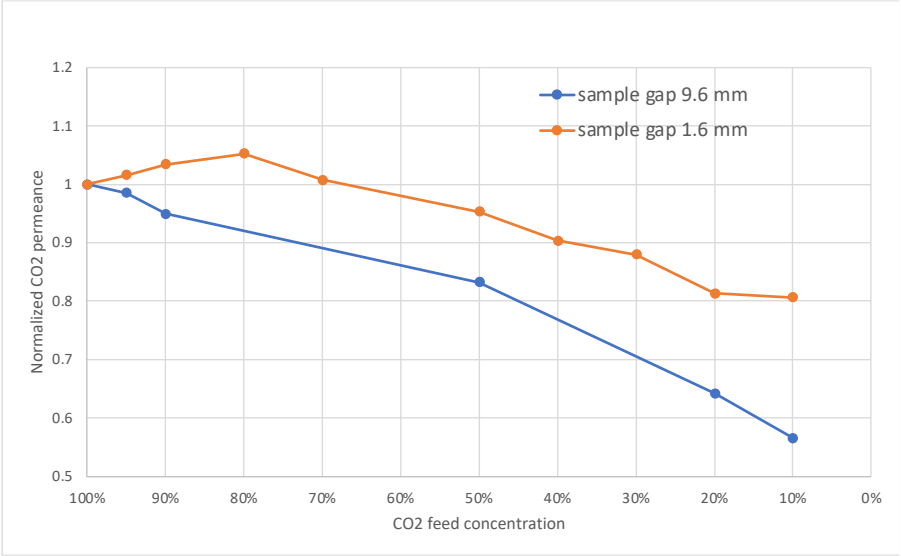

Figure 54. Normalized CO_2 permeance as a function of CO_2 feed concentration obtained from the same membrane with different feed channel thicknesses

To address concentration polarization, we used the same membrane-sealing strategy while adjusting the feed gap and making simplifications. The 3D design of the optimized membrane module is shown in Figure 19. The step-by-step assembly of the membrane module is shown in Figure 55. Table 3 shows the gas permeation results of a commercial PDMS membrane tested in the optimized membrane module

under single-component and equal-molar mixture feed gas. The consistency in gas permeance and selectivity demonstrated that the concentration polarization effect is minimal in the optimized module.

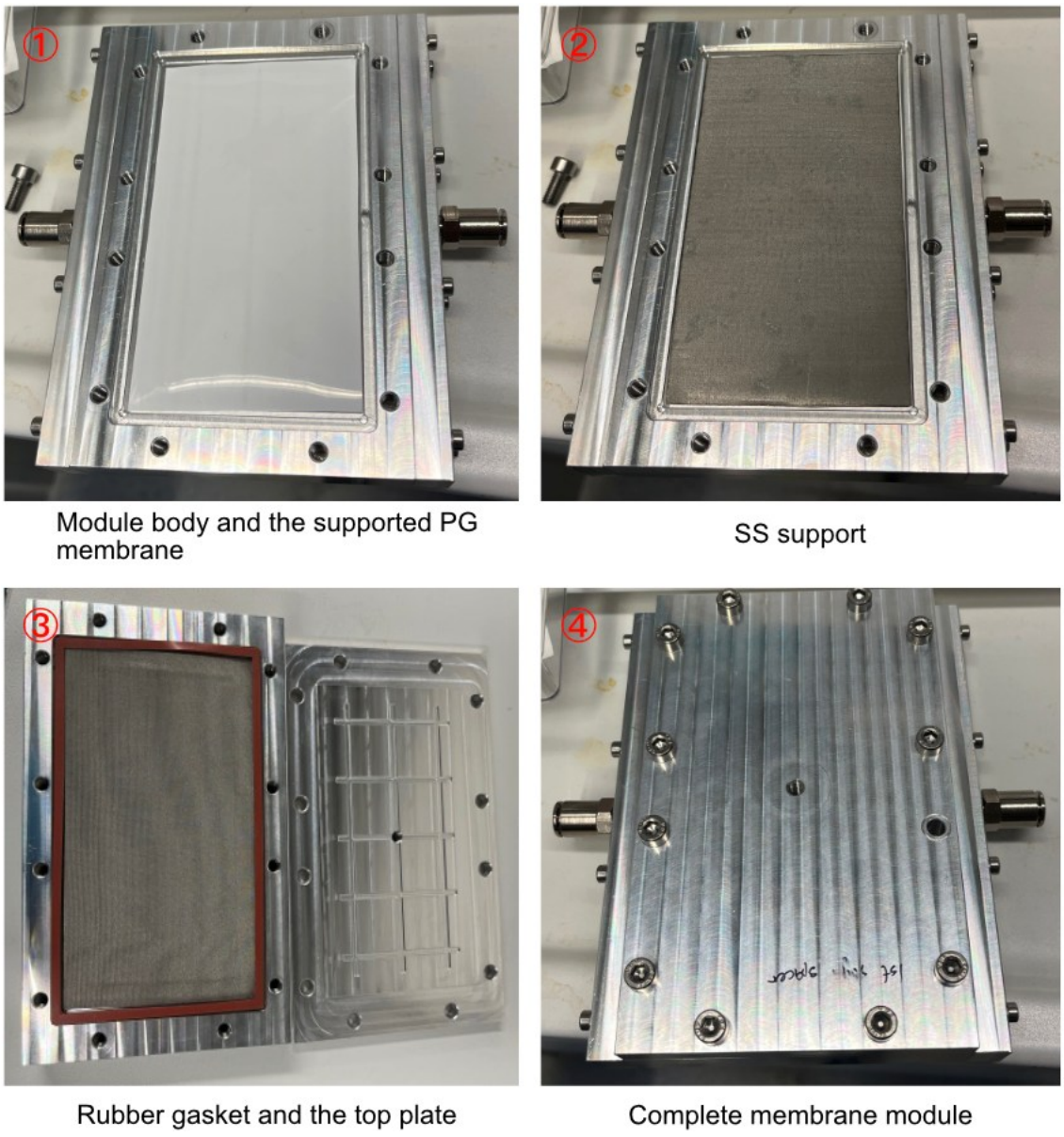

Figure 55. Step-by-step assembly of the optimized membrane module.

Table 3. Gas permeation results of the PDMS membrane from the optimized module.

	CO_2 permeance (GPU)	N_2 permeance (GPU)	CO_2/N_2 selectivity
Single-component feed	2131	226	9.4
Equimolar mixture feed	2388	240	9.9

4.6 Single-stage membrane stability test

Figure 56 shows month-long stability testing of a 50 cm^2 coupon under laboratory gas flow, demonstrating stable performance. A slight decrease in permeance over time was observed, which can be attributed to aging of the MRF (PTMSP in this case). Based on a three-month laboratory study, we have shown that this ageing is reversible. Indeed, heating the membrane to 130 ºC for 1 h restores its permeance (see regeneration in Figure 56). The alternate strategy would be to use non-aging MRF such as PDMS.

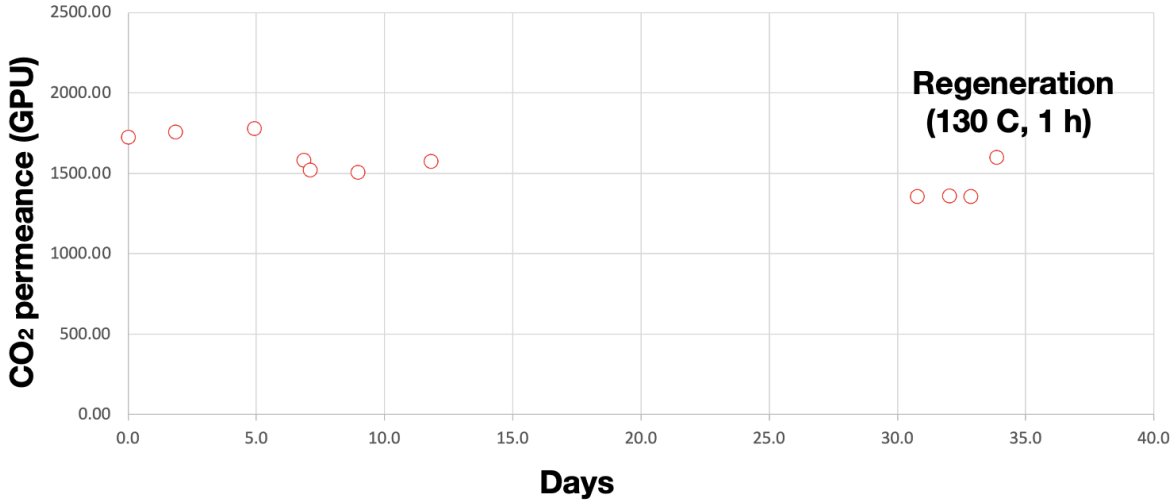

Figure 56. Month-long permeation testing of 50 cm^2 sized graphene membrane showing stable performance.

We performed a single-stage membrane stability test on a platform built in collaboration with GAZNAT (See section 7 for more details). The results are highly encouraging, showing excellent membrane stability in the flue gas from a combined heat and power (CHP) unit containing 50 ppm NOx (Figure 57). The data fluctuation is due to fluctuations in feed supply (CHP is not always on), and where flue gas was stored in a pressurized tank to allow for steady-state membrane operation.

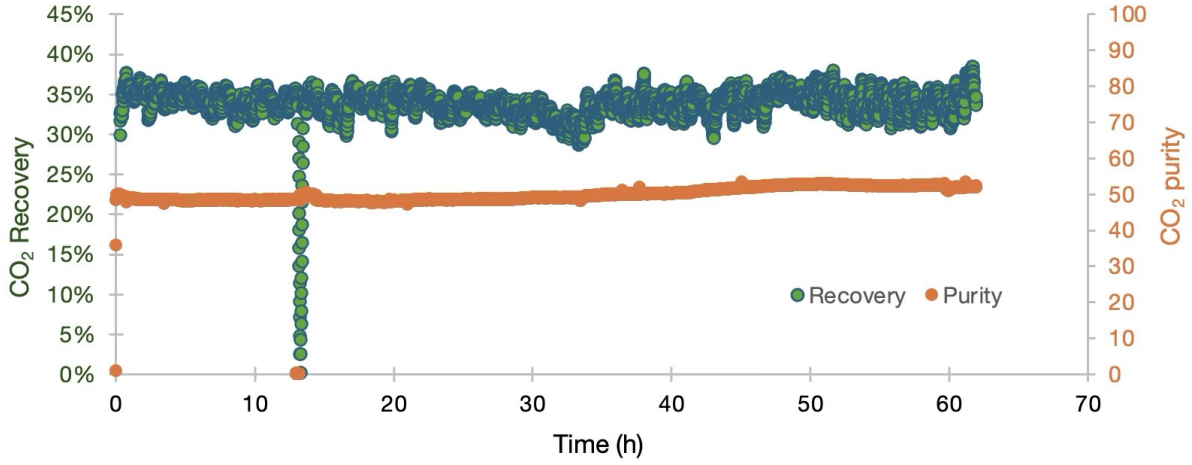

Figure 57. Recovery and purity data from a single-stage graphene membrane (50 cm^2) separating flue gas from GAZNAT CHP containing 50 ppm NOx.

4.7 Process design for pilot plant

We performed a techno-economic analysis of double-stage membrane processes for carbon capture from flue gas and from biogas. The technical model designs the process, i.e., estimates the membrane areas in each stage and the energy consumption of the vacuum pumps and the compressors for a given target of recovery and purity. The model requires a number of inputs and parameters, such as the composition and flow rate of the inlet feed stream, the efficiency of pressure equipment, and the membrane performance parameters. Then, the economic model calculates the capital and operating expenses, where the capital expenses are given by equipment costs, indirect costs, and contingency and fee costs, whereas the operating expenses are given by energy costs, fixed operating costs, and membrane replacement costs. The sum of the capital and operating expenses per year divided by the amount of CO_2 produced per year returns the capture penalty.

The techno-economic model can also identify the set of operating conditions (in particular, the pressures in the feed and permeate channels) that minimize the capture penalty.

Capture from flue gas

We considered various scenarios to include the variation of (i) membrane CO_2 permeance and CO_2/N_2 selectivity; (ii) membrane cost; and (iii) target of CO_2 purity. In particular, we used:

(i) Low-performance (CO_2 permeance and selectivity of 1000 GPU and 15, respectively), and high-performance (CO_2 permeance and selectivity of 10000 GPU and 30, respectively) specifications.

(ii) Conservative cost estimation of 500 $/m^2 and updated cost estimation based on lower-cost copper foil and mesh for support of 100 $/m^2;

(iii) Target purity of 90% and 98%, depending on the downstream process (either storage or utilization).

The simulations take into account a wet feed stream, saturated with water vapor at 50 ℃ and with an inlet CO_2 concentration of 11.8%. The simulations refer to a large-scale system with a capture rate of around 0.5 million tons per year and a target recovery of 90%.

With CO_2 permeance of 1000 GPU and CO_2/N_2 selectivity of 15, we found that a double-stage membrane process with the combination of feed compression and permeate under vacuum in the first stage is preferable to a process where the driving force relies only on vacuum in the permeate channel. This is because the permeance is relatively low, and when feed is compressed, the membrane area is always reduced. In particular, the optimal configuration presents feed and permeate pressures in the first stage of 5 and 0.08 bar and in the second stage of 1 and 0.1 bar.

The specific energy consumption is equal to 2.5 MJ/kgCO_2 for a purity of 90% and 5.0 MJ/kgCO_2 for a purity of 98%. The energy consumption increases with purity because higher recycle rates of the second retentate are needed. Mostly driven by the increase in energy consumption (Figure 58), the capture penalty increases from 87.2 to 153.4 $/ton, when purity increases from 90% to 98%.

When membrane cost reduces from 500 to 100 $/m^2, capture penalty is equal to 69.5 and 129.5 $/ton, for purity of 90 and 98%, respectively.

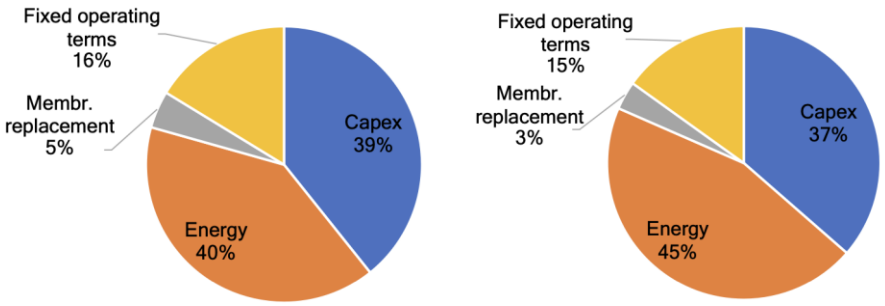

Figure 58. Breakdown of capture cost with purity target of 90% (left) and 98% (right), with CO2 permeance of 1000 GPU and CO_2/N_2 selectivity of 15, and with membrane cost of 500 $/m^2.

The capture penalties are significantly reduced with the high-performance graphene membrane; with CO_2 permeance of 10000 GPU and CO_2/N_2 selectivity of 30 (performance already achieved in our lab from porous graphene membrane even without nitrogen functionalization), a double-stage membrane process with vacuum in the permeate of both stages and ambient pressure in the feed channel is more economically competitive. The selected configuration presents permeate pressures of 0.05 bar in the first stage and 0.1 bar in the second stage. The energy consumption is 1.0 MJ/kgCO_2 and 1.6 MJ/kgCO_2 with purity of 90 and 98%, respectively. As in the previous case, capital costs and energy costs cover almost the same share of the total cost (~ 40%, see Figure 59). The total capture penalty in this case is very attractive and equal to 35.6 $/ton for 90% purity and 52.8 $/ton for 98% purity.

Membrane cost covers between 34 and 37% of the capital costs and the reduction of the specific membrane cost from 500 to 100 $/m^2 leads to a reduced capture penalty of 25.4 $/ton (90% purity) and 39.6 $/ton (98% purity).

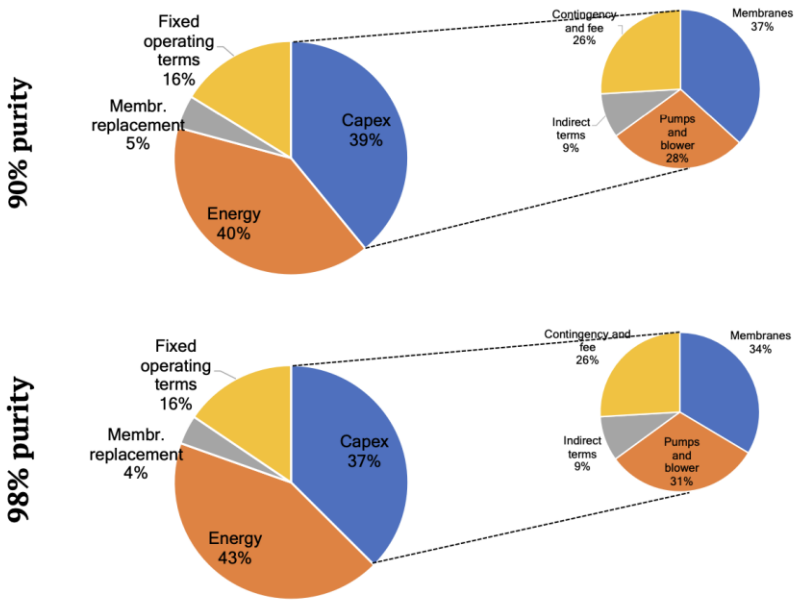

Figure 59. Breakdown of total cost and capital cost for capture from flue gas with purity target of 90% (up) and 98% (down), with CO2 permeance of 10000 GPU and CO_2/N_2 selectivity of 30, and with membrane cost of 500 $/m^2.

Module design – impact of channel thickness

An important aspect to consider, especially with highly permeable membranes, is the impact of non-ideal phenomena, i.e., pressure drops and concentration polarization. These non-ideal effects can be mitigated by proper module design, particularly by selecting the feed channel thickness appropriately. The thinner the feed channel, the smaller the concentration polarization, but also the larger the pressure drops. Therefore, we usually select the smallest channel thickness that allows us to keep the pressure drop below 0.1 bar/m threshold.

The selection of the thickness depends on the membrane parameters, especially permeance, because higher permeance corresponds to larger fluxes through the membrane, leading to stronger CO_2 depletion at the feed-membrane interface, i.e., stronger concentration polarization. In this regard, in Figure 60, we show how the required membrane area and the concentration polarization index vary with the channel thickness for the two ranges of membrane performances presented above. In all cases, the pressure drops are below 0.1 bar/m.

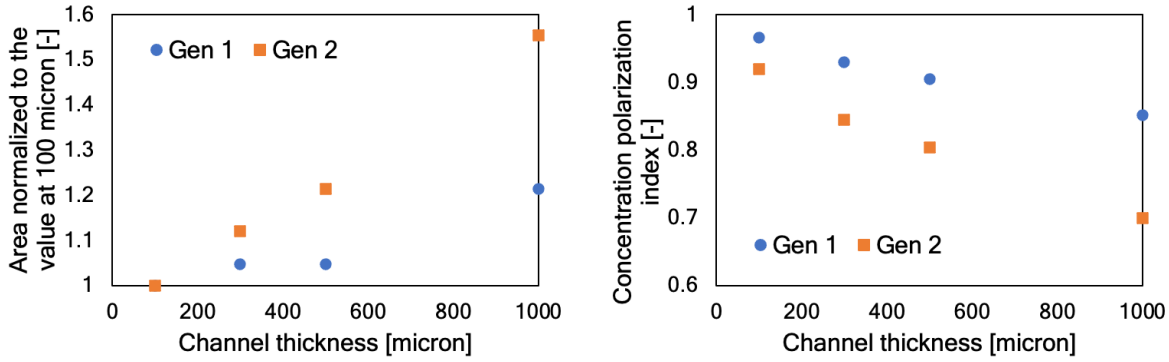

Figure 60. Impact of channel thickness on the membrane area (expressed as normalized area to the value found with channel thickness of 100 µm) and on the concentration polarization index (defined as the ratio between the concentration of CO_2 at the feed-membrane interface and the concentration in the feed bulk). Gen 1 refers to low-performance (CO_2 permeance and selectivity of 1000 GPU and 15, respectively) and high-performance (CO_2 permeance and selectivity of 10000 GPU and 30, respectively) membranes.

First, the membrane area required for the same targets of recovery and purity increases when channel thickness increases, because the effect of concentration polarization is stronger. This causes a decrease in the partial pressure driving force; thus, a larger membrane area is required for the same separation. The membrane area increases by around 20% and 60% when the channel thickness increases from 100 to 1000 µm with Generation 1 and 2 membranes, respectively. Generation 2 membranes are more impacted by the variation of channel thickness because of the higher permeance.

This is also evident from the chart reporting the concentration polarization index as a function of the channel thickness. The concentration polarization index is defined as the ratio between the concentration of CO_2 at the feed-membrane interface and the concentration in the bulk of the feed channel. The lower the index, the stronger the concentration polarization.

In line with what is already said for the variation of membrane area, the index decreases when the channel thickness increases and it goes down to 0.85 and 0.7 with Generation 1 and 2 membranes, respectively.

Overall, in order to reduce the loss of driving force due to concentration polarization, we should keep the channel thickness as low as possible while fulfilling the requirement for maximum pressure drops.

Process design and techno-economic analysis

We carried out the optimization of membrane processes for carbon capture by taking into account variable membrane performances (permeance and selectivity) in line with those found in the lab.

All simulations target 90% CO2 recovery and 95% CO_2 purity in the permeate stream, starting from a wet flue gas saturated with water vapor at 50 ºC and with a CO_2 concentration of 11.8%. The cost analyses refer to large-scale processes aiming at producing around 0.5 million tons of CO_2 per year. The main cost assumptions used for the simulations are reported in Table 4.[4]

Table 4. Main economic variables.

Cost variable	Value
Membrane cost [$/m^2]	100
Electricity cost [$/kWh]	0.05
Membrane replacement rate [y]	5
Contingency factor [-]	0.15 (project) + 0.2 (process)
Capital charge factor [-]	0.125
Vacuum pump efficiency [-]	0.7
Compressor efficiency [-]	0.85

All simulations refer to a double-stage process, where the partial pressure driving force is generated by the combination of feed compression and permeate under vacuum in the first stage, whereas in the second stage, the feed channel is at ambient pressure and the permeate channel is under vacuum (see Figure 61). The optimization variables are the pressures in the feed and permeate channels of the first stage and the permeate pressure in the second stage.

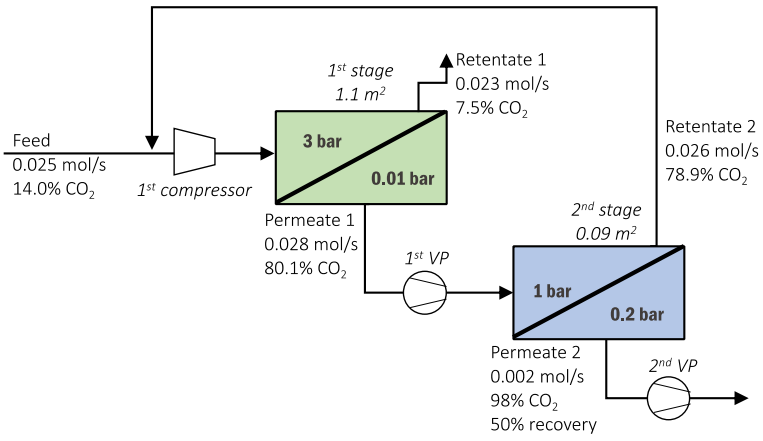

Figure 61. Scheme of the double-stage membrane process for 50% CO_2 recovery from dry feed with CO_2 purity of 98%.

The feed pressure generated in the compressor can range from 1 to 6 bar, whereas the permeate pressures are free to vary between 0.1 and 0.3 bar. In these analyses, we did not consider vacuum pressures below 0.1 bar as a higher vacuum is generally considered more difficult and expensive to realize at a large scale.

The variation of membrane performance parameters corresponds to important variations in overall cost, membrane area, and energy consumption.

We consider two membranes: (i) generation 1 with a CO_2 permeance of 1000 GPU and CO_2/N_2 selectivity of 20, and (ii) generation 2 with a CO_2 permeance of 10000 GPU and CO_2/N_2 selectivity of 50. In both cases, the CO_2/O_2 and the CO_2/H_2O selectivity are taken equal to 12.6 and 1, respectively. The optimal pressure configurations are presented in Table 5. Sets of pressure (bar) that minimize capture cost with the two generations of membranes. and the relevant results of the economic analysis are reported in Figure 62.

Table 5. Sets of pressure (bar) that minimize capture cost with the two generations of membranes.

	Membrane generation 1	**Membrane generation 2**
Feed channel 1	2.5	1.5
Permeate channel 1	0.1	0.1
Permeate channel 2	0.1	0.2

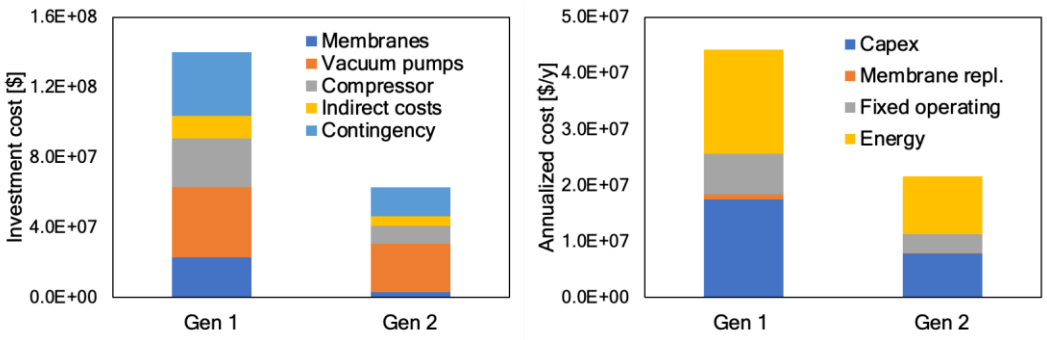

Figure 62. Results of the cost optimization with the two generations of membranes.

Generally speaking, the costs are much higher with Gen 1. In the investment costs, the difference is mostly driven by the membrane cost due to the different values of CO_2 permeance. Conversely, the lower selectivity of Gen 1 membranes causes an increase in energy consumption, because larger recycle rates are needed to achieve the same targets.

The total minimized capture penalty varies from 65.5 $/ton with Gen 1 membranes to 31.0 $/ton with Gen 2, and the specific energy from 2.0 to 1.1 MJ/kg. The capture penalty and the energy consumption with Gen 2 membranes are highly competitive with state-of-the-art polymeric membrane-based processes.

4.8 Process validation from the two-stage membrane separation pilot

We commissioned a demonstration site at the EPFL campus to serve as a testbed for continuous operation and stability evaluation of the membrane-based carbon capture system. A fully integrated pilot platform (Figure 14) was constructed to simulate CO_2 capture from waste incineration flue gas. The system enabled long-term operation with continuous data acquisition, real-time monitoring, and process visualization.

Prior to operation, the skid was thoroughly validated through gas leak testing, electrical checks, and calibration of all instrumentation (mass flow controllers, flow meters, and gas analyzers). The process control and data infrastructure were further optimized to ensure reliable operation and high-quality data

collection. The finalized process flow diagram and skid configuration are shown in Figures 13–14 and Figure 64.

Two 50 cm^2 porous graphene membranes were installed in a two-stage configuration. We used representative flue gas conditions (12.5% CO_2, 0.4 L/min feed, pressure of the first and second stage membranes were 3.5 bar and 1.5 bar, respectively). These are reflected in the user interface (Figure 65). The user interface in the skid can display the real-time process parameters and the overall purity and recovery plot from the start of the test, and is a useful tool for the operator. The system achieved an initial CO_2 recovery of 90.2% and purity of 90.0%. These results validate the process design and demonstrate the capability of the membrane platform to meet industrially relevant separation targets.

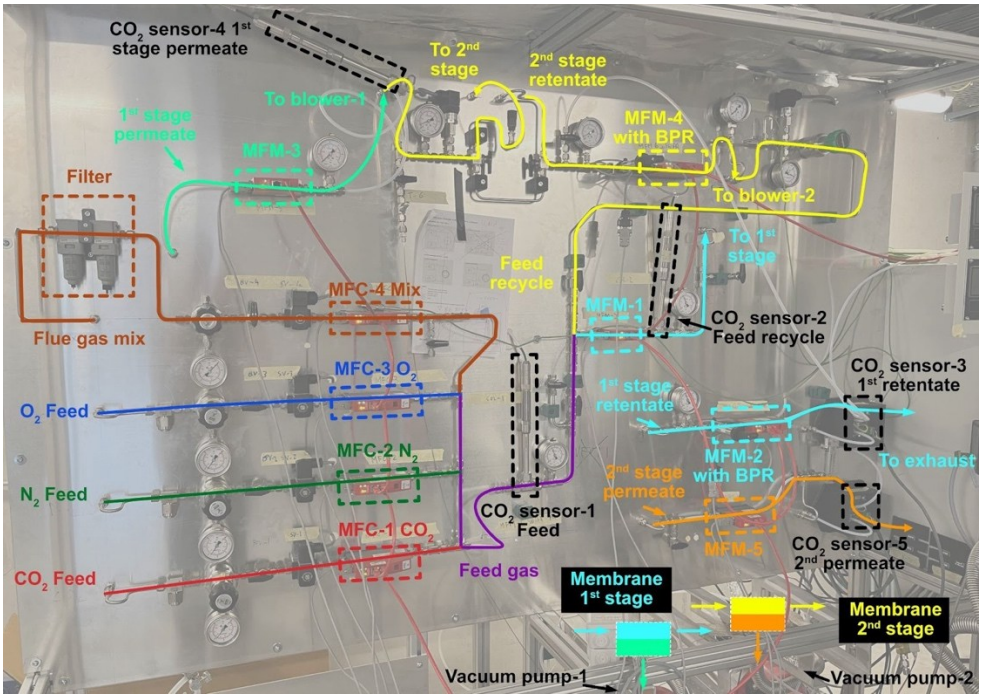

Figure 63. The carbon capture pilot platform and the details of the gas flow direction and equipment information.

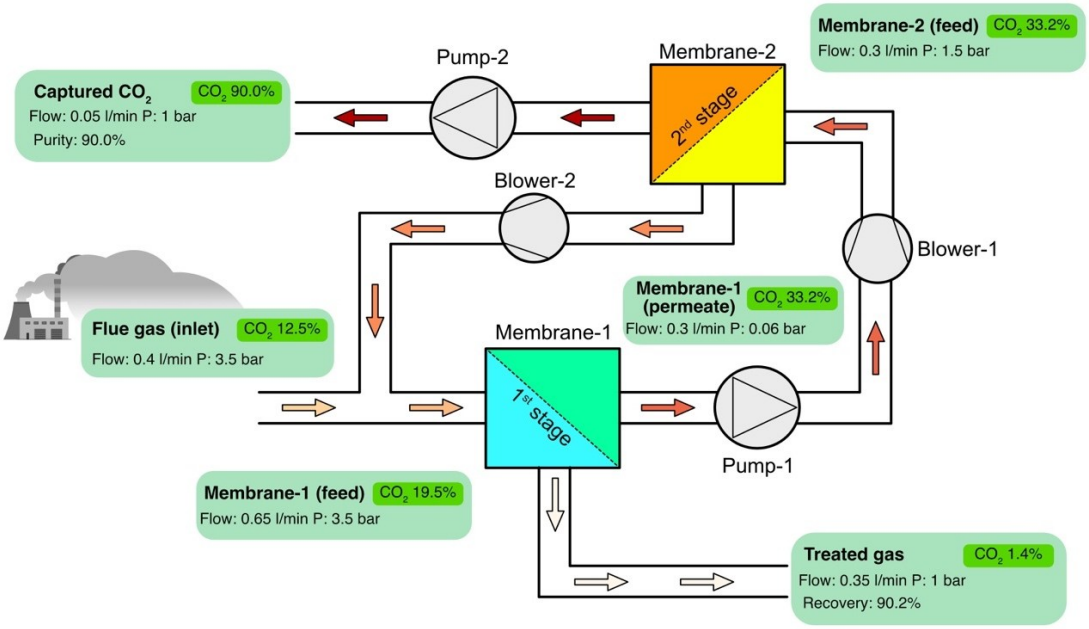

Figure 64. Process parameters of the initial test from the membrane skid.

System Stability and Operational Insights

Continuous operation over extended periods provided valuable insights into both system-level robustness and material behavior. During the initial campaign (Figure 66), a gradual decline in recovery and purity was observed. This behavior is consistent with the well-known physical aging of high-free-volume polymer materials, such as PTMSP, used in the membrane reinforcement layer (MRF), which evolves under operational conditions. This issue can be simply resolved by using stable MRF such as PDMS.

Importantly, the pilot system itself demonstrated stable operation, and deviations in performance were successfully traced to identifiable and correctable factors. We kept the process running continuously, and Figure 65 shows the recovery and purity data over time for the initial one-month test. We observed a monotonous decrease in the recovery and purity of both stage 1 and stage 2 membranes. This degradation is mainly due to the physical aging of the polymer MRF (PTMSP), which eventually controls the membrane performance. Physical aging of PTMSP could be reversed by a regeneration step: heating the membrane to 130 ºC. However, before we could regenerate the membrane, we observed instability in data acquisition, as indicated by the large jump in recovery and purity after 400 h of testing. This was because a leak in the blower of the setup. The leak allowed water vapor from the air to be injected into the membrane system, which then condensed at the exhaust of the vacuum pump of the second stage membrane. The condensed water damaged the mass flowmeter and the CO_2 concentration sensor (Figure 66). To solve this issue, we replaced the swing-piston blowers with diaphragm blowers which typically have a very low leak rate.

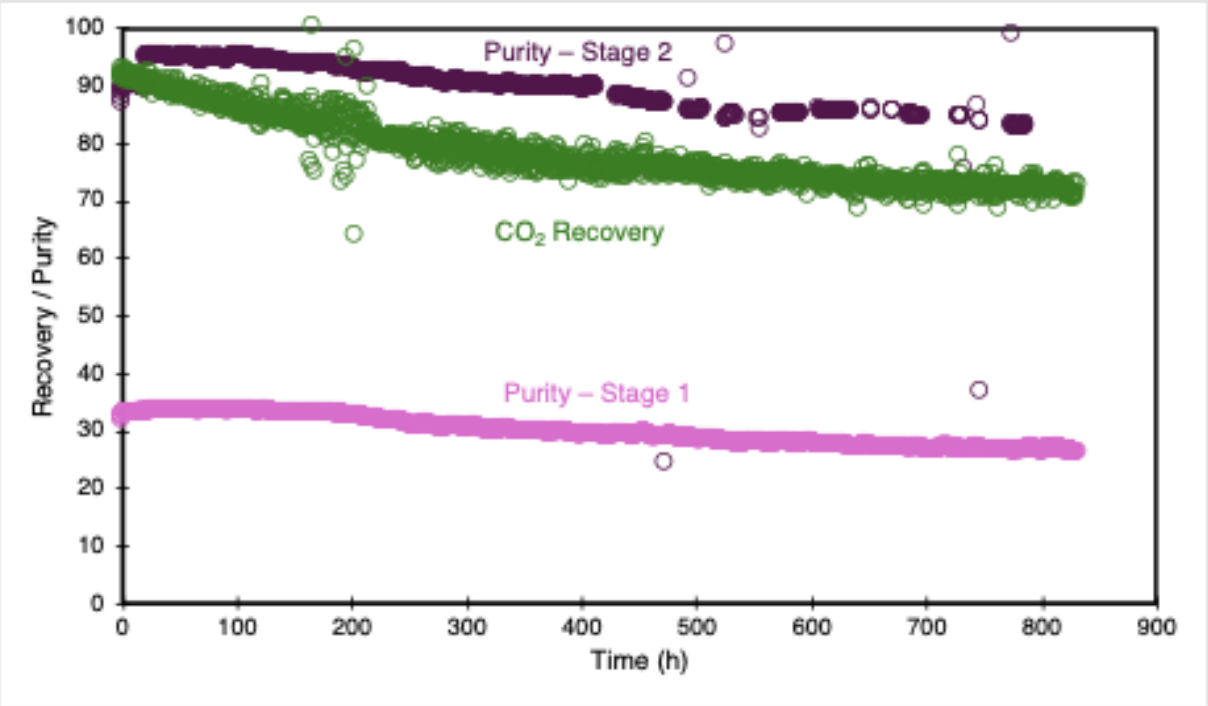

Figure 65. Recovery and purity data over time from the initial run.

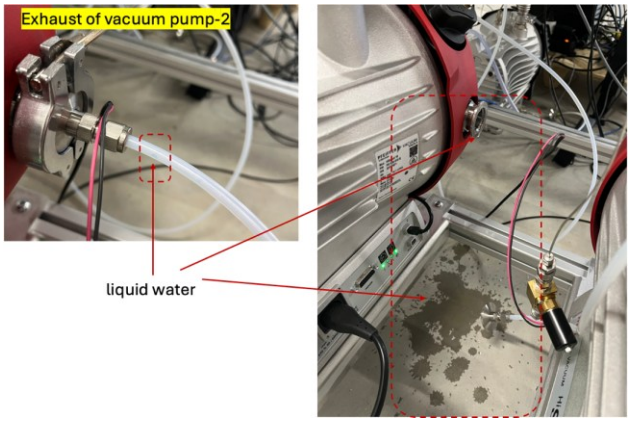

Figure 66. Photo of the condensed water in the exhaust of the vacuum pump.

Regeneration and Performance Recovery

A key advantage of the carbon capture pilot platform in this study is the ability to restore performance through in-situ regeneration. Thermal treatment (130 °C, 1 h) enabled recovery of ~90% of the initial separation performance after MRF (PTMSP)-aging-induced decline in the performance of porous graphene membrane (Figure 68). This demonstrates that the system can be operated with periodic regeneration cycles to maintain performance over extended operation. While repeated aging/regeneration cycles highlight intrinsic limitations of PTMSP-based MRFs, they also provide a clear pathway for MRF optimization. In particular, alternative MRF materials such as PDMS-based systems, which do not exhibit physical aging, will significantly enhance long-term stability of porous graphene membrane.

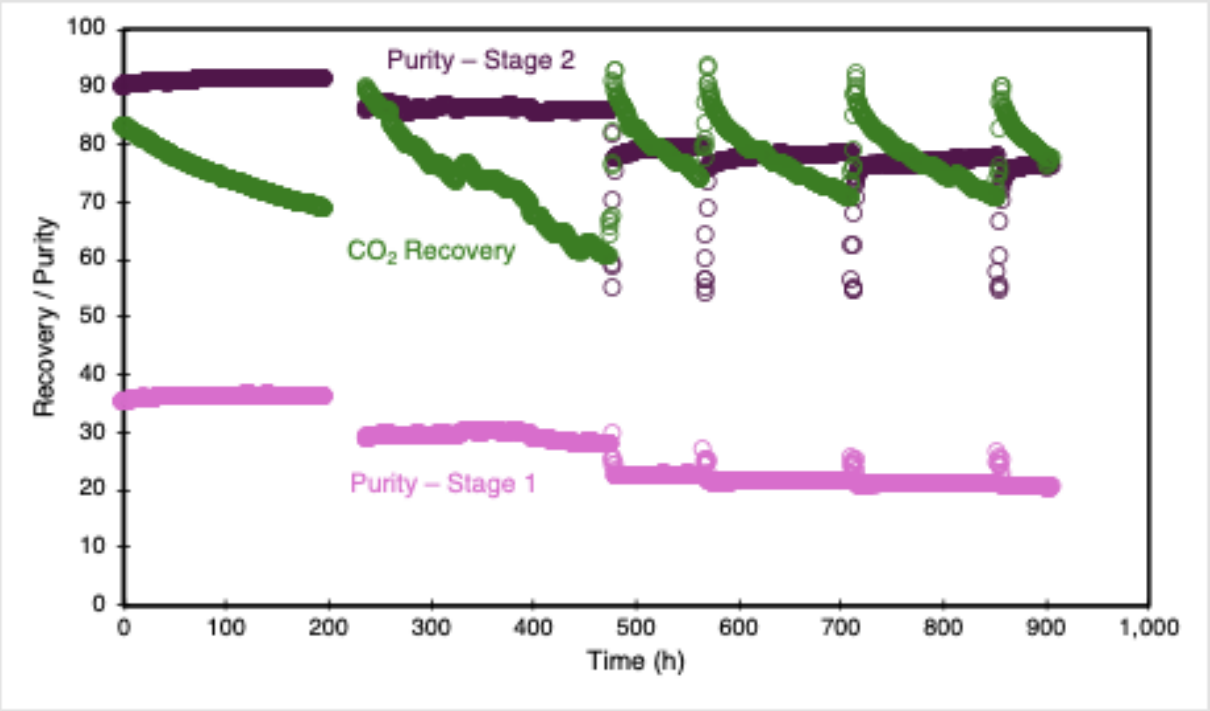

Figure 67. Recovery and purity data over time from the second run.

For the next step, we probed membrane stability under a humid gas atmosphere. To do that, we added a customized bubbler before the feed of the stage 1 membrane. The feed gas first bubbles through water at ambient temperature and then flows to the pilot plant. We have reached a relative humidity (RH) of ~50% at 25 ºC and 3.5 bar, which represents ~2% water vapor (molar basis) at standard conditions. To prevent water condensation in the system, we attached heating tape to the tubing in the pilot plant and maintained it at 35 ºC. The lines were then wrapped in aluminum foil to evenly distribute the heat. Figure 69 shows that recovery and purity are maintained at the target level (>90%) with minimal drop, indicating that the membranes remained stable under a humid atmosphere. This result is particularly important for industrial deployment, as it demonstrates that the membrane platform can operate reliably under humid flue gas conditions without performance degradation.

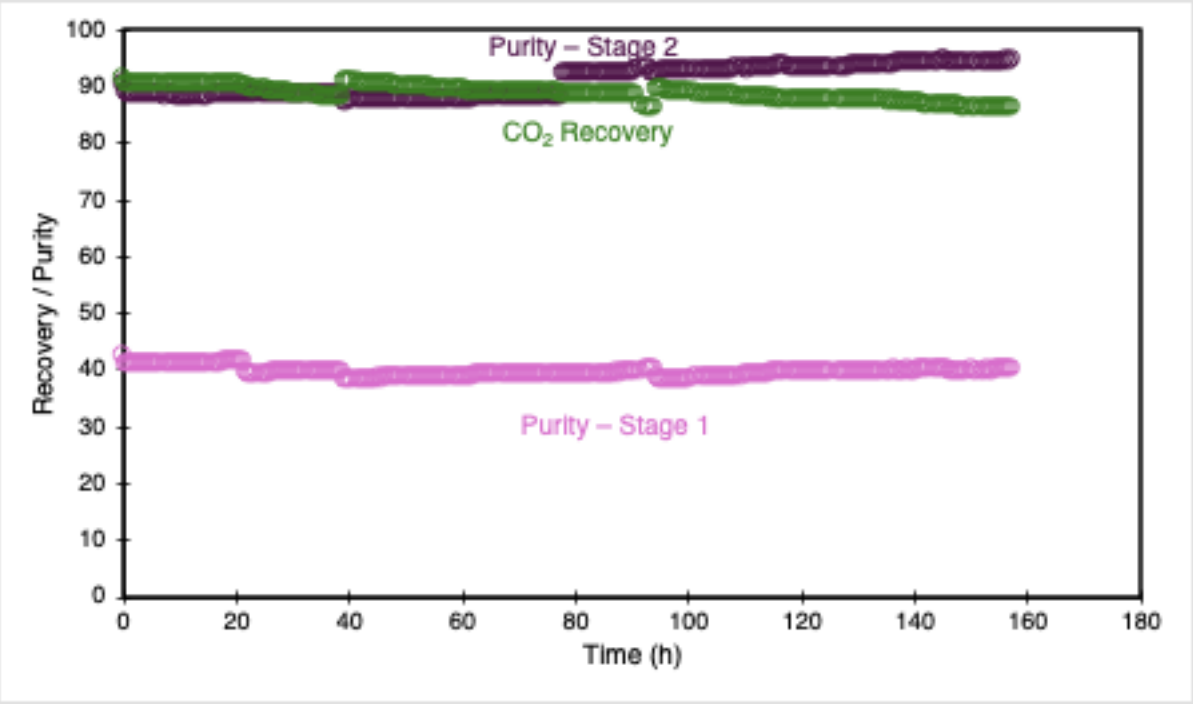

Figure 69. Recovery and purity data over time from the third run after introducing 0.5% water vapor.

5 Conclusion and outlook

Key insights, challenges, and measures

Before the start of this project, graphene membranes that demonstrated successful separation of CO_2 from N_2 were still on a scale of a millimeter or a centimeter. The success rate in the preparation of these membranes was low (e.g., 20%, which means that only one in five membranes would have a good performance). Overall, there has been significant progress since the start of the project, reflected by the successful design, commissioning, and validation of (i) a large-scale CVD reactor to produce graphene, (ii) an oxidation reactor to generate controlled porosity in large-area graphene, and (iii) testing and validation of large-area membranes for CO_2/N_2 separation. Our success rate in producing porous graphene and porous graphene membranes is now near 100%, thanks to the novel transfer-free membrane preparation step developed for larger area modules. We show that porosity in graphene is incorporated by ozone treatment successfully inside the reactor, making it convenient to prepare large-scale (27 cm x 12 cm) porous graphene films on a routine basis. We have validated cross-flow modules with an area of 10 cm^2 followed by an area of 50 cm^2. The process for separation has been optimized inside the scale-up reactor, learning from the conditions for small-scale membranes. The membranes produced by the large-scale reactor show promising performance, with permeance from a 50 cm^2 graphene membrane reaching close to 10000 GPU based on the resistance model. We have also successfully built and operated the two-stage membrane separation test bench based on the process design, and the performance of our graphene membranes was evaluated from the month-long continuous test.

One of the key advances in this project is that our success rate in producing graphene membranes is now close to 100%. We have achieved this owing to several factors. These include consistent quality of

graphene produced by CVD, extremely uniform oxidation of graphene in the scaled-up reactor setup thanks to improved mass transfer and uniform velocity, and finally, a novel membrane transfer process which allows crack-free transfer of large-area membranes.

We have made a decision to carry out oxidation at low (or even room temperature) to improve the scalability and uniformity of the method. This is one of the reasons for achieving a nearly 100% success rate in membrane production, as mentioned above. However, at low temperatures, oxidation kinetics is sluggish compared to high-temperature oxidation. We have explored improving the mass transfer of ozone by improving the velocity of ozone, as indicated by the extensive data on velocity generated in this project. The results are highly encouraging, with extremely promising results at room temperature oxidation by simply increasing ozone velocity (Figures 70 and 71).

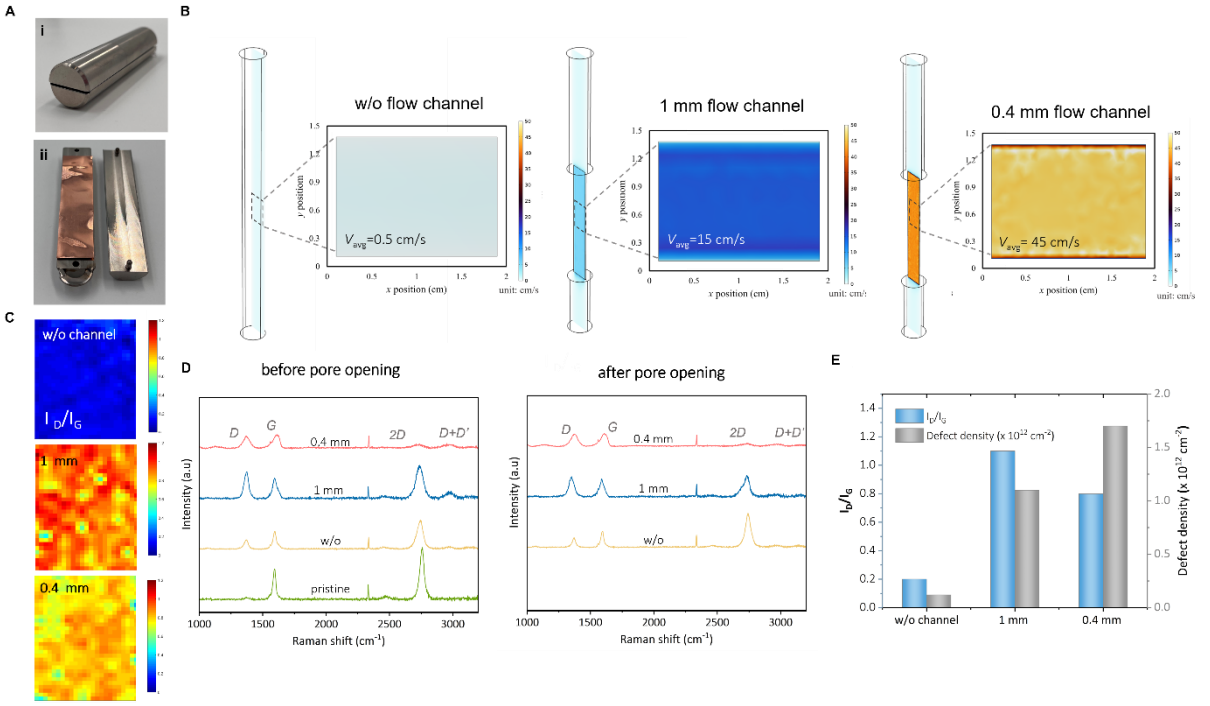

Figure 70. (a) Custom-made flow channel with 1 mm flow gap (i) assembled (ii) before sandwiching the graphene sample. (b) 3D models and 2D velocity profiles of O_3/O_2 flow on 1 mm above the graphene obtained with COMSOL for three conditions: without a flow channel, with a 1-mm flow channel, and with a 0.4-mm flow channel (c) Raman spectroscopy mapping of I_D/I_G for samples exposed to ozone flow under different conditions: without a flow channel, with a 1-mm flow channel, and with a 0.4-mm flow channel (d) Raman spectra of pristine graphene and ozone-treated samples at room temperature, comparing conditions without a flow channel and with 1-mm and 0.4-mm flow channels, both before and after pore opening. (e) The change in the I_D/I_G ratio and defect density, analyzed based on the carbon amorphization trajectory, for samples exposed to ozone and light under different oxidation conditions.

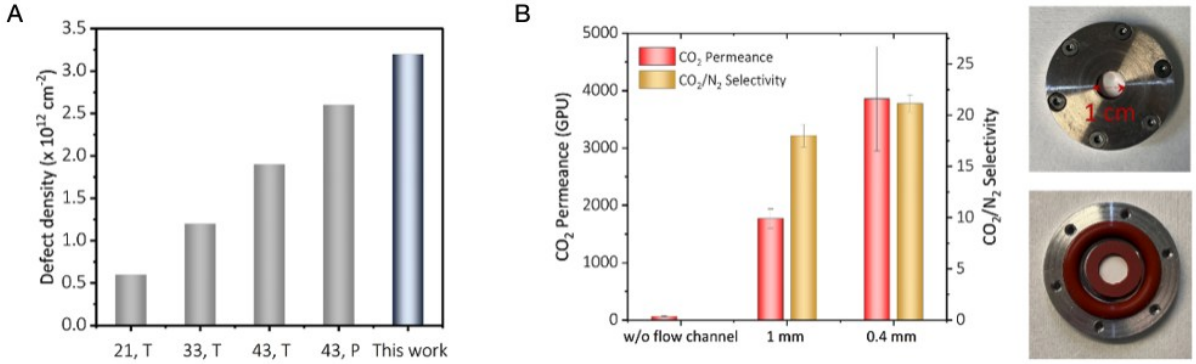

Figure 68. (a) Comparison of oxidative etching using high-temperature and room-temperature protocols. Membranes are labeled based on oxidation temperature (℃) and pore incorporation technique, where T represents thermal gasification (heating the samples), and P represents photonic gasification (light exposure). (b) Membrane separation performance of cm-scale membranes, prepared from oxidized graphene samples under different flow conditions: without a flow channel, with a 1-mm flow channel, and with a 0.4-mm flow channel. The right panel shows the pictures of a membrane module with a 1 cm-diameter membrane element.

We are also making progress in industrial testing of the membrane. The deployment of a pilot plant at the Agile site of GAZNAT (See section 7 for more details) has provided valuable operational feedback on the current skid design. Notably, the modularity has proven effective for rapid installation and troubleshooting. Mechanical integration was smoother than anticipated, though thermal insulation around certain fittings needs redesign to reduce water condensation during colder months. Lessons from onsite handling have led to considerations for more compact and transportable configurations, leading to an improved skid commissioned at EPFL, as shown in Figure 14.

Trade-off: permeance, selectivity, and economics

Membrane material inherently exhibits a trade-off between permeance and selectivity, a balance that fundamentally dictates process economics. Our achievement of approximately 10000 GPU in CO_2 permeance significantly reduces the required membrane surface area, which directly lowers the capital expenditure (CAPEX) for large-scale installations. While high permeance is critical for handling the massive volumes that exist in bulk separations like flue gas treatment, maintaining a selectivity of at least 30 is essential to achieving high-purity capture. High permeance reduces the energy consumption of the overall process, thereby decreasing the total carbon capture penalty and operational costs (OPEX). Conversely, in high-value sectors such as medical oxygen or specialty gas purification, selectivity, rather than permeance, becomes the dominant economic driver.

Our current membrane performance benchmark makes our membrane particularly suitable for post-combustion carbon capture, where the CO_2 concentrations typically range between 10% and 20%. In these sectors, where the emission volumes are vast, highly permeable membranes can significantly lower the cost. Furthermore, our membrane also demonstrates stability in the presence of SOx and NOx. This resistance to acidic industrial waste gases provides a significant advantage over traditional polymer membranes, which tend to degrade rapidly under such harsh conditions.

Next steps and R&D roadmap

Bridging the gap between our current laboratory prototypes and full-scale commercialization requires several key academic and engineering advancements. Currently, the membrane's supporting layer acts as a bottleneck for overall permeance. We are developing supports that offer higher permeability while facilitating the crack-free transfer of graphene. Besides, to boost CO_2/N_2 selectivity toward a target of 50, we are exploring the functionalization of graphene pores with pyridinic nitrogen on a large scale.

With regard to the pore formation process, the ozone reaction can be further optimized at room temperature. We have now adapted these results for our project on roll-to-roll fabrication of graphene membranes, where oxidation is designed at room temperature, reducing the process complexity. A spinoff on graphene membrane (Divea) has been created which is testing membrane stability and performance under various conditions. Divea has been testing porous graphene at waste-incinerator facility of Tridel at Lausanne. These membranes, now reinforced with PDMS as MRF (instead of PTMSP), show no sign of loss of permeance and recovery after month-long testing (proprietary data of Divea, not shown here).

Market entry strategy

The commercialization of this technology can be potentially realized by two approaches. Initially, the membranes can be introduced as specialized modular components (250 cm^2 to 1 m^2) to be implemented in existing pilot-scale research and industrial gas separation systems. To meet the demands of large-scale carbon capture, we will transition to roll-to-roll production. This shift allows for the continuous manufacturing of graphene membranes, drastically reducing the cost per square meter and making the technology competitive with traditional solvent-based absorption methods. Beyond component sales, our long-term strategy involves marketing complete, large-scale separation skids. These systems, modeled after our validated two-stage separation test bench, provide a “plug-and-play” solution for industries looking to integrate carbon capture or gas purification with minimal site disruption. Throughout this process, we maintain close collaboration with our industrial partners to accelerate the development cycle, allowing us to incorporate specialized feedback and operational data into our final system designs.

6 National and international cooperation

We have been collaborating with GAZNAT for carbon capture from flue gas from CHP using natural gas (Figure 69). Under this project, we have built a membrane skid that shows extremely promising data for flue gas separation (Figure 57).

Figure 69. Membrane skid for testing graphene membranes for the separation of flue gas from combined heat and power (CHP), installed in Aigle under the premises of GAZNAT.

At EPFL, our next step is to build a 1 tonCO_2/day test skid with capture at the waste incinerator site of Enevi near EPFL Valais. For this, graphene membranes will be produced by the recently developed roll-to-roll production tool, sponsored by EPFL Solutions4Sustainability project (*https://s4s-ccus.epfl.ch*) and Bridge Discovery project. We have started building and connecting all the components required for the Enevi test site. As shown in Figure 70, we will take the flue gas from the chimney and cool it down through two heat exchangers using cooling water with different temperatures (Figure 71). Then the flue gas is purified by three particle filters to avoid damage to the sensors. The driving force of the flue gas is provided by a centrifugal blower with a capacity of creating 2500 Pa differential pressure at a flow rate of 300 m^3/h. The remaining flue gas will be sent back to the chimney. This system will be used in the future for a larger capture capacity. For the small-scale demonstration, the flue gas after the blower will be sent through a compressor to the membrane skid. We plan to collect membrane stability data from the real flue gas for several months. We will make a projection on the lifespan of the membrane based on the above results.

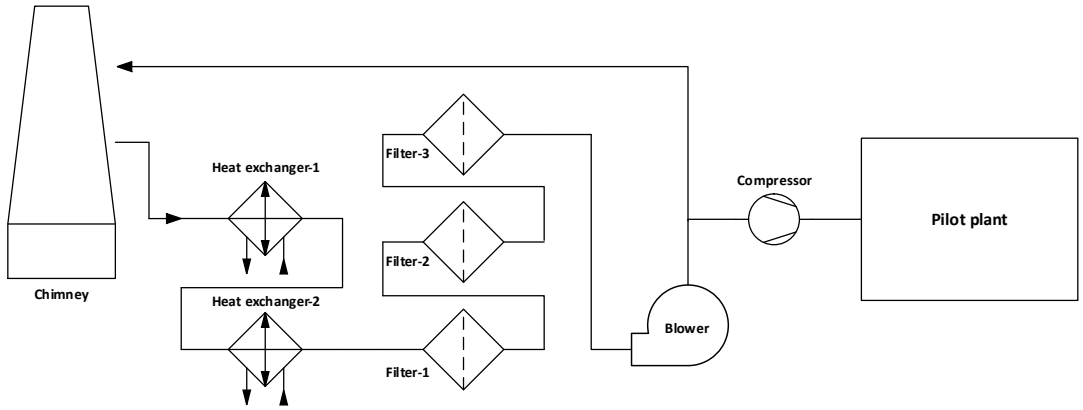

Figure 70. Process flow diagram of the connection from the chinmey in Enevi waste incineration plant.

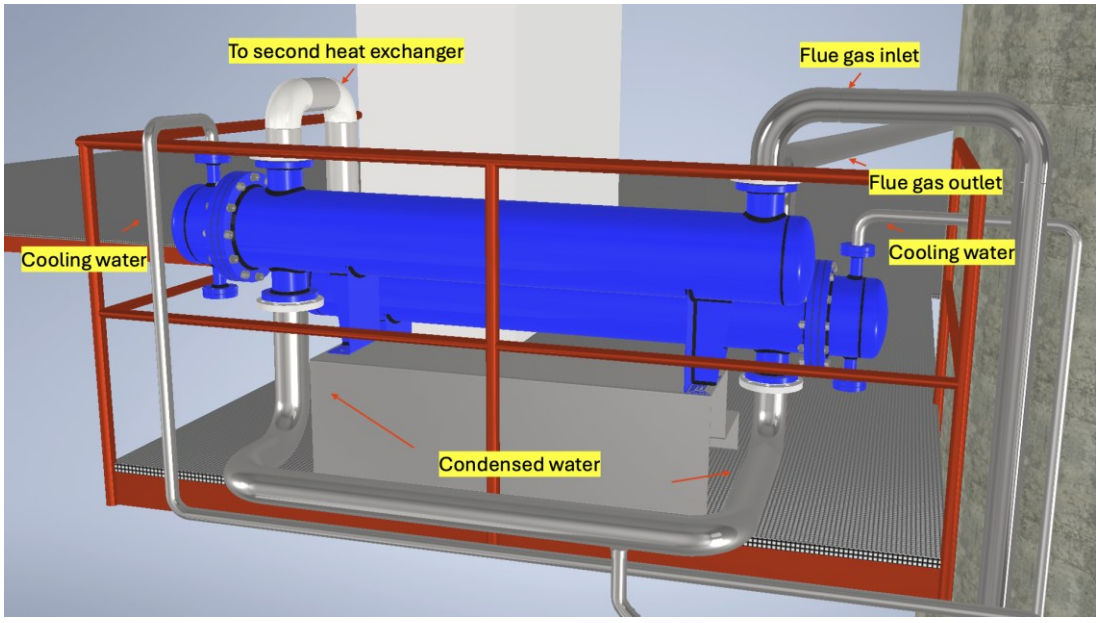

Figure 71. 3D design of the connection between the chimney and the heat exchanger on Enevi site.

7 Communication

There have been several communications on the scale-up activity of graphene membrane. In the scope of Valais demo project, this includes media news outlet.

1. https://www.rts.ch/info/regions/valais/2025/article/stockage-d-electricite-un-demonstrateur-power-to-gas-inaugure-a-sion-29066982.html
2. https://canal9.ch/fr/energypolis-une-technologie-valaisanne-pour-stocker-durablement-lenergie-sous-forme-de-gaz/
3. https://www.lenouvelliste.ch/valais/valais-central/sion-district/sion-commune/lepfl-et-la-hes-so-valais-presentent-une-machine-revolutionnaire-pour-stocker-et-redistribuer-lenergie-1476799
4. https://www.lfm.ch/actualite/suisse/romandie/un-nouveau-demonstrateur-energetique-power-to-gas-inaugure-a-sion/
5. https://latele.ch/articles/un-nouveau-demonstrateur-energetique-power-to-gas-inaugure-a-sion
6. https://www.rhonefm.ch/valais/transition-energetique--a-sion-une-installation-permet-de-stocker-l-electricite-sous-forme-de-gaz-1268198
7. https://www.bluewin.ch/fr/infos/suisse/un-nouveau-d-monstrateur-nerg-tique-power-to-gas-inaugur-sion-2974025.html
8. https://www.swissinfo.ch/fre/un-nouveau-d%c3%a9monstrateur-%c3%a9nerg%c3%a9tique-%22power-to-gas%22-inaugur%c3%a9-%c3%a0-sion/90426222
9. https://actu.epfl.ch/news/un-demonstrateur-place-le-valais-au-cur-de-la-tran/

In the scope of GAZNAT greengas project:

(1) Agrawal, K. V.; Bautz, R. "Capture Du Carbone". *Aqua & Gas* **2022**, 46–53.

http://www.aquaetgas.ch/fr/énergie/gaz/20220225_capture-du-carbone/

(2) René Bautz; Gilles Verdan, Noris Gallandat; Liping Zhong, Andreas Züttel; Kumar Varoon Agrawal, "Greengas - projet gazier innovant". *Aqua & Gas* **2024**, 36–44.

https://www.aquaetgas.ch/fr/énergie/gaz/20241031-greengas-projet-gazier-innovant/

There have been several presentations at invited lectures at international conference as follows:

1. Materials for Carbon Capture and Low Energy Separation Solutions, IISc Bangalore, Feb 2026.
2. Nanofluidics conference, Lake Tahoe, USA, 2026
3. 2nd International Conference on Sustainable Nanomaterials Integration and Organization for Energy and Environment (2nd-iSNIOE2), India, 2026
4. Carbon Capture Science and Technology (CCST) Conference, Online, 2025
5. World Chemical Engineering Congress, China, 2025.
6. NanoKorea Conference, Goyang, South Korea, 2025.
7. MedPore 2, Marrakech-UM6P campus, Morrocco, 2025.

8. Interdisciplinary Perspectives on Transport Mechanisms in Membranes and Nanopores, France, 2025.
9. International Conference on Carbon Capture and Utilization 2024 (ICCCU24), India, 2024.
10. International conference From Solid-state to Biophysics XI, Croatia, 2024.
11. Materials Research Society (MRS) Spring Meeting, Nanoscale Mass Transport Through 2D and 1D Nanomaterials, USA, 2024.
12. Gordon Research Conference (GRC) on Nanoporous Materials and Their Applications, Proctor Academy, USA, 2023.

We have also made presentations (contributed) to international conferences including American Institute of Chemical Engineers (AIChE) 2024 and 2025.

Finally, the progress has been disseminated in invited research seminars and research talks:

1. EPFL Engineering Industry day (500 industries present), EPFL March 2026.
2. EPFL Sustainability days, EPFL March 2026.
3. Seminar, Dalian Institute of Chemical Physics, Dalian, China, July 2025.
4. Seminar, Peking University, Beijing, China, July 2025.
5. Seminar, Yonsei University, Seoul, South Korea, July 2025
6. Research Talk, Center for Enhanced Nanofluidic Transport (CENT), August 2024.
7. Seminar, NTU Material Science Department, July 2024.
8. Research Talk, ETH Board, Lausanne, Switzerland June 2024.
9. Seminar, Yonsei University, Jan 2024.
10. Seminar, Tianjin University, Fall 2023.
11. Seminar, Suzhou University, Fall 2023.
12. Seminar, University of Texas at Austin, Fall 2023.
13. Seminar, Ohio State University, Fall 2023.
14. Seminar, IISC Bangalore, 2023.
15. Seminar, Shell, June 2023.
16. Seminar, Yonsei University, Jan 2023.

8 Publications

Some of the results indirectly and directly related to this project have been published here:

1. L. Bondaz, A. Ronghe, G. Ayappa*, K. V. Agrawal*, "Decisive role of pore edge termination in determining the CO_2 selectivity of Å-scale pores in graphene", preprint at ChemRxiv. doi: 10.26434/chemrxiv-2026-trxcq

2. M. Micari*, K.-J. Hsu, K. V. Agrawal*, "Energy-Efficient and Cost-Effective Carbon Capture from Dilute Emissions Using Pyridinic-Graphene Membranes", **Nature Sustainability**, 9, 164–175 2026.
3. Hsu, K. J., Micari, M., Shen, Y., Li, S., Song, S., & Agrawal, K. V. (2025). Tuning Pore Size in Porous Graphene Membrane for O_2/N_2 Separation, **Advanced Materials**, e19645, 2025.
4. K. Černevičs, L. Bondaz, K. V. Agrawal*, O. Yazyev*, "Mechanistic insights into oxidation-induced carbon vacancy formation in graphene". **Cell Reports Physical Science**, 6, 12, 2025.
5. C. Kocaman, L. Bondaz, Y. Shen, M. Chevalier, J. Hao, M. Mensi, K. V. Agrawal*, "Scalable room temperature incorporation of CO_2-selective ångström-scale pores in graphene for carbon capture", **Nature Communications**, 16, 10380, 2025.
6. L. Bondaz, A. Ronghe, K. G. Ayappa*, K. V. Agrawal*, "Gated CO_2 Permeation across Dynamic Graphene Pores", **Nature Communications**, 16, 6252, 2025.
7. K.-J. Hsu, H.-Y. Chi, Y. Shen, S. Huang, R. Goswami, K. V. Agrawal*, "Modulation of Graphene Oxidation Using Substrate-Induced Electron-Hole Puddles Advancing Molecular Separation", **Advanced Functional Materials**, 2503121, 2025.
8. J. Hao, P. Gebolis, P. Gach, M. Chevalir, L. S. Bondaz, C. Kocaman, K.-J. Hsu, K. Bhorkar, D. J. Babu, K. V. Agrawal*, "Scalable Synthesis of CO_2-Selective Porous Single-Layer Graphene Membranes", **Nature Chemical Engineering**, 2, 241–251, 2025.
    - Highlighted on the front cover page with cover page graphics.
9. R. Bautz; G. Verdan, N. Gallandat; L. Zhong, A. Züttel; K. V. Agrawal, "Greengas - project gazier innovant", **Aqua & Gas**, 11 (31 October), 36–44, 2024.

Available at https://www.aquaetgas.ch/fr/énergie/gaz/20241031-greengas-projet-gazier-innovant/

10. T. Emmerich, N. Ronceray, K.V. Agrawal*, S. Garaj*, M. Kumar*, A. Noy*, A. Radenovic*, "Nanofluidics". **Nature Review Methods Primers** 4, 69, 2024.
11. M. Micari*, K. V. Agrawal, "Optimization of High-Performance Membrane Processes for Post-Combustion Carbon Capture", **Computer Aided Chemical Engineering** 53, 997, 2024.
12. K.-J. Hsu, S. Li, M. Micari, H.-Y. Chi, L. Zhong, L. F. Villalobos, S. Huang, X. Duan, A. Züttel, K. V. Agrawal*, "Graphene membranes with pyridinic nitrogen at pore edges for high-performance CO2 capture". **Nature Energy**, 9, 964–974, 2024.
13. S. Li, K.V. Agrawal*, "Nanolithography of the nanocorral structure of chemisorbed oxygen atoms on the graphitic lattice", **Carbon**, 221, 118897, 2024.
14. M. T. Vahdat, S. Li, S. Huang, L. Bondaz, N. Marzari*, K. V. Agrawal*, "Mechanistic Insights on Functionalization of Graphene with Ozone". **Journal of Physical Chemistry C,** 127, 22015–22, 2023.
15. L. Bondaz, A. Ronghe, S. Li, K. Čerņevičs, J. Hao, O. Yazyev, K. G. Ayappa, K. V. Agrawal*, "Selective Photonic Gasification of Strained Oxygen Clusters on Graphene for Tuning Pore Size in Å-Regime". **JACS Au**, 3, 2844-54, 2023.
    - Invited manuscript.
16. M. T. Vahdat, S. Li, S. Huang, C. A. Pignedoli, N. Marzari*, K. V. Agrawal*, "Unraveling the Oxidation of Graphitic Lattice : Structure Determination of Oxygen Clusters". **Physical Review Letters**, 131, 16, 168001, 2023.

17. S. Huang, L. F. Villalobos, S. Li, M. T. Vahdat, H.-Y. Chi, K. Hsu, L. Bondaz, V. Boureau, N. Marzari, K. V. Agrawal*, “In Situ Nucleation-Decoupled and Site-Specific Incorporation of Å-Scale Pores in Graphene via Epoxidation”, **Advanced Materials**, 2206627, 2022.
    - Featured in supplementary cover page
18. L. F. Villalobos, D. J. Babu, K. Hsu, C. Van Goethem, K. V. Agrawal*, “Gas Separation Membranes with Atom-Thick Nanopores: The Potential of Nanoporous Single-Layer Graphene”. **Accounts of Material Research**, 3, 1073-1087, 2022.
19. K. V. Agrawal*, R. Bautz*, “Capture du carbone par membranes en graphène à nanopores”, Capture Du Carbone. **Aqua & Gas**, 2022, 46–53 (2022).

    Available at https://www.aquaetgaz.ch/fr/énergie/gaz/20220225_capture-du-carbone/
20. S. Li, M. T. Vahdat, S. Huang, K.-J. Hsu, M. Rezaei, N. Marzari, K. V. Agrawal*, “Structural Evolution during the Oxidation of Graphitic Materials for the Generation of Vacancy Defects” **JACS Au**, 2, 723-730, 2022.
    - Featured on the cover page.
21. S. Huang, S. Li, K.-J. Hsu, L. F. Villalobos, K. V. Agrawal*, “Systematic design of millisecond gasification reactor for the incorporation of gas-sieving nanopores in single-layer graphene”, **Journal of Membrane Science**. 637, 119628, 2021.
    - Invited article (ICOM issue)
22. K.-J. Hsu, L. F. Villalobos, S. Huang, H. Chi, W. Lee, G. He, M. Mensi, K. V. Agrawal*, “Multi-pulsed millisecond ozone gasification for predictable tuning of nucleation and nucleation-decoupled nanopore expansion in graphene for carbon capture”, **ACS Nano**, 15, 13230-13239, 2021.
23. M. Micari, M. Dakhchoune, K. V. Agrawal*, “Techno-economic assessment of postcombustion carbon capture using high-performance nanoporous single-layer graphene membranes”, **Journal of Membrane Science,** 624, 119103, 2021.
24. S. Huang, S. Li, L. F. Villalobos, M. Micari, D. J. Babu, M. T. Vahdat, M. Mensi, E. Oveisi, K. V. Agrawal*, “Millisecond lattice gasification for high-density CO_2- and O_2-sieving nanopores in single-layer graphene”, **Science Advances**, 7, eabf0116, 2021

9 References

(1) Bui, M.; Adjiman, C. S.; Bardow, A.; Anthony, E. J.; Boston, A.; Brown, S.; Fennell, P. S.; Fuss, S.; Galindo, A.; Hackett, L. A.; Hallett, J. P.; Herzog, H. J.; Jackson, G.; Kemper, J.; Krevor, S.; Maitland, G. C.; Matuszewski, M.; Metcalfe, I. S.; Petit, C.; Puxty, G.; Reimer, J.; Reiner, D. M.; Rubin, E. S.; Scott, S. A.; Shah, N.; Smit, B.; Trusler, J. P. M.; Webley, P.; Wilcox, J.; Dowell, N. M. Carbon Capture and Storage (CCS): The Way Forward. ***Energy & Environmental Science*** 2018, *11* (5), 1062–1176. https://doi.org/10.1039/C7EE02342A.

(2) Change (IPCC), I. P. on C. Summary for Policymakers. In *Global Warming of 1.5°C: IPCC Special Report on Impacts of Global Warming of 1.5°C above Pre-industrial Levels in Context of Strengthening Response to Climate Change, Sustainable Development, and Efforts to Eradicate Poverty*; Cambridge University Press, 2022; pp 1–24.

(3) Melet, A.; Meyssignac, B.; Almar, R.; Le Cozannet, G. Under-Estimated Wave Contribution to Coastal Sea-Level Rise. ***Nature Climate Change*** 2018, *8* (3), 234–239. https://doi.org/10.1038/s41558-018-0088-y.

(4) Merkel, T. C.; Wei, X.; He, Z.; White, L. S.; Wijmans, J. G.; Baker, R. W. Selective Exhaust Gas Recycle with Membranes for CO2 Capture from Natural Gas Combined Cycle Power Plants. ***Industrial & Engineering Chemistry Research*** 2013, *52* (3), 1150–1159. https://doi.org/10.1021/ie302110z.
(5) Merkel, T. C.; Lin, H.; Wei, X.; Baker, R. Power Plant Post-Combustion Carbon Dioxide Capture: An Opportunity for Membranes. ***Journal of Membrane Science*** 2010, *359* (1), 126–139. https://doi.org/10.1016/j.memsci.2009.10.041.
(6) Wang, L.; Pérez-Fortes, M.; Madi, H.; Diethelm, S.; herle, J. V.; Maréchal, F. Optimal Design of Solid-Oxide Electrolyzer Based Power-to-Methane Systems: A Comprehensive Comparison between Steam Electrolysis and Co-Electrolysis. ***Applied Energy*** 2018, *211*, 1060–1079. https://doi.org/10.1016/j.apenergy.2017.11.050.
(7) Rubin, E. S.; Davison, J. E.; Herzog, H. J. The Cost of CO2 Capture and Storage. ***International Journal of Greenhouse Gas Control*** 2015, *40*, 378–400. https://doi.org/10.1016/j.ijggc.2015.05.018.
(8) Micari, M.; Hsu, K.-J.; Bempeli, S.; Agrawal, K. V. Energy- and Cost-Efficient CO2 Capture from Dilute Emissions by Pyridinic-Graphene Membranes. ***Nature Sustainability*** 2026, *9* (1), 164–175. https://doi.org/10.1038/s41893-025-01696-5.
(9) Huang, S.; Li, S.; Villalobos, L. F.; Dakhchoune, M.; Micari, M.; Babu, D. J.; Vahdat, M. T.; Mensi, M.; Oveisi, E.; Agrawal, K. V. Millisecond Lattice Gasification for High-Density CO_2- and O_2-Sieving Nanopores in Single-Layer Graphene. ***Science Advances*** 2021, *7* (9), eabf0116. https://doi.org/10.1126/sciadv.abf0116.
(10) Villalobos, L. F.; Goethem, C. V.; Hsu, K.-J.; Li, S.; Moradi, M.; Zhao, K.; Dakhchoune, M.; Huang, S.; Shen, Y.; Oveisi, E.; Boureau, V.; Agrawal, K. V. Bottom-up Synthesis of Graphene Films Hosting Atom-Thick Molecular-Sieving Apertures. ***Proceedings of the National Academy of Sciences*** 2021, *118* (37). https://doi.org/10.1073/pnas.2022201118.
(11) Bondaz, L.; Ronghe, A.; Li, S.; Čerņevičs, K.; Hao, J.; Yazyev, O. V.; Ayappa, K. G.; Agrawal, K. V. Selective Photonic Gasification of Strained Oxygen Clusters on Graphene for Tuning Pore Size in the Å Regime. ***JACS Au*** 2023, *3* (10), 2844–2854. https://doi.org/10.1021/jacsau.3c00395.
(12) Hsu, K.-J.; Li, S.; Micari, M.; Chi, H.-Y.; Villalobos, L. F.; Huang, S.; Zhong, L.; Song, S.; Duan, X.; Züttel, A.; Agrawal, K. V. Graphene Membranes with Pyridinic Nitrogen at Pore Edges for High-Performance CO_2 Capture. ***Nature Energy*** 2024, *9* (8), 964–974. https://doi.org/10.1038/s41560-024-01556-0.
(13) Micari, M.; Dakhchoune, M.; Agrawal, K. V. Techno-Economic Assessment of Postcombustion Carbon Capture Using High-Performance Nanoporous Single-Layer Graphene Membranes. ***Journal of Membrane Science*** 2021, *624*, 119103. https://doi.org/10.1016/j.memsci.2021.119103.
(14) Koenig, S. P.; Wang, L.; Pellegrino, J.; Bunch, J. S. Selective Molecular Sieving through Porous Graphene. ***Nature Nanotechnology*** 2012, *7* (11), 728–732. https://doi.org/10.1038/nnano.2012.162.
(15) Yuan, Z.; Govind Rajan, A.; Misra, R. P.; Drahushuk, L. W.; Agrawal, K. V.; Strano, M. S.; Blankschtein, D. Mechanism and Prediction of Gas Permeation through Sub-Nanometer Graphene Pores: Comparison of Theory and Simulation. ***ACS Nano*** 2017, *11* (8), 7974–7987. https://doi.org/10.1021/acsnano.7b02523.
(16) Bondaz, L.; Ronghe, A.; Ganapathy Ayappa, K.; Agrawal, K. V. Gated CO2 Permeation across Dynamic Graphene Pores. ***Nature Communications*** 2025, *16* (1), 6252. https://doi.org/10.1038/s41467-025-61518-2.
(17) Li, S.; Vahdat, M. T.; Huang, S.; Hsu, K.-J.; Rezaei, M.; Mensi, M.; Marzari, N.; Agrawal, K. V. Structure Evolution of Graphitic Surface upon Oxidation: Insights by Scanning Tunneling Microscopy. ***JACS Au*** 2022, *2* (3), 723–730. https://doi.org/10.1021/jacsau.1c00570.
(18) Vahdat, M. T.; Li, S.; Huang, S.; Bondaz, L.; Bonnet, N.; Hsu, K.-J.; Marzari, N.; Agrawal, K. V. Mechanistic Insights on Functionalization of Graphene with Ozone. ***The Journal of Physical Chemistry C*** 2023, *127* (45), 22015–22022. https://doi.org/10.1021/acs.jpcc.3c03994.

(19) Vahdat, M. T.; Li, S.; Huang, S.; Pignedoli, C. A.; Marzari, N.; Agrawal, K. V. Unraveling the Oxidation of a Graphitic Lattice: Structure Determination of Oxygen Clusters. ***Physical Review Letters*** 2023, *131* (16), 168001. https://doi.org/10.1103/PhysRevLett.131.168001.
(20) Novoselov, K. S. Electric Field Effect in Atomically Thin Carbon Films. ***Science*** 2004, *306* (5696), 666–669. https://doi.org/10.1126/science.1102896.
(21) Li, X.; Cai, W.; An, J.; Kim, S.; Nah, J.; Yang, D.; Piner, R.; Velamakanni, A.; Jung, I.; Tutuc, E.; Banerjee, S. K.; Colombo, L.; Ruoff, R. S. Large-Area Synthesis of High-Quality and Uniform Graphene Films on Copper Foils. ***Science*** 2009, *324* (5932), 1312–1314. https://doi.org/10.1126/science.1171245.
(22) Deng, B.; Liu, Z.; Peng, H. Toward Mass Production of CVD Graphene Films. ***Advanced Materials*** 2019, *31* (9), 1800996. https://doi.org/10.1002/adma.201800996.
(23) Kidambi, P. R.; Mariappan, D. D.; Dee, N. T.; Vyatskikh, A.; Zhang, S.; Karnik, R.; Hart, A. J. A Scalable Route to Nanoporous Large-Area Atomically Thin Graphene Membranes by Roll-to-Roll Chemical Vapor Deposition and Polymer Support Casting. ***ACS Applied Materials & Interfaces*** 2018, *10* (12), 10369–10378. https://doi.org/10.1021/acsami.8b00846.
(24) Huang, S.; Dakhchoune, M.; Luo, W.; Oveisi, E.; He, G.; Rezaei, M.; Zhao, J.; Alexander, D. T. L.; Züttel, A.; Strano, M. S.; Agrawal, K. V. Single-Layer Graphene Membranes by Crack-Free Transfer for Gas Mixture Separation. ***Nature Communications*** 2018, *9* (1), 1–11. https://doi.org/10.1038/s41467-018-04904-3.
(25) Huang, S.; Villalobos, L. F.; Li, S.; Vahdat, M. T.; Chi, H.-Y.; Hsu, K.-J.; Bondaz, L.; Boureau, V.; Marzari, N.; Agrawal, K. V. In Situ Nucleation-Decoupled and Site-Specific Incorporation of Å-Scale Pores in Graphene via Epoxidation. ***Advanced Materials*** 2022, *34* (51), 2206627. https://doi.org/10.1002/adma.202206627.
(26) Kocaman, C.; Bondaz, L.; Shen, Y.; Goswami, R.; Chevalier, M.; Hao, J.; Mensi, M.; Agrawal, K. V. Scalable Room Temperature Incorporation of CO_2-Selective Ångström-Scale Pores in Graphene for Carbon Capture. ***Nature Communications*** 2025, *16* (1), 10380. https://doi.org/10.1038/s41467-025-65336-4.
(27) Suk, J. W.; Kitt, A.; Magnuson, C. W.; Hao, Y.; Ahmed, S.; An, J.; Swan, A. K.; Goldberg, B. B.; Ruoff, R. S. Transfer of CVD-Grown Monolayer Graphene onto Arbitrary Substrates. ***ACS Nano*** 2011, *5* (9), 6916–6924. https://doi.org/10.1021/nn201207c.
(28) Hao, J.; Gebolis, P. M.; Gach, P. M.; Chevalier, M.; Bondaz, L. S.; Kocaman, C.; Hsu, K.-J.; Bhorkar, K.; Babu, D. J.; Agrawal, K. V. Scalable Synthesis of CO_2-Selective Porous Single-Layer Graphene Membranes. ***Nature Chemical Engineering*** 2025, *2* (4), 241–251. https://doi.org/10.1038/s44286-025-00203-z.

10 Appendix

Computational fluid dynamics (CFD) simulation

Model physics and geometry:

To systematically analyze the gas flow profile within the tubular furnace, we performed 3D CFD simulations using the COMSOL Multiphysics® 6.1 platform. The geometry was modeled to match the physical dimensions of the 12 cm-diameter quartz reactor, including the internal sample substrate and the quartz semi-cylindrical block. Given the low velocities and reactor dimensions, the Laminar Flow interface was utilized. The fluid properties were modeled based on O_2 at the reaction temperature 85 ℃, accounting for the temperature-dependent changes in gas density and dynamic viscosity.

Boundary conditions and numerical setup:

The simulation was governed by the steady-state Navier-Stokes and continuity equations. The following boundary conditions were applied to ensure physical accuracy.

a) Inlet: Defined as a fully developed flow with a customized volumetric flow rate (e.g., 2 l/min). This boundary condition ensures that the velocity profile at the entrance of the chamber represents the actual flow as it emerges from the upstream piping.

b) Outlet: Set to a static pressure of 0 Pa, simulating an exhaust to the ambient atmosphere or a controlled vacuum system.

c) Walls: All solid boundaries, including the reactor shell, quartz block, and sample substrate, were assigned a no-slip condition.

Mesh strategy and grid independence:

The model was discretized using COMSOL's physics-controlled "Fine" mesh sequence. This sequence automatically generates a combination of unstructured tetrahedral elements in the bulk flow and triangular elements on the boundaries. To accurately resolve the fluid-solid interface at the graphene surface, we utilized boundary layer meshing, which creates a dense layer of thin, high-aspect-ratio elements to capture the velocity gradients within the viscous sublayer. To ensure the accuracy of our results while maintaining computational efficiency, we applied the following logic regarding grid independence.

a) Predefined Resolution: By utilizing the "Fine" mesh setting, we ensured a high enough element density to avoid significant numerical diffusion.

b) Geometric Consistency: A formal mesh sensitivity analysis was not performed because the reactor geometry in the immediate vicinity of the sample position remained unchanged across our primary comparisons.

c) Comparative Focus: Since all other boundary conditions and parameters were held consistent, our analysis focused exclusively on the macroscopic differences between distinct reactor geometries. By maintaining a stable, high-resolution mesh configuration in the region of interest, we ensured that the observed variations in the gas flow profile were a direct result of geometric changes rather than discretization errors.

All simulation results, including the extraction of velocity magnitude data and the generation of 2D and 3D plots, were performed directly within the COMSOL Multiphysics® data analyzing node.